Design of polyelectrolyte multilayer particles for nucleic acid delivery

Chen, Averil Min Hui

2012

Chen, A. M. H. (2012). Design of polyelectrolyte multilayer particles for nucleic acid delivery. Master’ s thesis, Nanyang Technological University, Singapore.

https://hdl.handle.net/10356/50610

https://doi.org/10.32657/10356/50610

DESIGN OF POLYELECTROLYTE MULTILAYER PARTICLES FOR NUCLEIC ACID DELIVERY

CHEN MIN HUI AVERIL

A thesis submitted to Nanyang Technological University

in partial fulfillment of the requirement for the degree of

Master of Engineering

School of Chemical and Biomedical Engineering

Nanyang Technological University, Singapore

2012

Acknowledgements

First, I would like to thank three individuals whose united efforts had sparked this collaborative bioengineering project. My supervisor, Associate Professor Dr. Björn H. Neu, for offering me an opportunity to be part of his PEM particles research group and his constant encouragement. Professor Dr. Subbu S. Venkatraman for the collaboration with School of Materials Science and Engineering (MSE) and his expert advice and suggestions on polymer research work. Dr. Tina Wong for the collaboration with Singapore Eye Research Institute (SERI), her insights in eye-related research and continuous encouragement. I am very grateful for being part of this collaboration which I had learnt so much from.

To the research group members involved with PEM particles, Dr. Jacqueline E. Leβig and M. Shaillender, thank you for listening, understanding (only you will truly understand the problems!), and encouraging me through my project. Your suggestions and friendships enabled me to move forward and made each day in lab more enjoyable. Thank you Jacqueline, for your invaluable help and guidance through my thesis. Thank you Shaillender for all the priceless nuggets of information. I will remember all the good times we all shared.

I would also like to thank Dr. Uta Reibetanz, for introducing and sharing her expertise about polyelectrolyte multilayer particles system. Thank you for imparting to

me some of your research skills and knowledge which were essential for the completion of this thesis.

To the researchers at MSE, Dr. Scott A. Irvine for his encouragement and informative advice on biological works and Dr. Ma Lwin Lwin for her help with equipments in MSE.

To SCBE professional and technical staff, Dr.Yu Shucong, Yeo Kah Yan, Noor Haslinda Binte Abdullah, Chitra Devi D/O Subramaniam for their trainings and technical support. Special thanks to Kah Yan for processing with the lab's orders and repairs, and my transportation claims!

A special thank you to SERI research staff, Toh Li Zhen, Sharon N. Finger, Roseline Su, Stephanie Chu and Yonathan Lukito for their friendly assistance with experiments held in SERI. Thank you Li Zhen and Sharon for introducing and helping me with the equipments especially for bookings and data retrieval! I will remember all the laughter and lunches we shared.

Researchers in the laboratory group, Gao Jie, Zhang Zhengwen, Yang Yang, Stephanie, Samar Rad, Rani Kaliyaperumal, Deng Xiao Peng; and FYP students Kelvin Qu, Winston Tan, Gan Yan Li, Petrie Cheah, Qiao Mei, Sharon Kaur, Lim Ying Ling and Teo Zi Yong; thank you for your company and help in the laboratory!

Fellow SCBE post-graduate students Bernice Oh, Ng Shu Rui, Lau Ting Ting, Teo Ailing, Vu Thi Thu Thao, Wong Wei Chang; thank you for your friendship, the birthday celebrations and all the various presents brought back from overseas.

A special thank you to my family members for their constant love and support, especially to my mother who heart-warmingly prepares dinner for me even when I am home late.

Lastly, thank you to my close friends and my love Nai Chiau Kwang, who were always there for me, patiently listening to my complains, continuously being my pillars of support and making my life so much more beautiful!

Table of Contents

Abstract

Polyelectrolyte multilayer (PEM) particles fabricated using the layer-by-layer (LbL) method provides the advantage of being highly customizable despite its simple assembly process. An array of sizes and materials can be selected for the particle template and polyelectrolyte multilayer to tailor for its anticipated purpose. Substances can be encapsulated within the core, in between the multilayer or coated on the outermost surface to provide added functionality of the resultant PEM particles. Biopolymers which are biocompatible and biodegradable are beneficial in biomedical applications of PEM particles such as carrier systems, bioreactors, biosensors, etc. The focus of this project is to bridge the gap between biomedical applications of PEM particles and delivery of active biomacromolecules through the systematic design and development of biodegradable PEM particles for nucleic acid delivery in a biological environment. Encapsulation of reporter plasmid DNA and siRNA within bio-relevant PEM particles (including PEM nanoparticles, microparticles and microcapsules) was explored as well as the interaction of these nucleic acid loaded PEM particles with HEK293T, FibroGRO and HTF cells. Furthermore, cytotoxic studies of the PEM particles were executed to determine the threshold levels for cellular applications. The long term goal is to develop the PEM particles as multifunctional tailor-made biodegradable drug carrier systems with controlled drug release and additional functionalities.

List of abbreviations

ARG	Poly-L-arginine hydrochloride
$CaCO_3$	Calcium carbonate
CLSM	Confocal laser scanning microscopy
DNA	Deoxyribonucleic acid
DXS	Dextran sulfate
FibroGRO	Human foreskin fibroblasts
FITC	Fluorescein isothiocyanate
FSC	Forward scattering
GFP	Green fluorescent protein
HA	Hydroxyapatite
HEK293T	Human embryonic kidney cells
HTF	Human tenon fibroblasts
LbL	Layer by layer
MTT	Thiazolyl blue tetrazolium bromide

NaCl	Sodium chloride
PEM	Polyelectrolyte multilayer
PRM	Protamine sulfate
RNA	Ribonucleic acid
RNAi	Ribonucleic acid interference
RITC	Rhodamine isothiocyanate
SEM	Scanning electron microscopy
siRNA	Short interfering ribonucleic acid
SSC	Side scattering

List of figures

Publications

1) Uta Reibetanz, Min Hui Averil Chen, Shaillender Mutukumaraswamy, Zi Yen Liaw, Bernice Hui Lin Oh, Subbu Venkatraman, Edwin Donath, Björn Neu; *Colloidal DNA Carriers for Direct Localization in Cell Compartments by pH Sensoring.* Biomacromolecules, 2010. **11**(7): p. 1779-1784.

2) Reibetanz, Uta; Chen, Min Hui Averil; Mutukumaraswamy, Shaillender; Liaw, Zi Yen; Oh, Bernice Hui Lin; Donath, Edwin; Neu, Björn; *Functionalization of Calcium Carbonate Microparticles as a Combined Sensor and Transport System for Active Agents in Cells.* Journal of Biomaterials Science, Polymer Edition, 2011. **22**(14): p. 1845-1859.

3) Min Hui Averil Chen, Jacqueline Lessig, Tina Wong, Subbu Venkatraman, Björn Neu; Delivery of reporter siRNA by biocompatible PEM nanoparticles, in preparation.

Conferences

1) 2nd International Conference on Cellular & Molecular Engineering (ICCMB2), 2010

   Polyelectrolyte multilayer particles as nucleic acid carriers

   Min Hui Averil Chen, Bernice Hui Lin Oh, Mutukumaraswamy Shaillender, Uta Reibetanz, Subbu Venkatraman, Björn Neu

2) Biomedical Engineering Society 5th Scientific Meeting (BES5SM), 2011

   Polyelectrolyte microcapsules coated with red blood cell membranes for passive targeting

   Mutukumaraswamy Shaillender, Min Hui Averil Chen, Björn Neu, Subbu Venkatraman

CHAPTER 1
Introduction

1.1 Introduction

This project examines the design and development of biodegradable PEM particles for the delivery of active biomacromolecules. The potential of PEM particles as nucleic acid carriers for therapeutic purposes is explored. The following sub-chapters give an introductory overview of the two areas which are combined in this project, namely LbL coated PEM particles and therapeutic uses of nucleic acids.

1.1.1 Introduction to PEM particles

The layer-by-layer (LbL) assembly method, based on the sequential absorption of polycations and polyanions on a substrate, was started by Decher and fellow workers [1]. The major advantages of this method are its simple fabrication steps and customizability, which arises from the individual addition of each layer during the fabrication process, thus the multilayer components can be altered to suit multiple purposes.

Primarily, the LbL constructed multilayer is held through electrostatic attraction of the oppositely-charged polyelectrolytes. However, LbL has also been extended to hydrophobic interactions [2, 3], hydrogen bonding [4-6], DNA hybridization [7], etc. to secure the thin films together.

Initially, the LbL technique was applied to planar surfaces to create multilayer thin films. The evolution to use colloidal particles [8, 9] as layering substrates allowed the development of polyelectrolyte multilayer capsules. Figure 1.1 illustrates the fabrication process using particles, where centrifugation washes are executed to remove excess polyelectrolytes before the adsorption of next alternately-charged polyelectrolyte. After several repetitions to the form a multilayer shell held together by electrostatic attraction, the core substrate can be sacrificed to create a hollow capsule.

Due to the versatility of the LbL technique, PEM particles have been tailored for a wide range of applications including reactor systems [10, 11], sensor [12], immunoassay [13] and controlled carrier systems [14, 15]. Comprehensive reviews are available about the numerous works on PEM particles for various functions [16, 17].

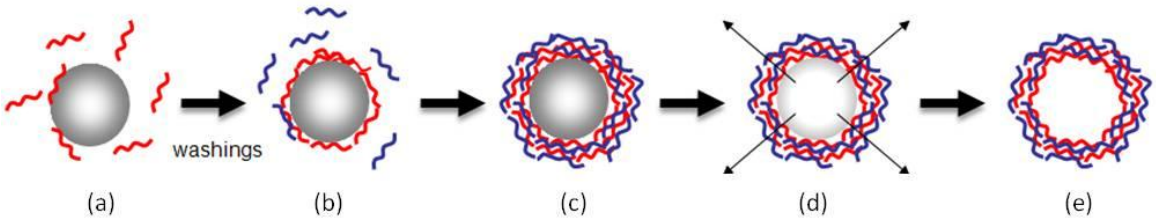

Figure 1.1 Schematic illustration of LbL coating to fabricate PEM particles. (a) Coating of the first polyelectrolyte onto the particle substrate. (b) After centrifugation washes to remove the excess polyelectrolyte, the alternately-charged polyelectrolyte is adsorbed. (c) After several coatings of the polyelectrolyte pairs, a polyelectrolyte multilayer shell is formed. (d) Dissolution of the particle core. (e) Formation of a polyelectrolyte multilayer capsule with a hollow core.

1.1.2 Introduction to nucleic acid as biological drugs

Gene therapy aims to modify specific genes, by the administration of genetic material, for therapeutic purposes [18]. Insertion of DNA was primarily developed for treatment of genetic diseases, but has expanded to treatment of other diseases like cancer [19], arthritis [20], vascular diseases [21] etc.

Another way to alter gene expression is through post-transcriptional gene silencing or also known as RNA interference. RNA interference was first discovered by Fire, Mello and colleagues, when double-stranded RNA (dsRNA) injected into *Caenorhabditis elegans* caused silencing of the complementary gene [22].

The silencing mechanism begins with the long dsRNA being cleaved by the dicer to short interfering RNA (siRNA) of 21-23 base pairs. After the duplex siRNA associates with the RNA-induced silencing complex (RISC) and unwinds, the sense strand of the siRNA is degraded while the anti-sense strand is utilized as a template for targeting the complementary mRNA bound for degradation. The activated RISC can execute degradation cycles of the specific mRNA repeatedly. As such, no protein is produced, and the gene which encodes the mRNA is effectively silenced [23-26].

Vector systems used to deliver genes can be classified into two categories, viral and non-viral vectors. Viral vectors exploit the efficient gene transfer by viruses [27], but come with the safety and pathogenic concerns [28]. Despite being less efficient then viral vectors, the research into non-viral vectors has been increased, due to its non-pathogenic advantages [29].

1.2 Thesis outline

The first few chapters of this thesis give an overview of the background information which facilities the comprehension of the results presented in the later chapters. Chapter 1 introduces the topic of research, overall research objectives and specific aims, scope and limitations, and significance of research. The second chapter provides an in depth review of literature on PEM. Information about biocompatible PEM particles and their encapsulation abilities are presented as well as studies on their interactions with cells. Chapter 3 details the materials and research methodologies used to achieve the data in the following chapters.

Chapter 4 through 8 represents the research work completed in this thesis. Fabrication of the PEM particles is covered in Chapter 4, presenting the data used to verify each layer is coated on the particles. Absorption of PRM/DXS and ARG/DXS layer pairs was examined on PEM nanoparticles and microparticles. The fabrication of PEM microcapsules from PEM microparticles was also verified.

Successful fabrication of PEM particles lead to loading of the useful material into the particles. Chapter 5 studies two types of nucleic acids encapsulation methods in PEM particles, namely layer and core encapsulation. Encapsulation of both reporter plasmid DNA and siRNA were accomplished in PEM nanoparticles and microparticles/capsules.

Chapter 6 examines the cellular uptake of the different sizes of PEM particles in HEK293T, FibroGRO and HTF cells. The cells readily uptake the PEM particles presented, as particles were observed to be within the cell membrane using confocal microscopy. To differentiate PEM particles attached on the cell membrane and PEM particles within the cells, trypan blue quenching was employed during flow cytometry.

Additionally, cellular processing of PEM nanoparticles was studied by staining the particle-treated cells with acidic organelle stain Lysotracker Red. The absence of co-localization of fluorescent PEM particles with the stained lysosomes suggested that the particles were not within acidic environments such as endolysosomes.

After the uptake of the particles, Chapter 7 follows with the potential of intracellular delivery nucleic acids by PEM particles. Reporter DNA and siRNA gave straightforward indication of successful delivery by PEM particles. This was observed in PEM nanoparticles as well as PEM microcapsules.

To apply the PEM particles as nucleic acid carriers, cytotoxic studies gave a deeper understanding on the threshold levels which could be used with cellular interaction experiments. Chapter 8 presents the cell proliferation assays of HEK293T, FibroGRO and HTF cells when incubated with different amounts of PEM particles.

To end with, Chapter 9 summarizes and concludes the findings established in this thesis. Final recommendations of future experiments for the development of PEM particles as nucleic acid carriers are also suggested.

1.3 Overall research objectives and specific aims

The overall objective of this project is to utilize PEM particles as a biological drug delivery system. It encompasses bio-relevant particles fabricated using the LbL technique in micron and sub-micron sizes, encapsulated with reporter DNA and siRNA as biological drugs. The studies of cellular interaction, cytotoxicity, as well as the drug delivery capabilities of the PEM particles propel the development of PEM particles as novel nucleic acid carriers. The specific aims achieved in this project are as follows:

1.3.1 Fabrication and characterization of biodegradable PEM particles

Commercially-available particles (hydroxyapatite (HA) ($Ca_5(PO_4)_3(OH)$) nanoparticles) as well as fabricated biocompatible particles (calcium carbonate ($CaCO_3$) particles) were explored as template cores for the layer-by-layer adsorption of alternately-charged biodegradable polyelectrolytes. Polyelectrolyte layers were successfully coated on micron and sub-micron particles as characterized by qualitative confocal microscopy figures and quantitative data from zeta potentials and flow cytometry. A number of polyelectrolyte pairs were studied including PRM/DXS and ARG/DXS. Additionally, microcapsules were achieved through the dissolution of the $CaCO_3$ template cores after formation of the multilayer.

1.3.2 Loading of nucleic acids into PEM particles

Loading of nucleic acids (reporter DNA or siRNA) was studied in two ways: inside the template core, as well as sandwiched within different layers of the polyelectrolyte multilayer. This was analyzed using confocal microscopy and flow cytometry. The amount of encapsulated drug was determined by UV/Vis measurements of the supernatants before and after incubation with the PEM particles. Loading efficiencies within the multilayer depended on particle size and the polyelectrolyte layers used.

1.3.3 Cellular interaction with PEM particles

Cellular interaction of PEM particles with HEK293T, HTF and FibroGRO cells were examined by co-incubation of the cells with PEM particles possessing fluorescent-labeled components. In-vitro cellular uptake and processing of the particles in these cell types were elucidated through analysis with confocal microscopy and flow cytometry in combination with specific cell organelle stains. Cellular uptake of the fluorescent PEM particles was visualized by overlapping of CLSM fluorescence images with their

transmission light images or using fluorescent cell membrane stains. Flow cytometry of cells allowed the comparison of fluorescent intensities of cells with and without fluorescent PEM particle incubation. In order to determine if the PEM particles were within the cytoplasm or stuck in endolysosomal compartments after cellular uptake, processing within the cells was further investigated using Lysotracker Red, a stain which stains the acidic organelles as lysosomes within the cells. Co-localization of fluorescent PEM particles with the stained lysosomes would indicate that the particles were trapped within the acidic compartments, while its absence would imply that the particles have escaped to the cytoplasm.

1.3.4 PEM particles as biological drug delivery system

Applications of biodegradable PEM particles as nucleic acid carriers were studied using reporter DNA and siRNA. The reporter DNA is a plasmid which codes for fluorescent proteins (GFP, DsRed), and when successfully transfected, the cells will appear fluorescent. As for the reporter siRNA, siGLO Green a transfection indicator is exploited as it is easily detectable when transfected due to its accumulation within the cell nuclei. The nucleic acids were encapsulated within the PEM particles and incubated with various cell types. Confocal microscopy was utilized to observe for delivery success; fluorescent cells for DNA delivery and fluorescent nuclei for siRNA delivery. Intracellular delivery of reporter DNA and siRNA was accomplished through PEM particles carrier system.

Furthermore, cytotoxicity of the carriers was studied with two proliferation studies, xCelligence real-time proliferation assay and the traditional MTT assay. The investigation of cell viabilities with increasing amounts of PEM particles enabled the investigation of the tolerable amounts of PEM particles to be used as drug carriers.

1.4 Scope and limitations of the study

This project encompasses bio-relevant particles fabricated using the LbL technique in micron and sub-micron sizes, with reporter DNA and siRNA as biological drugs. Reporter nucleic acids give distinct indications if PEM particles have definite potential applications in nucleic acid delivery. Plasmid DNA coding for fluorescent proteins allow for uncomplicated detection of effective DNA delivery as successfully transfected cells will produce fluorescent proteins and be straightforwardly indentified. siGLO Green transfection indicator is a fluorescent, specially coded RNA duplex that accumulates within the cell nuclei upon successful RNAi transfection. This permits easy and immediate detection of RNAi transfection success.

Straightforward detection of nucleic acid delivery enables preliminary investigations of the abilities of the proposed drug carriers. However, effectiveness of the biological drug released from PEM nanoparticles have to be studied in further depths for future drug developments. Most importantly is the true functionality of the DNA or siRNA, expressing or silencing specific genes, when it is delivered and released from PEM particles within the cell. This requires additional studies which investigate the specific gene being expressed or silenced such as PCR at RNA level and/or at the protein level with Western blots.

Additionally, several other factors have to be considered for a drug delivery system to be applied *in vivo* including drug loading efficiency, efficacy of the delivery system in cells, optimal amount and duration of loaded drug released etc. These factors will need to be optimized for optimal therapeutic effect with minimal toxicity.

1.5 Significance of research

The novelty of the highly customizable and multi-functional PEM particle system lies in the LbL fabrication of PEM particles; which enables them to be specifically designed to fit the required purposes and yet have a simple production process. In this project, the strengths of each tailored PEM particle system will be exploited and further explored for drug delivery applications. The use of biopolymers plus its encapsulation ability poses an excellent platform to utilize PEM particles as drug carrier systems, as the drug trapped within the particles can be released as the particles degrade within the cell. The components of the PEM particle system, its drug loading efficiency and drug release rate can be modified to achieve the desired drug effect with minimal cytotoxicity. The LbL system allows for time-controlled or low-dose drug release which can be accomplished by varying the number of polyelectrolyte layers between and above the drug layers. Additional functionalities can also be included in the PEM particles, such as the inclusion of the ability to track the particles within the cells as detailed below, as well as specific cell targeting. These factors will play important roles in functionalizing PEM particles as biological drug carriers, specifically for the novel application of cellular delivery of nucleic acids.

1.5.1 Fabrication of PEM particles

The template core used at the beginning of the multilayer fabrication determines the size of the final PEM particles. Micron sized particles can be easily fabricated without the use of complex steps and also, they permit the encapsulation of a large volume of substance within the cores. Furthermore, PEM microcapsules can be formed from dissolution of the microparticle core, leaving a shell of polyelectrolyte multilayer encapsulating the active

substance. In particular, the calcium carbonate cores used in this project utilize mild conditions for dissolution, which is essential in preserving the nucleic acid loads.

On the other hand, nano-sized particles offer a high surface to volume ratio. That allows for encapsulation of a high amount of substance on its surface. They can also be taken up by cells more readily due to its smaller size as compared to microparticles. However, nanoparticles are more difficult to fabricate in uniformed sizes and shapes. The choice of commercially-available particles allows a ready-to-use option and they are more uniformly-sized and shaped than self-fabricated particles. This is favorable for studying factors that pertain to the polyelectrolyte multilayer, as the particle core remains consistent. HA nanoparticles offer an excellent choice as cores for the fabrication of PEM nanoparticles as they are biocompatible and cheaply commercially available. Thus they would be useful in the investigation of biocompatible and biodegradable PEM nanoparticles, as layer encapsulation is the focus of these nano-sized particles.

Both sizes of PEM particles has its own advantages, hence in this thesis both types were studied to exploit their individual strengths for the development of a biodegradable nucleic acid carrier system.

1.5.2 Drug loading within PEM particles

The LbL coating scheme allows for encapsulation within the core or within the multilayer, of which both can be specifically modified to suit the delivery requirements. Varied amounts of drug can be encapsulated within the particle core during the fabrication process, and after subsequent coating of the PEM, the core can be dissolved to form capsules encapsulating the drug. With multilayer encapsulation, drug dosage can be

tweaked by adjusting the number of layers of drug adsorbed on the particles. More layers of drug on a particle will correlate to a higher drug dosage per particle.

Moreover, for both type of encapsulation methods, controlled release can be envisioned by varying the number of polyelectrolyte layers between and above the drug layers. An increased number of polyelectrolyte layers will possibly increase the amount of time needed for the particle to degrade before the release of encapsulated drug.

The delivery of biological drugs like proteins, DNA and RNA requires protection as they are prone to degradation. The intracellular delivery of nucleic acids using PEM particles is not yet well studied; with few studies about DNA and RNA delivery by PEM particles. Hence this project will be a significant contribution to developing PEM particles as a biological drug carrier system.

1.5.3 Cellular interaction of PEM particles

Cellular processing of PEM particles is not yet well studied including its cellular uptake pathway, degradation within the cell, release of encapsulated material inside the cell and its effects on the cellular activities, etc. In this project, fluorescent labeled nucleic acids encapsulated within the PEM particles and co-incubated with different cell lines allowed for intracellular tracking. With the combination of specific cell organelle stains, the results which can lend insights for investigation of the above intracellular processing factors. Specifically, Lysotracker Red was utilized in this project to stain the acidic organelles in particle-treated cells. The co-localization of the fluorescent PEM particles and acidic compartments was examined to determine if the particles were stuck within endolysosomes or had escaped to the cytoplasm. Furthermore, the reporter characteristics like plasmid DNA for the expression of fluorescent proteins as well as siRNA

transfection indicator that accumulates within the cell nucleus will further elucidate the cell's interaction with PEM particles.

The cytotoxicity of the particles is also an important aspect to investigate, as the carrier system should work below the toxic threshold. A novel real-time cell proliferation assay is used to continuously monitor cell growth with the presence of particles over a period of 7 days. The traditional MTT assay is utilized to cross-check the proliferation data. This contributes knowledge to the development of PEM particles as drug carriers as the possible amounts of PEM particles which can be applied for low cytotoxic drug delivery will be explored.

CHAPTER 2
Review of literature

2.1 Biocompatible PEM particles

The versatility of PEM particles fabricated by the LbL technique led to its numerous applications, and one of the recent developments is for biomedical purposes like drug delivery, bioreactors and biosensors [30-35]. For PEM particles to act as therapeutic agent there is a need for biocompatibility and degradability, so as to release the encapsulated drug as well as disappearing from the human body after it has served its purpose. The PEM particle is comprised of two components: the core and the polyelectrolyte multilayer, and both can be customized for the design of a biodegradable PEM particle suitable for applications in the biological field.

A number of materials have been studied to serve as the template core. Some templates can be sacrificed after adsorption of the polyelectrolyte layers, resulting in hollow capsules with no core in the final product. Silica [36-38] and melamine formaldehyde (MF) particles [39-41] have been utilized widely, but their dissolution makes use of harsh chemicals which may pose toxicity issues. Biocompatible cores such as cells [42, 43], calcium carbonate [44-46], poly(lactide-co-glycolide) (PLGA) [47-50] etc. are more suitable for biomedical applications, and furthermore the dissolution of cells and calcium

carbonate particles require milder chemicals. In addition, sub-micron sized biocompatible particles have increasingly been used as templates [51], such as gold nanoparticles [52-54], quantum dots [55], PLGA nanoparticles [49, 50], poly-L-lactic acid (PLA) nanoparticles [56] etc.

Various biodegradable polymers have been utilized in PEM particle fabrication, and their permutations have led to formation of an even wider array of biodegradable PEM particles. Examples of positively-charged biopolymers include protamine sulfate [57-59], poly-L-arginine [44], poly-L-lysine [59-61], chitosan [49, 62], etc. The particular positively-charged polymer is paired with a negatively-charged biopolymer including dextran sulfate [44, 57], alginate [49], etc. More specialized biopolymers are also used including PEG-grafted polymers [63].

2.2 Encapsulation in PEM particles

Encapsulation can take place in either the core or the multilayer, or both. It is highly flexible due to the LbL fabrication technique. Several substances have been encapsulated into PEM particles and functionalizing them differently in the process. Encapsulation of fluorescent substances that changes intensity with surrounding pH conditions passes the pH sensor characteristics to the PEM particles. Fluorescein-labeled poly(acrylic acid) encapsulated within PEM microcapsules and $CaCO_3$ PEM microparticles displayed pH sensor response from pH 3 to 8 [64]. PEM microcapsules encapsulating fluorescent seminaphtho-rhodafluor-1-dye (SNARF-1) were able to show the dye's inherent unique changes in fluorescence intensities related to the local pH environment (with increasing pH, the fluorescence emission intensity at 580 nm decreases, while the intensity at 640 nm increases). The ratio of the intensities enables absolute pH determinations from pH 6

to 8 [65]. Also, encapsulation of pH-sensitive fluorescent materials allows for tracking of the multifunctional PEM particle within the cell. Intracellular pH can be utilized as a marker, as endolysosomes would be more acidic than the cytoplasm [66].

Chemical drugs have also been successfully integrated into the PEM particles, functionalizing them as drug carriers. Anti-tumor drug doxorubicin [62], anti-cancer drug daunorubicin [67], anti-cancer curcumin [68] and gentamicin molecules used as a model drug [69] were loaded into pre-formed PEM microcapsules. Anti-inflammatory drug ibuprofen which has low solubility in low pH solutions but is soluble in higher pH solutions, allowed ibuprofen crystals to be coated LbL and then dissolved to form PEM microcapsules encapsulated with ibuprofen [70]. Lipid-based drugs have also been loaded in PEM microcapsules [71].

Most importantly, biological drugs such as enzymes [72, 73], proteins [45, 74-76] including therapeutic protein like insulin [77], and deoxyribonucleic acid (DNA) [36, 78-80] have been encapsulated in PEM particles. Biological substances are prone to degradation and PEM particles offers protection from substances that can degrade the biological drug. Furthermore, encapsulation in PEM particles present other advantages as a non-viral drug carrier system such as controlled dosage and release through the regulation of the amount of drug and rate of drug release can be achieved by changing the number of layers of the polyelectrolyte multilayer. Additionally, the possibility of additional customizable functionalities can be included to the PEM particles, resulting in multifunctional systems such as DNA carriers with pH sensoring abilities [81, 82].

2.3 Cellular interaction with PEM particles

Although LbL-fabricated biocompatible particles are extensively researched on, less has been explored for its interaction with cells. Several groups have showed the cellular uptake of PEM particles and capsules and their intracellular delivery of specific drugs, including in various cancer cells [83-87], HEK293T cells [66], bone-marrow derived dendritic cells [44], differentiated macrophage-like U937 cells [88], mouse embryonic fibroblasts NIH 3T3 [89], etc. However, few had studied the uptake mechanism and cellular processing of PEM particles inside the cell including its degradation within the cell, location of the particle and release of encapsulated material in the cell, and its effects on the cellular activities; especially for sub-micron sized PEM particles. These factors will be essential in the development of PEM particles as drug carriers. One of the more in depth study of cellular interaction of PEM microparticles was reported by Javier et al. within NIH 3T3 fibroblasts and MCF7 cells. The authors mentioned that PEM microparticles with intact template cores do not deform while PEM microcapsules may deform when incorporated into cells, but there is no uncontrolled release of the cargo during the process. Although the PEM microparticles/capsules were never located in the nucleus, the final location of the PEM microparticles/capsules was still inconclusive [89]. Also, Rathmann et al. studied the processing of PEM microparticles with polymorphonuclear leukocytes (PMN). PEM microparticles between 3 μm and 5 μm showed the high and faster interaction rates with PMNs, instead of those with 1 μm diameter [90]. This highlights that size of the PEM particles as well as the interaction times of the cells with the particles affect uptake rate of the particles.

There are also few *in-vivo* studies of the PEM particles and capsules. De Koker et al. demonstrated *in-vivo* uptake and degradation of PEM microcapsules when they were injected subcutaneously in mice. As for biocompatibility, moderate immune reaction similar to tissue reaction for other types of biodegradable microspheres was observed [44]. Han et al. presented *in-vivo* drug delivery mediated by PEM microcapsules by the injection of biocompatible microcapsules loaded with anti-cancer drug daunorubicin at the tumor site in mice, which showed better inhibition of tumor growth than with the free drug [91]. This proposes the possibility of PEM particles and capsules applications in the field of drug delivery.

CHAPTER 3
Research methodology

3.1 Materials

Hydroxyapatite (HA) nanoparticles (dispersion, 10 wt % in H_20, < 200 nm), calcium chloride ($CaCl_2$), sodium carbonate (Na_2CO_3), poly-L-arginine hydrochloride (ARG) (MW > 70,000), protamine sulfate sodium salt from herring (PRM), dimethyl sulfoxide (DMSO), rhodamine isothiocyanate (RITC), Sephadex G25 chromatography gel, trypan blue and thiazolyl blue tetrazolium bromide (MTT) were purchased from Sigma-Aldrich, Singapore. ~3 μm silica particles (2.76 μm ± 0.15 μm, 50 mg/ml) were from microparticles GmbH. Dextran sulfate sodium salt (DXS) (MW 36,000 – 50,000) was from MP Biomedicals LLC. siGLO green transfection indicator was obtained from Dharmacon, Thermo Scientific. Plasmid DNA pEGFP-C1 and pDsRed were purchased from Clontech. SPARC siRNA (Sense Seq 5' AAC AAG ACC UUC GAC UCU UCC 3') was acquired from Biorev. Nucleic acid labeling kit was from Mirus. Lysotracker Red DND-99 and CellMask Orange plasma membrane stain were from Invitrogen. FibroGRO human foreskin fibroblasts were from Millipore. Human tenon fibroblasts (HTF) were acquired from Singapore Eye Research Institute (SERI). HEK293T/17 cells were obtained from ATCC. DMEM high glucose with L-glutamine, Dulbecco's PBS without

calcium and magnesium, trypsin-EDTA, penicillin-streptomycin, and fetal bovine serum (FBS) "gold" were from PAA laboratories.

3.2 Fluorescent labeling of polyelectroytes

RITC labelling of PRM, described in [36], was initiated in 0.1M carbonate buffer (pH 8.5). RITC dissolved in a methanol solution was subsequently added drop wise. The solution was protected from light during continuous stirring for 2 days and free RITC was removed via gel chromatography using sephadex 25 G. The resultant RITC-PRM solution was collected and lyophilized.

Labelling of ARG with RITC was performed as detailed in [44]. Briefly, ARG and RITC was dissolved in 0.1 M borate buffer and constantly stirred for 1 day, protected from light. The residual RITC was removed via dialysis with Millipore water for several days with occasional change of Millipore water. The resultant RITC-ARG solution was aliquoted and lyophilized.

3.3 PEM nanoparticle fabrication

HA nanoparticles were washed twice with 0.2 μm filtered Millipore water through centrifugation. Ultrasonication and vortex mixing of the particle suspension were executed when needed to thoroughly disperse the nanoparticles. The polyelectrolytes were dissolved in 0.1 M sodium chloride (NaCl) solution to give a concentration of 3 mg/ml for PRM/DXS layer pair and 0.5 mg/ml for ARG/DXS layer pair. The coating process was achieved by rapid and uniform mixing of 1 mg of HA nanoparticles into 1 ml of the respective polyelectrolyte solution. To allow for the coating of the polyelectrolyte layer the particle suspension was incubated for 10 minutes under gentle shaking. Subsequent washings were performed with 0.1M NaCl to remove excess polyelectrolytes

before incubation with the next polyelectrolyte solution. The coating steps were repeated until a polyelectrolyte multilayer (e.g. $[ARG|DXS]_2|ARG$) is formed on the nanoparticles. When coating with fluorescent labeled polyelectrolytes, the particle suspension was protected from light during the incubation steps.

3.4 PEM microparticle/capsule fabrication

Silica particles of size ~3 μm were washed twice with 0.2 μm filtered Millipore water before coating. While commercially available silica particles offer a convenient and standard template for PEM particle fabrication, self-fabricated calcium carbonate ($CaCO_3$) particles present the advantage of encapsulation within the core as well as dissolution to form PEM microcapsules. Several journals [45, 76, 92] had exploited a simple method to obtain uniformly-size $CaCO_3$ microparticles, which was through the precipitation of equal volumes of 0.33 M calcium chloride ($CaCl_2$) and sodium carbonate (Na_2CO_3). This was executed under rapid continuous vortex mixing for 3 minutes was left to rest for 1 minute to form microparticles. The particles were washed 4 times with Millipore water to remove unused reactants before coating of the polyelectrolytes. To fabricated PEM microparticles, similar fabrication steps for the adsorption of polyelectrolytes on PEM nanoparticles were used.

To form PEM microcapsules, the coated PEM microparticles were subjected to 0.2 M EDTA, pH 7 [65, 92]. The particle suspension was uniformly mixed using the vortex and incubated in the dark for 10 minutes. Subsequent centrifugation washes with 0.1 M NaCl were performed to achieve PEM microcapsules. After core dissolution, a small amount of the PEM microcapsules were checked under the microscope each time, which appeared as almost transparent capsules instead of solid $CaCO_3$ PEM particles.

3.5 Encapsulation in PEM particles

Plasmid DNA was stored in Tris-EDTA (TE) buffer (1 µg/µl) and siGLO dissolved in siRNA buffer (100 µM) according to manufacturer's instructions stored at -20 ^{o}C were used for loading in the particles. Fluorescent labeled nucleic acids were achieved using the nucleic acid labeling kit according to manufacturer's protocol. Briefly, the fluorescent dye was added to the nucleic acid diluted in buffer and incubated at 37 ^{o}C for 1 hour. Residual dye was removed using G 50 microspin purification column provided in the kit.

For layer encapsulation of negatively charged nucleic acids, PEM particles with a positively-charged surface layer were utilized. The nucleic acids were diluted with 0.1 M NaCl and the PEM particles were incubated in the nucleic acid solution for at least 30 minutes under gentle shaking at 4 ^{o}C. An example of the coating configurations for layer encapsulation is ARG|DXS|ARG|nucleic acid|ARG. Subsequent washes with 0.1 M NaCl were executed prior to absorption of the next positively-charged layer.

Core encapsulation of nucleic acids was achieved in $CaCO_3$ particles. The nucleic acids were added to $CaCl_2$ solution and uniformly mixed before the addition of Na_2CO_3. Subsequent coating as well as dissolution steps as detailed earlier were performed to fabricate core-loaded PEM microparticles/capsules.

Once loaded with nucleic acids, the PEM particles were constantly stored on ice or at 4 ^{o}C. PEM particles loaded with fluorescent labeled nucleic acids were also kept away from direct light. Supernatants before and after the nucleic acid loading step were collected for absorbance measurements.

3.6 Cell culture

FibroGRO, HTF and HEK293T cells were cultured in a complete medium of DMEM with 10 % FBS, 1X penicillin streptomycin and incubated at 37 ^{o}C, 5 % CO_2. Cells were detached using 1X trypsin-EDTA, and passaged at ratios of 1:2 to 1:4 for FibroGRO and HTF cells, and 1:10 for HEK293T cells. HTF cells were cultured to a maximum of 6 passages.

3.7 Zeta potential

A charged particle surface would distribute the surrounding ions in the solution into an electrical double layer. The zeta potential is the potential at the slipping plane. To measure the zeta potential, an electric field is employed across the particle dispersion causing the particles to move toward the oppositely-electrode with a certain velocity. Laser Doppler anemometry is utilized to measure the particle velocity, where phase shift of the laser initiated by the moving particles is recorded as particle mobility. Using Smoluvhowski or Huckel theories, the zeta potential is calculated from the particle mobility.

In this thesis, examination of the zeta potential of the particles facilitated the study of polyelectrolyte layer growth on the template cores. If the particle was successfully coated with a positively charged polyelectrolyte, one would expect its surface charge and zeta potential to be positive. Hence, the zeta potential of the particle could demonstrate if the charged polyelectrolyte was successfully coated on the PEM particles. Examination of the zeta potential of particles after each layer adsorption enabled the analysis of the multilayer growth of the PEM particles.

After absorption of the specific layer, the surface charge of the PEM particles was examined by fully suspending the PEM nanoparticles in 0.2 μM filtered 0.01 M NaCl and measured with Zetasizer (Malvern) immediately. A total of 3 readings were collected for each sample, and experiments were repeated at least 3 times to obtain mean zeta potentials and standard deviations.

3.8 Scanning electron microscopy (SEM)

The advantage of using SEM as compared to traditional transmission microscopy is its high resolution. This is made possible as SEM utilizes an electron optical system, consisting of an electron gun, condenser lens and objective lens, to produce a small electron probe to scan the sample. When the electron beam hits the sample, various electromagnetic waves and electrons are emitted. The secondary electrons emitted from the sample are detected by the secondary electron detector, and its output signal is subsequently amplified and used to produce the SEM image. This enables morphological observation of the sample at high magnification.

JEOL JSM-6390 LA Analytical Scanning Electron Microscope enabled the examination of the size and morphologies of the PEM microparticles/capsules. Silicon chips were treated hydrochloric acid and washed with Millipore water to achieve hydrophilic surfaces. The PEM particles were re-suspended in Millipore water and a drop of the suspension was carefully placed on the silicon chips. The chips were placed in the oven until completely dried. The samples were sputtered with platinum before analysis with SEM.

3.9 Transmission and fluorescence microscopy

An Olympus IX71 inverted microscope was utilized to capture transmission light and fluorescence pictures of PEM particles and cells, using 20x objective lens. The fluorescence system (U-LH100HG, Manual/motorized Reflected Fluorescence System, Fluorescence Mirror Unit U-MWB2, Excitation wavelength 490 nm) allowed fluorescent images to be recorded. Images from the microscope were acquired using a CCD camera DP30BW with DP Controller software and analyzed using DP Manager.

3.10 Nucleic acid quantification

The NanoDrop 1000 spectrophotometer allowed for UV/VIS spectrophotometry of small sample amounts (as little as 1 μl), which was advantageous in measuring samples without dilution. The sample is directly pipetted on to the pedestal of the microspectrophotometer, eliminating traditional need for cuvettes. The sample is held by surface tension in a vertical orientation between the pedestal and arm, and the path length of 1mm and 0.2mm are used during each measurement. Using fiber optic technology, the light from a xenon flash lamp is passed through the sample and the detected light is analyzed by a liner CCD array.

Specifically for nucleic acids, the absorbance was measured at 260 nm and 280 nm wavelengths. The 260/280 ratio indicated the purity of the sample, with DNA having a ratio of about 1.8 and RNA of about 2.0 [93]. The nucleic acid concentrations of the solutions were determined from the absorbance at 260 nm using Beer's Law. The extinction coefficients used were 50 L mol^{-1} cm^{-1} for DNA and 40 L mol^{-1} cm^{-1} for RNA.

Solutions before and after nucleic acid encapsulation, either by core particle precipitation or coated as layer, as well as following washing steps supernatants were analyzed. The

amount of solution was also recorded to calculate the total amount of nucleic acid encapsulated. Experiments were repeated at least 3 times to obtain mean absorbance measurements and their standard deviations.

3.11 Flow cytometry

Flow cytometry enables the study of several properties of each individual particle or cell as it flows thorough the laser beam path. This is accomplished by injecting the sample into a running stream of sheath fluid, hence allowing the particle or cell to pass through the laser individually. When a particle or cell intercepts the laser, it scatters light in all directions. The scattered light in the forward direction (in line with the laser) is collected by the forward scatter (FSC) detector, while side scattered light is focused through a lens system and detected by the side scatter (SSC) detector.

Besides gathering information about its size (FSC channel) and granularity (SSC channel), the fluorescence intensity of the particle or cell can also be measured. As the fluorescent particle or cell passes through the laser, it is excited in the process. The emitted light is collected and subsequently split using filters and dichroic mirrors to direct into appropriate fluorescence detectors.

FACSCalibur (BD Biosciences) possessed laser excitation wavelength of 488 nm for siGLO Green and FITC detection in FL1-H channel and FL2-H for RITC detection, while the 635 nm wavelength laser was for Cy5 detection in FL4 channel. 10^4 events were recorded and analyzed using WinMDI software. The difference in size (FSC channel) and granularity (SSC channel) allowed for the differentiation of the particles and the cells.

Fluorescent nucleic acid loaded PEM particles constantly kept away from light and on ice until ready to be analyzed. The particles were thoroughly mixed and diluted with 0.22 µm filtered 0.1 M NaCl before flow cytometry analysis. Experiments were executed 3 times and one representative data was presented.

For flow cytometry analysis of cell-particle interaction, $2x10^5$ FibroGRO cells per well were first seeded overnight in 6 well plates. The medium was changed to reduced serum medium before addition of PEM particles. Following 4 hours incubation, the cells were detached by incubation in trypsin-EDTA for 5mins at 37 ^oC and mixed gently using a pipette to achieve single cells before addition of twice the volume of complete medium. Complete removal of the medium was achieved by centrifugation at 300 rcf and subsequent washes with PBS. The cells were carefully re-suspended in filtered PBS and constantly stored on ice and in the dark until ready for flow cytometry. Flow cytometry of the cells was executed immediately, and then followed by addition of trypan blue to the samples to quench the membrane-bound particles and measured again. Trypan blue quenches the fluorescence signal from external and memebrane –bound particles as detailed in [82]. Each experiment is repeated 3 times and one representative data was presented.

3.12 Confocal laser scanning microscopy (CLSM)

The advantages of CLSM lie in its ability to capture sharp images and its optical sectioning capability. Coupled with fluorochrome combinations, a great deal of information can be retrieved from biological samples using CLSM. The microscope uses a laser light source passed into the scanning head through a fiber optic. This laser source is focused into a parallel beam using a collimator and then reflected by a principal

dichroic beam splitter. Subsequently, the microscope objective focuses the laser into the focal plane to excite the fluorescent structures within the plane, and hence a sharp image of the plane can be created. A pinhole diaphragm blocks light emitted from weakly activated fluorescent structures above and below the focal plane, thus only signal from the focal plane enters the detector. Three dimensional pictures can be also be obtained by means of compiling several two dimensional optical slices at various Z-planes

CLSM allowed the cross-section of the cells and microparticles to be observed, which is specifically beneficial for investigating intra-cellular spaces. $4x10^3$ cells were seeded in 8 well glass-bottom chamber slide (Nunc) overnight in DMEM with 10 % FBS. The medium was changed to reduced serum medium before addition of siGLO-loaded PEM nanoparticles. After 4 hours incubation, the medium was changed back to DMEM with 10 % FBS and kept in the incubator until ready for analysis. After the specific incubation time, the medium was carefully replaced with PBS before CLSM. For tracking of acidic organelles within the cells, Lysotracker Red dye was added according to manufacturer's instructions. Confocal micrographs were captured using Zeiss LSM 510, with Ar/Kr or He/Ne laser and 40X/1.3 OIL Plan-Neofluar. Zeiss image browser software was utilized to analyze the images. Each experiment was repeated three times and representative images were presented.

3.13 xCelligence real-time cell proliferation assay

The xCELLigence system (Roche) provides real-time monitoring of cells by measuring electrical impedance across micro-electrodes integrated on the bottom of tissue culture plates [94]. Additionally, using electrical impedance the system is able to provide information about the cells without the use of labels. The bottom of the tissue culture well

is covered with gold electrodes and the presence of cells on the electrode changes the electrode impedance. Electrode impedance increases when a larger number of cells attach as well as with increased cell spreading or adhesion. Hence, the Cell Index (CI) (a dimensionless parameter which reflects the cell status relative to the change in measured electrical impedance) gives information about cell viability, adhesion and morphology.

In this thesis, the xCELLigence system enabled continuous examination of the cells when incubated with PEM particles for a period of about 7 days. This allowed the cytotoxicity of the PEM particles to be studied as well as the effects of exposure to increasing amounts of PEM particles.

The 96-well electrode plate was first blanked with 100 µl of complete medium and subsequently $4x10^3$ cells were placed in each well. PEM particles at various amounts were added to the cells in triplicates. The plate was left at room temperature for 30 minutes before carefully placing into the xCELLigence instrument. Cell growth was continuously monitored for about 7 days, with 25 sweeps of 5 minutes intervals, followed by 24 sweeps of 15 minutes interval and subsequent measurements at 1 hour intervals. The cell indexes were plotted against time interval in Origin software. Each sample was loaded in triplicates, and the mean cell index and standard deviations were presented.

3.14 MTT cell proliferation assay

Thiazolyl blue tetrazolium bromide (MTT) is commonly used as a colorimetric cell proliferation assay, as mitochondrial dehydrogenases of live cells convert the yellow water soluble MTT to purple formazan crystals. The crystals are then dissolved in fixed amounts of solvent and quantified by spectrophotometric means. Since reduction of MTT

is only possible in metabolically active cells, the amount of formazan produced relates to cell proliferation [95, 96].

MTT assay was used to examine cell viability when the cells were exposed to various amounts of PEM particles. $4x10^3$ cells per well were seeded in 96-well plates overnight in complete medium. Various amounts of particles in the same volume were added to the cells in triplicates and carefully placed in the incubator for specific incubation times.

To perform the MTT assay, 5 mg/ml of MTT in PBS was added at 10 % of total culture volume and incubated at 37 ^oC for 3 hours. Subsequently, the solution was carefully removed from the wells and 100 µl of DMSO was added to each well. The plate was shaken gently for 1 hour or more to allow the crystals to dissolve while remaining constantly covered and kept away from direct light. Then, absorbance of each well was measured at a wavelength of 595 nm (Victor3 multilabel plate reader, Perkin Elmer). Experiments were repeated 3 times and the means and standard deviations were presented. The values were normalized with the control cells and plotted as a percentage of the control cells' viability using Microsoft Office Excel 2007 software.

CHAPTER 4
Fabrication of PEM particles

4.1 Introduction

Biodegradable PEM particles were assembled using the LbL technique on micron and nano sized particles. Commercially available 200 nm HA nanoparticles as well as fabricated $CaCO_3$ particles were the template cores for polyelectrolyte adsorption. Polyelectrolyte pairs including PRM/DXS and ARG/DXS and their fluorescent labeled derivatives were coated LbL on the particles. Samples were collected after coating of specific layers to analyze the LbL layer adsorption on the particles.

By means of zeta potential measurements the LbL coating of alternatively charged polyelectrolytes onto the template particles was determined. Additional confocal microscopy figures and flow cytometry data of the PEM particles coated with fluorescent labeled polymers further supported the successful fabrication of a multilayer on the PEM particles. Furthermore, $CaCO_3$ particles coated with ARG/DXS layers were exposed to dissolution conditions to form microcapsules.

4.2 Results

4.2.1 LbL assembly on HA nanoparticles

HA nanoparticles were LbL coated as detailed in Chapter 3. The HA particles coated with PRM/DXS or ARG/DXS layers were analyzed for their surface charge after the

coating of each polyelectrolyte layer. The zeta potentials of each layer are plotted in Figure 4.1a and Figure 4.1b for PRM/DXS and ARG/DXS layers, respectively. Both layer pairs showed alternating zeta potentials, but ARG/DXS layers displaying larger differences between the positive and negative in zeta potentials than the PRM/DXS layers.

ARG/DXS layer adsorption on HA nanoparticles was further studied with fluorescent labeled ARG. ARG was tagged with RITC according the protocol detailed in Chapter 3, and coated on the template in place of the ARG layers. Samples were collected after coating of each ARG-RITC layer and analyzed by flow cytometry. Figure 4.2a and Figure 4.2b compares the RITC intensities (FL2-H axis) of PEM particles coated with 1, 2 and 3 layers ARG-RITC in the odd numbered layers, with blank HA particles as control. Figure 4.2a clearly shows a right shift of the graphs with increasing number of ARG-RITC layers. The Gmean of the RITC histograms in Figure 4.2a of PEM nanoparticles with different number ARG-RITC layer(s) are as follows: $Gmean_{0layer} = 1$, $Gmean_{1layer} = 22$, $Gmean_{2layers} = 59$, $Gmean_{3layers} = 104$. The above Gmeans were determined and plotted in Figure 4.2b. A linear increase in the RITC intensity is observed with increasing number of ARG-RITC layers.

Confocal micrographs of the PEM nanoparticles coated with ARG-RITC are displayed later in Chapter 4.3.

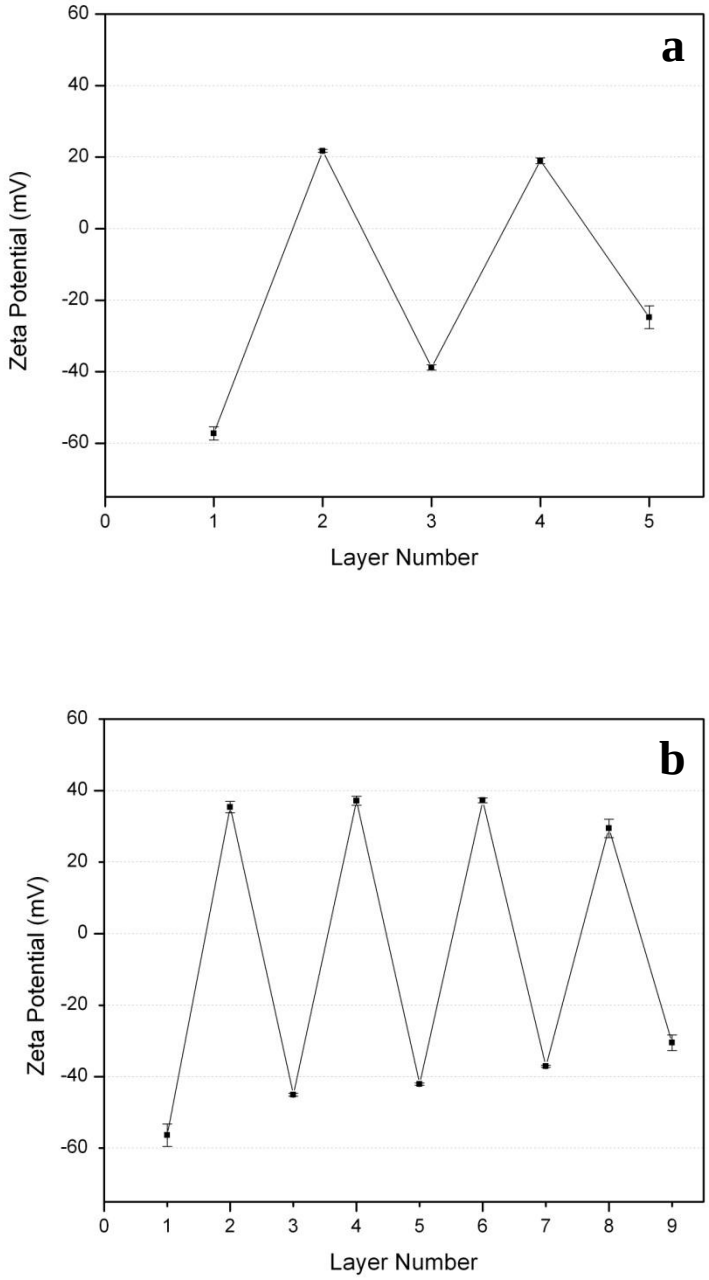

Figure 4.1 Zeta potentials of HA nanoparticles LbL coated with PRM/DXS and ARG/DXS layers. (a) Zeta potentials of particles were coated with negatively charged DXS as the first layer, followed by positively charged PRM as the second layer and repeated until layer 5 (HA|DXS|PRM|DXS|PRM|DXS). (b) Zeta potentials of PEM particles alternately coated with ARG/DXS layers (DXS|[ARG|DXS]$_4$). Shown are means and standard deviations of three independent measurements.

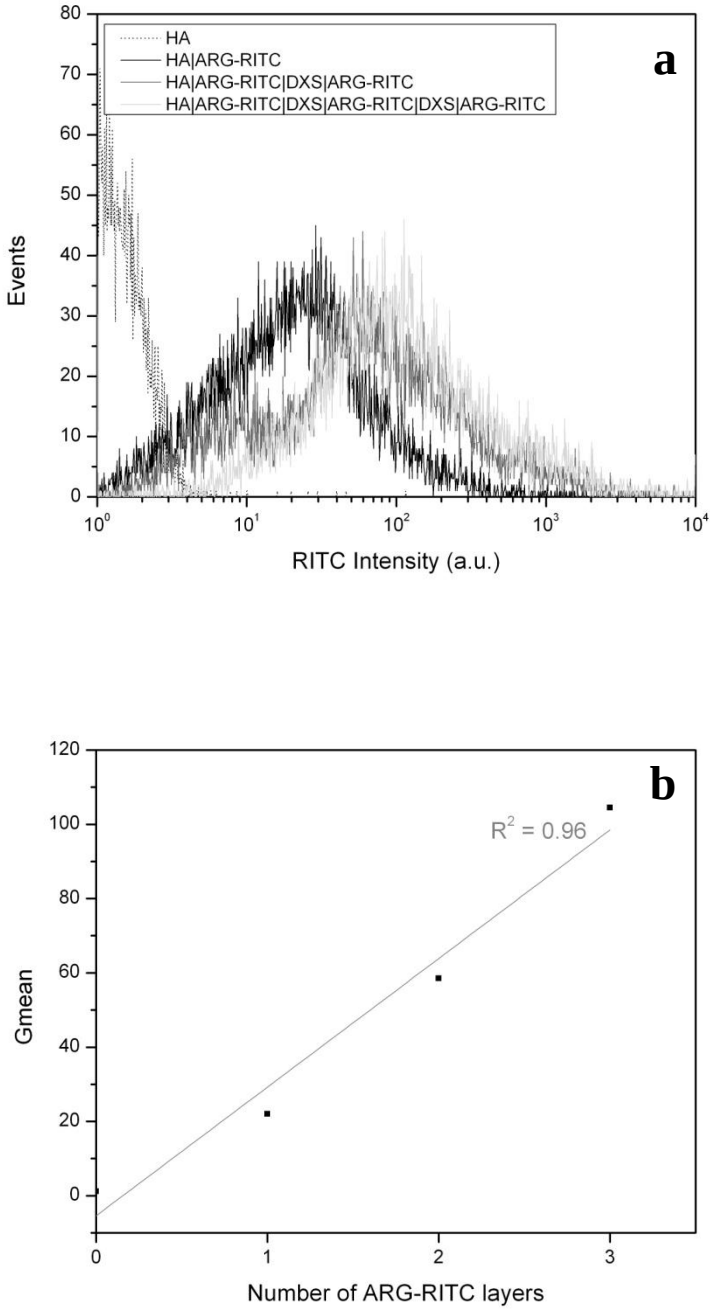

Figure 4.2 RITC fluorescent intensities of HA nanoparticles with ARG-RITC in different layers. (a) RITC intensity histograms of HA nanoparticles coated with 0 (dotted line), 1 (black line), 2 (grey) and 3 (light grey) layers of ARG-RITC. One representative histogram of three independent measurements is shown. (b) Gmean determined from the histograms in (a) showed a linear increase in RITC intensity with coating of each ARG-RITC layer.

4.2.2 LbL assembly on CaCO3 particles

First, $CaCO_3$ particles were fabricated as detailed in Chapter 3. The transmission light micrographs of the fabricated $CaCO_3$ particles in Figure 4.3a showed that the particles formed were spherical and uniform in size. The size was comparable to commercially available $CaCO_3$ particles displayed in Figure 4.3b. The SEM micrograph in Figure 4.3c confirmed the fabricated $CaCO_3$ particles to be around 3-5 μm, and spherical with a rough surface morphology.

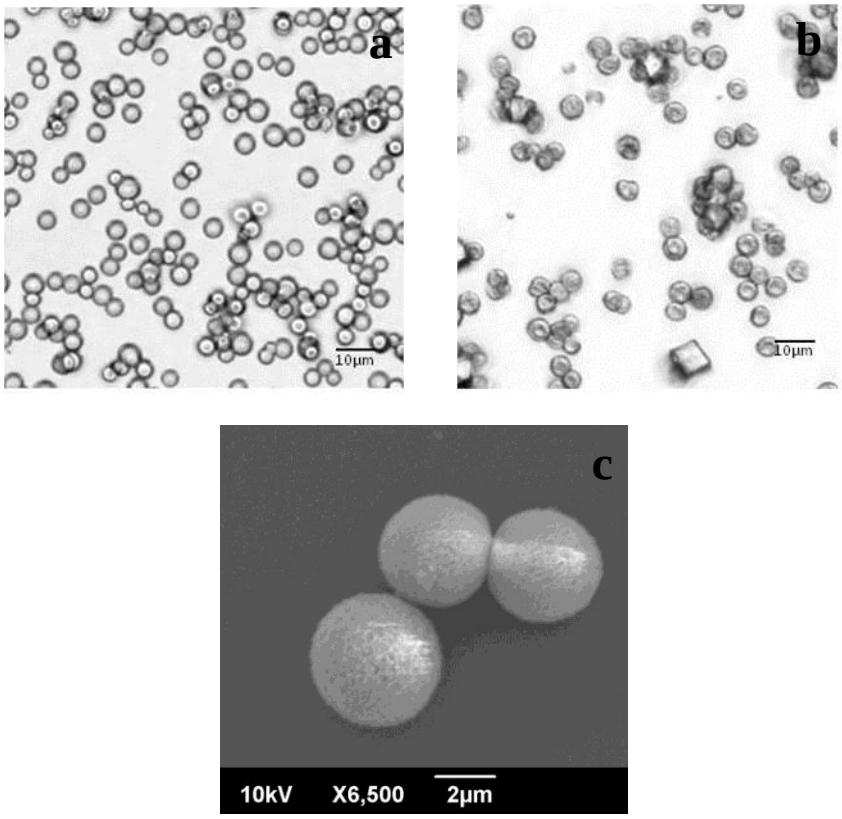

Figure 4.3 Transmission light and SEM micrographs of CaCO3 particles. (a) Transmission light pictures of fabricated $CaCO_3$ particles. (b) Commercially available 5 μm $CaCO_3$ particles. (c) SEM micrograph of fabricated $CaCO_3$ particles. Shown are representative images of three independent measurements.

Similarly to the LbL coating procedure, the fabricated $CaCO_3$ particles were coated with PRM/DXS and ARG/DXS layers. Figure 4.4a and Figure 4.4b display the alternating zeta potentials of the particles after each layer coating for PRM/DXS and ARG/DXS layers respectively. While the DXS layers appear to have similar zeta potentials, ARG layers were more positively charged than PRM layers.

ARG-RITC/DXS layers were adsorbed to investigate the multilayer buildup on $CaCO_3$ particles, where $CaCO_3$ particles with 0, 1, 2 and 3 layers of ARG-RITC were analyzed with flow cytometry. Likewise to the data for HA nanoparticles, an increase in the number of layers of ARG-RITC corresponded with an increase in RITC intensity. The definite RITC intensity increase is illustrated in Figure 4.5a due to the right shift of the RITC fluorescence intensity in the histogram with increasing number of ARG-RITC layers. Gmeans of RITC fluorescence intensity of PEM particles with different number ARG-RITC layer(s) are as follows: $Gmean_{0layer} = 1$, $Gmean_{1layer} = 178$, $Gmean_{2layers} = 790$, $Gmean_{3layers} = 1280$. The Gmeans of the histograms from Figure 4.5a are plotted in Figure 4.5b showing a linear increase in the RITC intensity with more ARG-RITC layers.

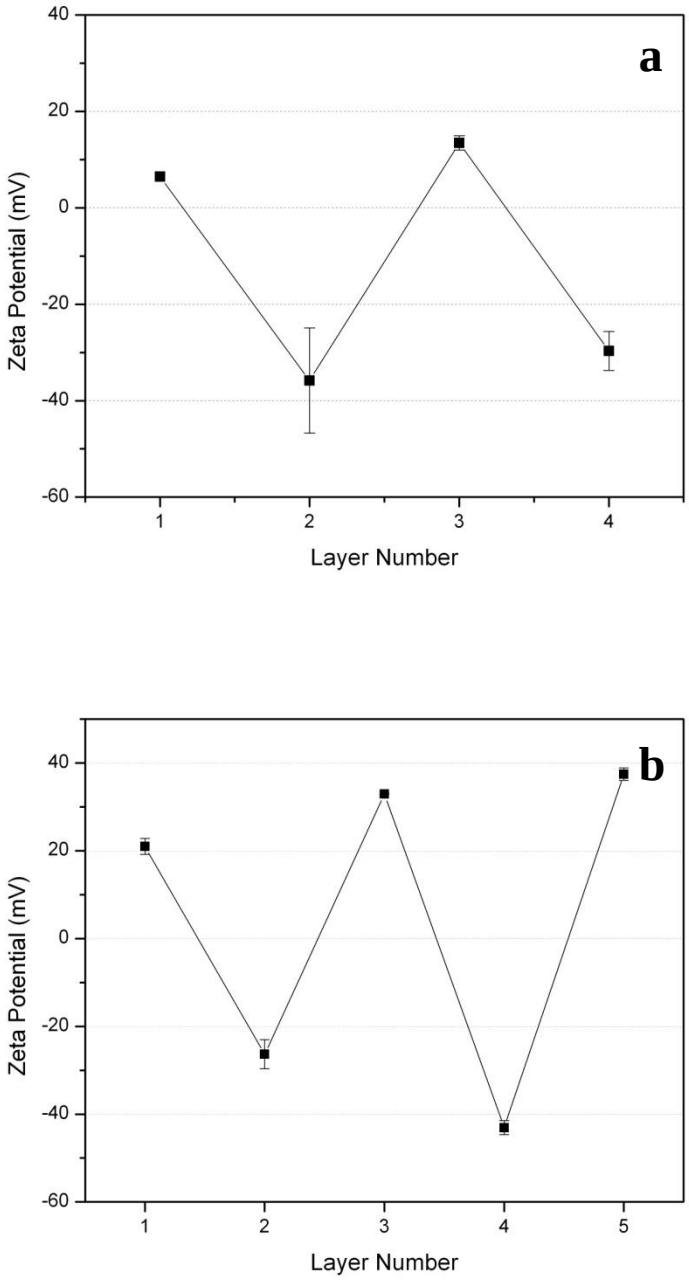

Figure 4.4 Zeta potentials of CaCO3 particles coated with PRM/DXS or ARG/DXS layers. Positively charged (a) PRM or (b) ARG was coated in the odd numbered layers, while DXS was coated in the even number layers. Means and standard deviations of three independent measurements are shown.

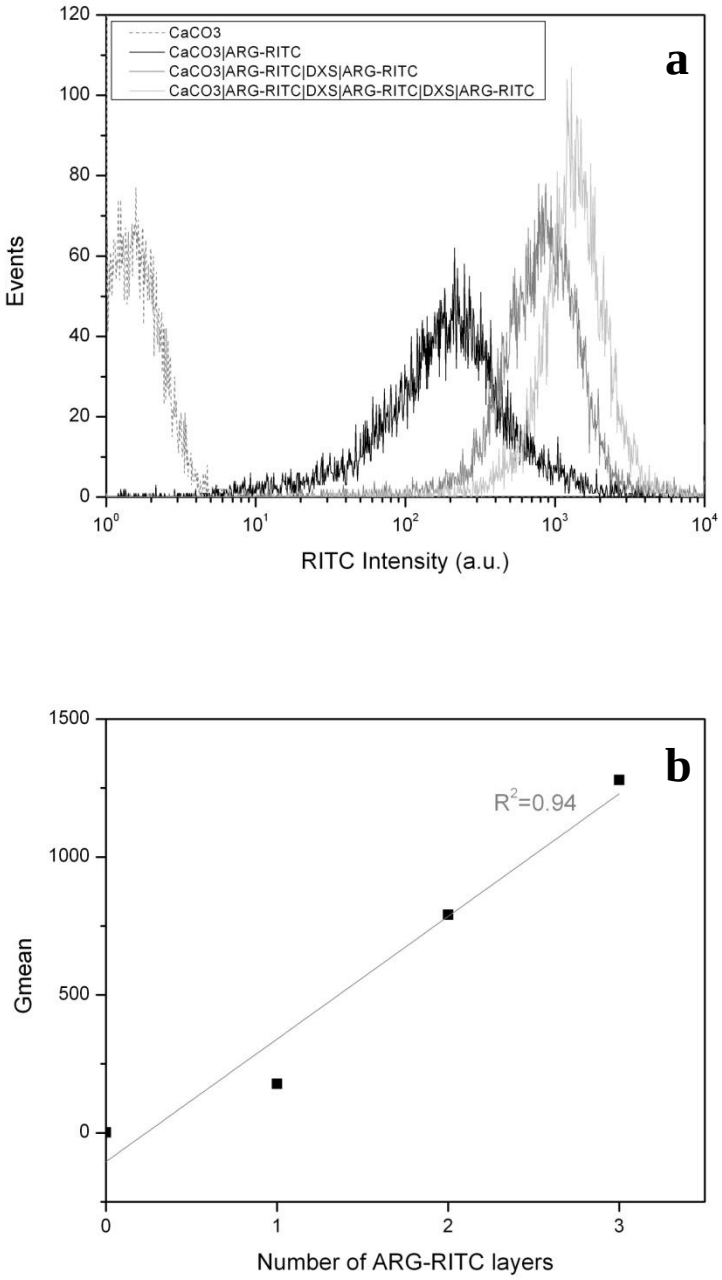

Figure 4.5 RITC fluorescent intensities of $CaCO_3$ microparticles with ARG-RITC layers. (a) RITC intensity histograms of $CaCO_3$ microparticles coated with 0, 1, 2 and 3 layers of ARG-RITC. Shown is one representative histogram of three independent measurements. (b) Gmean determined from the histograms in (a) showed a linear increase in RITC intensity with coating of each ARG-RITC layer.

4.2.3 Fabrication of microcapsules

$CaCO_3$ particles coated with ARG|[DXS|ARG]$_2$ layers were subjected to dissolution conditions to dissolve the $CaCO_3$ cores. Empty shells of ARG/DXS layers were achieved which were easily identified as the capsules appear as almost transparent rings under the transmission light microscope, as opposed to the solid spheres. Figure 4.6a and Figure 4.6b compares the changes in appearance of the PEM microcapsules and microparticles respectively. A more definite image of the microcapsule formed is the SEM micrograph in Figure 4.6c, showing a deflated capsule, due to the drying conditions required during processing of the samples for SEM imaging. It is evidently different from the $CaCO_3$ spheres pictured in Figure 4.6d which were subjected to the same drying process.

Comparison data obtained by means of flow cytometry before and after core dissolution of PEM microparticles is summarized in Figure 4.7. Figure 4.7a shows particles with only 1 polyelectrolyte layer (ARG-RITC) displayed a drop in RITC intensity after dissolution. This was not the case for particles with 3 (ARG-RITC|DXS|ARG-RITC) and 5 ([ARG-RITC|DXS]$_2$|ARG-RITC)polyelectrolyte layers, where the RITC fluorescence intensity was similar before (light grey graph) and after (black graph) core dissolution, as portrayed in Figure 4.7b and Figure 4.7c.

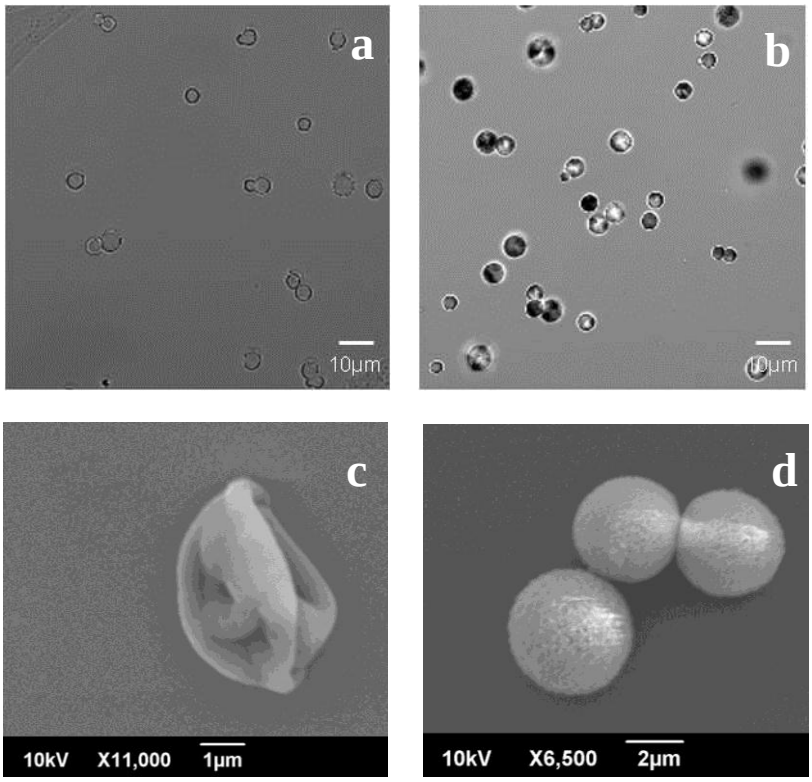

Figure 4.6 Comparison of transmission light and SEM micrographs of PEM microparticles before and after core dissolution (PEM microcapsules). $CaCO_3$ particles LbL coated with ARG|[DXS|ARG]$_2$ layers were exposed to dissolution conditions to remove the particle cores. (a) Hollow shells of the polyelectrolyte multilayer were formed. (b) Filled solid spheres before dissolution. (c) SEM micrograph of a PEM microcapsule, which shrunk after drying to form a deflated structure. (d) SEM micrograph of $CaCO_3$ particles exposed to the same drying process. One representative data of three independent measurements are displayed.

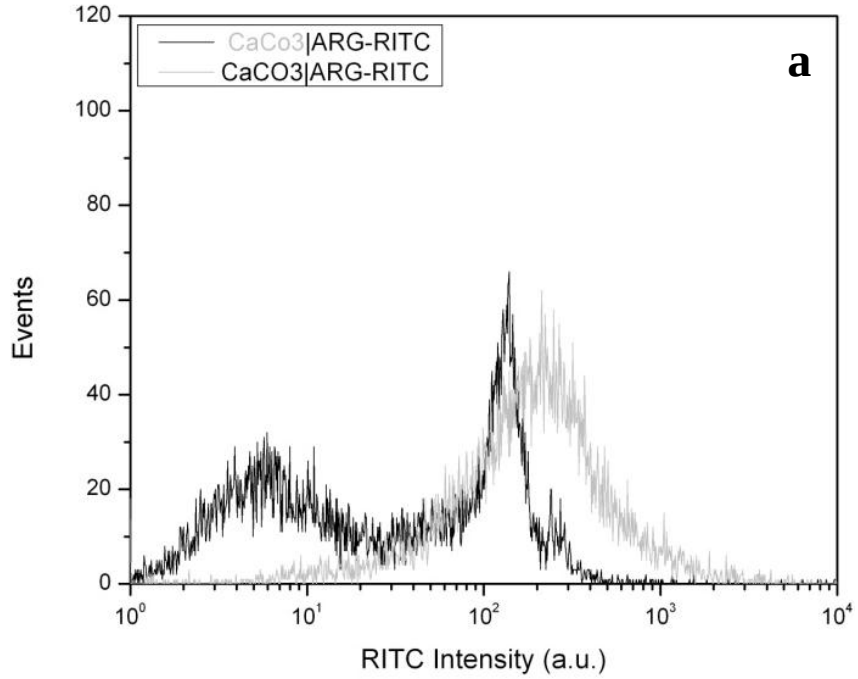
a
CaCo3|ARG-RITC
CaCO3|ARG-RITC
Events
RITC Intensity (a.u.)
0
20
40
60
80
100
120
10^0
10^1
10^2
10^3
10^4

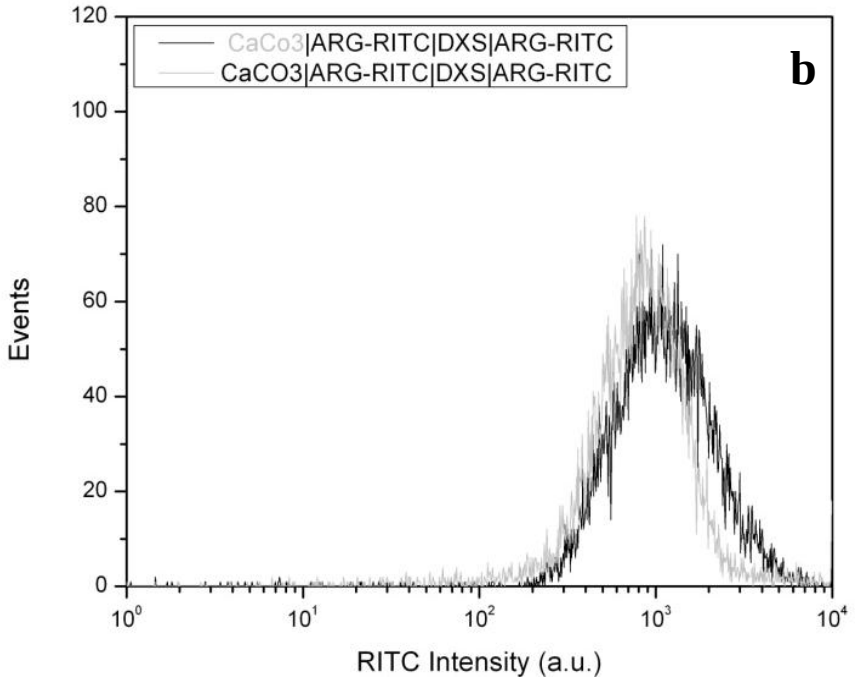
b
CaCo3|ARG-RITC|DXS|ARG-RITC
CaCO3|ARG-RITC|DXS|ARG-RITC
Events
RITC Intensity (a.u.)
0
20
40
60
80
100
120
10^0
10^1
10^2
10^3
10^4

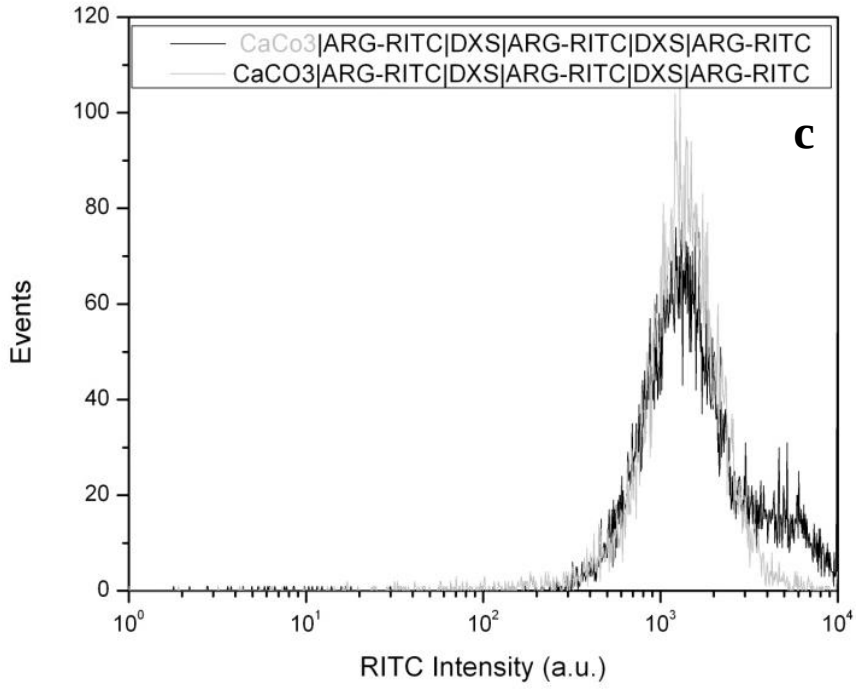

Figure 4.7 RITC intensity histograms of PEM microparticles and -capsules (before and after core dissolution). (a) PEM particles with 1 polyelectrolyte layer, (b) PEM particles with 3 polyelectrolyte layers, and (c) PEM particles with 5 polyelectrolyte layers. Light grey graphs are before core dissolution, black graphs are after core dissolution.

4.3 Discussion

In this chapter we studied the LbL assembly of PRM/DXS and ARG/DXS polyelectrolyte layers on HA nanoparticles and $CaCO_3$ microparticles as well as -capsules. Samples were collected after coating specific layers and analyzed with zetasizer and flow cytometry.

HA nanoparticles (< 200 nm) were used as template for nano LbL carriers. Although LbL coating on HA nanoparticles is not reported, they have the advantage of high absorbability and high binding affinity with a variety of biomolecules and used in a various drug delivery applications such as gene delivery [97], proteins [98] and various drugs [99] due to their excellent biocompatibility [100, 101].

In this work, it was shown that LbL assembly on HA nanoparticles was possible as both polyelectrolyte pairs showed alternating zeta potentials after coating each layer. Particles with outermost layer as positively-charged PRM or ARG layers displayed positive zeta potentials while those with negatively-charged DXS showed negative zeta potentials. ARG/DXS layers displayed larger zeta potential difference alternating between -40 mV and 40 mV, while PRM/DXS layers showed around -40 mV to 20 mV for negative and positive layers respectively.

During fabrication, ARG/DXS coated nanoparticles were easily dispersed when exposed to ultrasonication, and continued to show alternating zeta potentials even up till layer 9. However for PRM/DXS nanoparticles, the particles become increasingly difficult to disperse after layer 5. This is an indication that ARG/DXS nanoparticles are more stable than PRM/DXS nanoparticles, as PRM/DXS nanoparticles tend to aggregate to achieve a more stable configuration. A probable reason is that ARG is more positively charged than PRM, hence the nanoparticles experience larger repulsive forces with particles of like charges. Also, ARG has a much larger molecular weight (>70 kDa), which can cover the coating surface area better than the smaller sized PRM (~4 kDa). A strongly positive charged particle will attract more negatively charged DXS during the subsequent coating step, thus leading to a more stable multilayer fabrication. Confocal micrographs displaying the two different PEM particle populations discussed in the next chapter will further illustrate the aggregation of PRM/DXS nanoparticles.

Besides examining the surface charge of the particles, polyelectrolyte layer buildup can be tracked by coating several layers of fluorescent labeled polymer and investigating the resulting fluorescent intensity of the particles after each fluorescent layer. The linear

increase of RITC intensity with each layer of ARG-RITC proposes that an even layer of ARG-RITC was coated on the nanoparticles each time. It also indicates that the DXS layers were successfully adsorbed as without the negatively charged layer, the subsequent positively charged ARG-RITC will not be coated.

Fabrication of $CaCO_3$ particles of 3-5 μm was achieved using simple bench top techniques. Creating the core particles gave the advantage of enabling encapsulation of materials within the template core, which will be discussed in the next chapter. The fabricated particles were spherical, uniformly sized and were able to be coated with PRM/DXS and ARG/DXS layers. Both layer pairs showed similar alternating zeta potentials as those with HA nanoparticles. This was in correlation with previous research on PRM/DXS layers on $CaCO_3$ microparticles [81] as well as De Koker et al. [44] work on ARG/DXS absorption on $CaCO_3$ microparticles. Coating of polyelectrolytes on microparticles required less dispersion techniques than with nanoparticles, as normally mixing with the vortex or pipette was sufficient to disperse the particles without the need of ultrasonication.

Investigation with ARG-RITC layers also displayed similar linear RITC intensity increase with each ARG-RITC layer coated. More interestingly was the formation of PEM microcapsules from PEM microparticles. Under the transmission light microscope, the solid PEM microparticles appeared as almost transparent rings when exposed to EDTA, indicating the formation of microcapsules. Comparing SEM micrographs in Figure 4.6c (PEM microcapsules) with Figure 4.6d ($CaCO_3$ particles), it further demonstrates the hollow space created by the dissolution of the template core as it

collapsed after being exposed to drying processes used for SEM. The deflated structures of PEM microcapsules under SEM were similar to those reported in [44].

From the comparison of the RITC intensities of PEM particles before and after core dissolution in Figure 4.7, it is clear that the multilayer was still intact for 3 and 5 polyelectrolyte layers as the RITC intensity remained the same. However for $CaCO_3$ particles with only 1 polyelectrolyte layer, in this case the ARG-RITC layer, a drop in fluorescent intensity was recorded after dissolution conditions. It is probable that the one polyelectrolyte layer was not strong enough to uphold the microcapsule configuration. Hence, at least 3 polyelectrolyte layers (ARG|DXS|ARG) were needed to produce PEM microcapsules. This is supported by the work of De Koker et al. as they reported they were able to produce PEM microcapsules using just 1 ARG/DXS bilayer, i.e. 2 polyelectrolyte layers (DXS|ARG) [44]. As for PRM/DXS PEM microcapsules, 5 polyelectrolyte layers were not sufficient to produce microcapsules, as no capsules were observed under transmission light microscope after dissolution. Perhaps many more layers of PRM/DXS were needed to be adsorbed before core dissolution in order to stabilize the microcapsule configuration as Jin et al. successfully fabricated PRM/DXS microcapsules using PSS-doped $CaCO_3$ particles with $[PRM/DXS]_6$ [58]. Hence, ARG/DXS was more favorable in fabrication of PEM microcapsules as they require less polyelectrolyte layers to produce stabilized microcapsules after core dissolution.

4.4 Conclusion

Various types of PEM nanoparticles, microparticles and microcapsules were achieved using the LbL assembly technique. Successive adsorption of PRM/DXS and ARG/DXS layers on HA nanoparticle and $CaCO_3$ microparticle cores was shown by alternating zeta potential measurements. Although both layer pairs can be coated, ARG/DXS layers were more stable than PRM/DXS layers as shown by the larger zeta potential difference. This allowed for coating up to 9 polyelectrolyte layers on HA nanoparticles with easy dispersion and less aggregation. Also for the fabrication of microcapsules, ARG/DXS layer pair was more promising as microcapsules can be formed with as little as 3 polyelectrolyte layers. Hence, ARG/DXS layer pair was chosen for the future experiments for the development of PEM particles as nucleic acid carriers.

CHAPTER 5
Encapsulation in PEM particles

5.1 Introduction

Encapsulation in PEM particles can be achieved either in the core or within the multilayer. The investigations on encapsulation of fluorescent labeled and unlabeled nucleic acids within PEM nanoparticles, microparticles and microcapsules are summarized in this chapter. The fluorescent nucleic acids were either purchased or unlabeled nucleic acids were fluorescently tagged using a nucleic acid labeling kit. This allows the examination of nucleic acid absorption onto the PEM particles using confocal microscopy and flow cytometry. Additionally, unlabeled nucleic acids were encapsulated within PEM particles to investigate the nucleic acid encapsulation efficiency of the particles. Supernatant before and after the nucleic acid coating step was collected and analyzed for absorbance measurements at 260 nm and 280 nm.

5.2 Results

5.2.1 Nucleic acid layer encapsulation in PEM nanoparticles

5.2.1.1 siRNA

Fluorescently labeled siRNA (Cy5-labeled SPARC siRNA or reporter siRNA, siGLO Green) were encapsulated within the PRM/DXS and ARG/DXS layers on HA nanoparticles to investigate siRNA loading on PEM nanoparticles. Both,

HA|PRM|DXS|PRM|Cy5-siRNA|PRM and HA|ARG|DXS|ARG|siGLO|ARG PEM particles, displayed fluorescent signals from the fluorescently labeled siRNA as shown in confocal micrographs of Figure 5.1. PRM/DXS nanoparticles were more aggregated, appearing as bigger clumps than ARG/DXS nanoparticles. ARG/DXS nanoparticles were dispersed and remained their small sizes with few clumps.

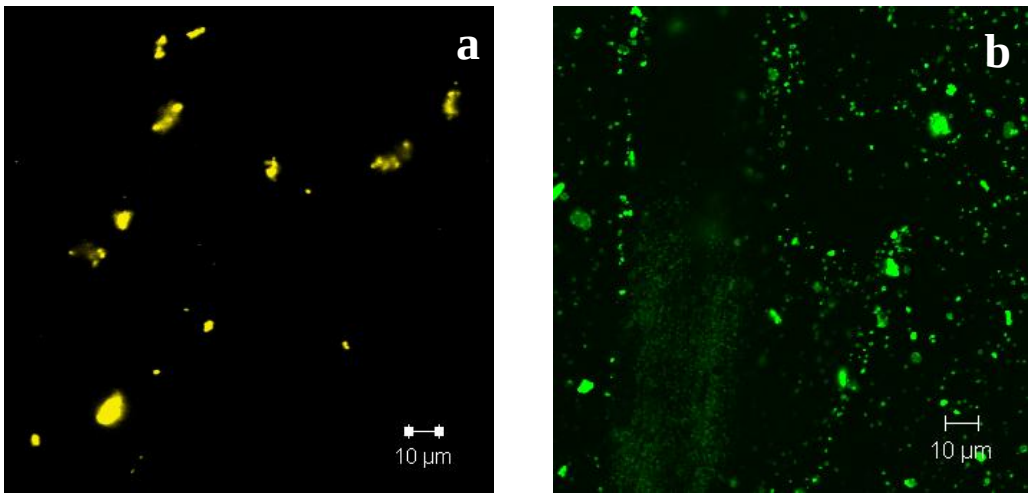

Figure 5.1 Confocal images of siRNA loaded PEM nanoparticles. (a) PRM/DXS nanoparticles encapsulated with Cy5-siRNA. (b) ARG/DXS nanoparticles with siGLO encapsulated in the fifth layer. Shown are representative confocal images of three independent measurements.

Absorbance measurements (260 nm and 280 nm) of the supernatants before and after absorption of the siRNA layer revealed higher encapsulation efficiency of ~95 % for ARG/DXS layers as compared to ~75 % for PRM/DXS layers, for the same amount of PEM nanoparticles and siRNA.

Thus, ARG/DXS nanoparticles were further studied for coating of more siRNA layers. An additional layer of siGLO was loaded, giving the layer configuration

HA|ARG|DXS|ARG|siGLO|ARG|siGLO|ARG. Samples were collected at each layer and the surface charge of the particles was determined by zetasizer. Alternating zeta potentials were observed as shown in Figure 5.2a. The odd numbered layers of ARG generally displayed stable positive zeta potentials of about 40-60 mV, while the even numbered layers of DXS and siGLO normally showed negative zeta potentials. The zeta potential of the DXS coating is stronger negative (about -45 mV) than the siGLO coatings with zeta potentials between -20 and -35 mV. Negligible amount of siGLO was left in the supernatants for 0.5 mg of PEM nanoparticles with 200 pmol of siGLO per layer.

The ARG/DXS PEM nanoparticles coated with 1 and 2 layers of siGLO were analyzed with flow cytometry, together with non-fluorescent control particles. The FITC intensity histograms in Figure 5.2b demonstrates that the PEM nanoparticles which had 1 siGLO layer (black graph, GMean = 203) had higher fluorescence intensity than the control particles (grey graph, Gmean = 1), and 2 layers of siGLO possessed an even higher fluorescence (light grey graph, Gmean = 336).

Furthermore, first results of PEM nanoparticles with the polyelectrolyte pair ARG/siRNA are presented. Here, siRNA completely replaces the negatively charged polymer DXS. Schemes are as follows: $[ARG|siRNA]_3|ARG$. Zeta potential of the particles were examined after absorption of each layer and plotted in Figure 5.3. The odd number layers consisted of ARG, which displayed zeta potentials of about -50 mV. The even number layers were siRNA, which showed a relatively small zeta potential value of about -8 mV for layer 2 but increase to higher values of about -30 mV and -45 mV for layer 3 and 5. From absorbance measurements of supernatants, it was discovered that 0.5 mg HA PEM

nanoparticles can coat 400 pmol of siRNA per layer with negligible amounts of siRNA left in the supernatants for the first and second siRNA layers. The third siRNA layer showed a drop in loading efficiency to about 80 %.

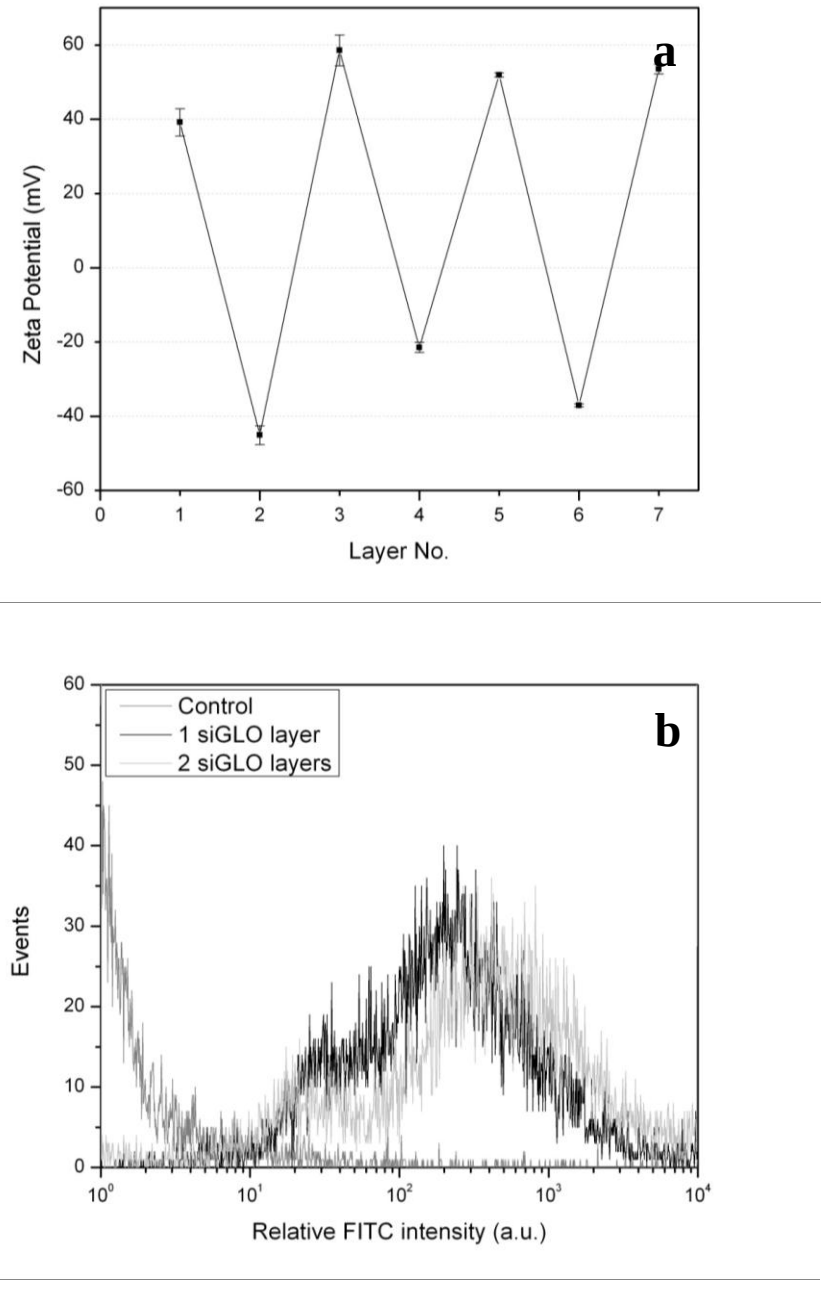

Figure 5.2 Loading of siGLO layers in ARG/DXS PEM nanoparticles. (a) Zeta potential measurements of PEM nanoparticles HA|ARG|DXS|ARG|siGLO|ARG|siGLO|ARG. Means and standard deviations of three independent measurements are shown. (b) FITC

intensity histograms of non-fluorescent control particles (grey), PEM nanoparticles with 1 siGLO layer HA|ARG|DXS|ARG|siGLO|ARG (black), and PEM nanoparticles with 2 siGLO layers HA|ARG|DXS|ARG|siGLO|ARG|siGLO|ARG (light grey). One representative histogram of three independent measurements is shown.

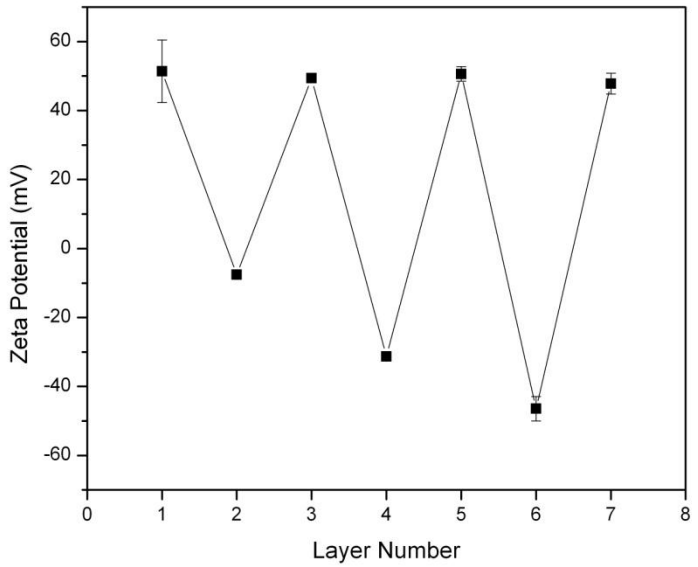

Figure 5.3 Zeta potentials of ARG/siRNA PEM nanoparticles. Odd and even number layers consist of ARG and siRNA respectively. Means and standard deviations of three independent measurements are shown.

5.2.1.2 DNA

Layer encapsulation of plasmid DNA on PEM nanoparticles were investigated by coating ARG|DXS|ARG|DNA|ARG on HA nanoparticles. Samples were collected at each layer and analyzed for their zeta potentials. As pictured in Figure 5.4, the fourth layer which was the coating of DNA reflected an opposite zeta potential from the previous positively

charged ARG layer, with a negative zeta potential of about -40 mV. The subsequent layer of ARG continued the alternating zeta potential trend, with an average reading of 40 mV.

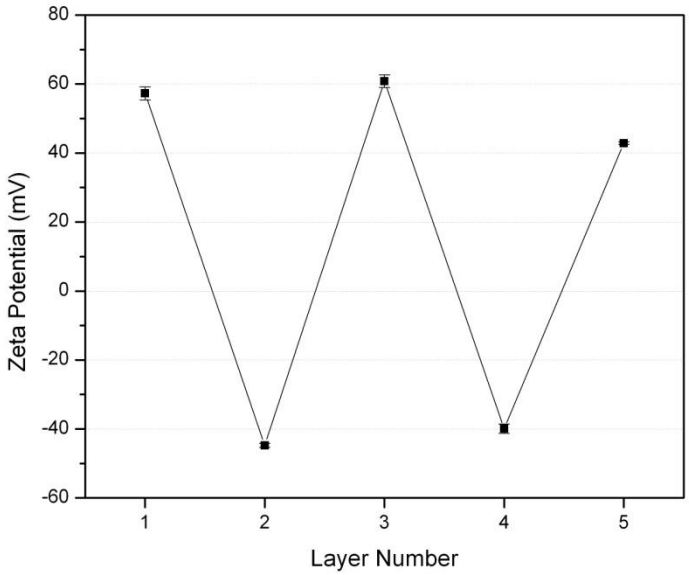

Figure 5.4 Zeta potential of PEM nanoparticles with layer encapsulated plasmid DNA. The coating configuration was ARG|DXS|ARG|DNA|ARG on HA nanoparticles. Means and standard deviations of three independent measurements are shown.

5.2.2 Layer encapsulation in PEM microparticles

Commercially available 3 μm silica particles were chosen to study layer encapsulation for PEM microparticles as they are ready-to-use and are particularly useful in studying factors that pertain to the polyelectrolyte multilayer with the particle core remaining consistent. Silica particles were coated with $[PRM|DXS]_2|PRM|$nucleic acid$|PRM$, where Figure 5.5a shows Cy5 labeled siRNA, Figure 5.5b and Figure 5.5c shows FITC labeled plasmid DNA as the nucleic acid encapsulated. Fluorescent rings are seen when the fluorescent nucleic acid PEM microparticles are analyzed with confocal microscopy. Flow cytometry data shows an increase in fluorescence intensity for PEM microparticles

possessing a FITC-DNA layer (green trace) as compared to non-fluorescent control particles (black trace).

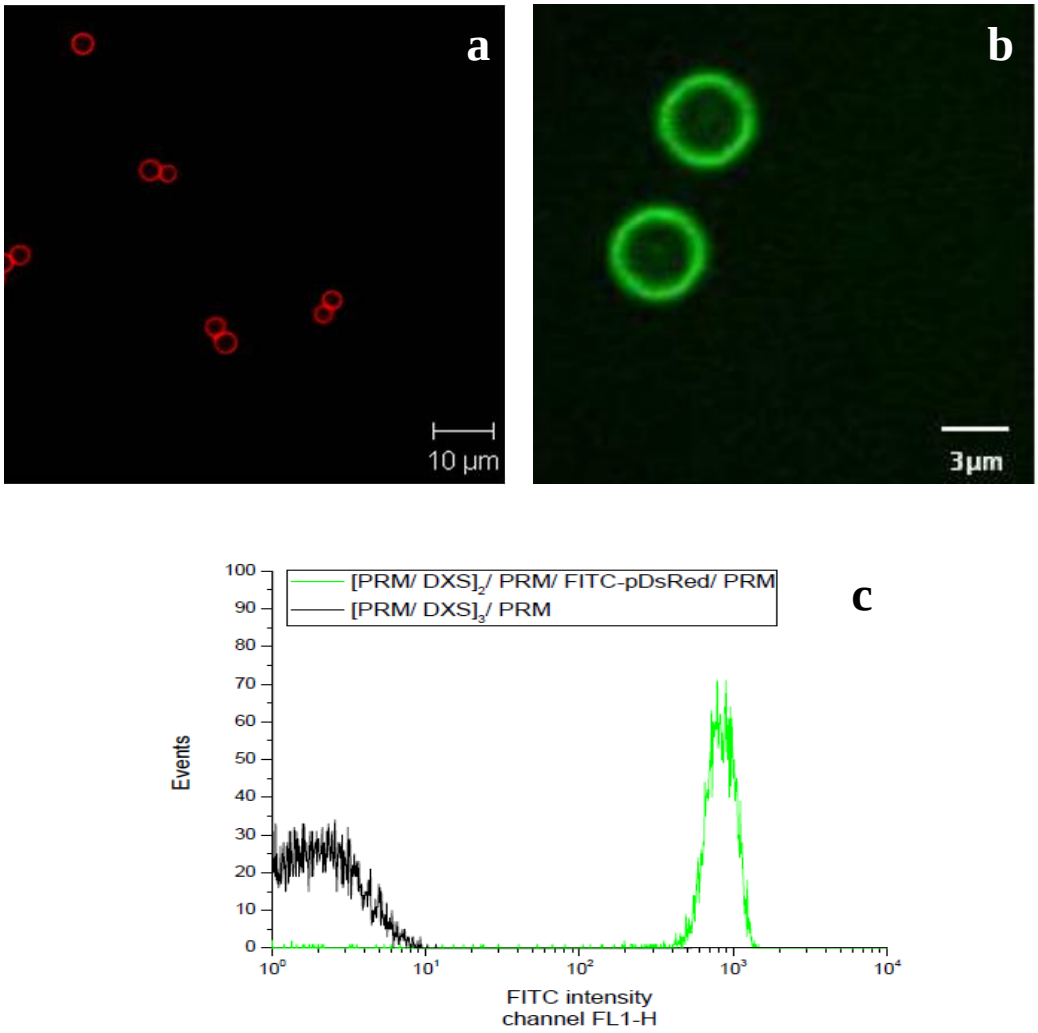

Figure 5.5 Layer encapsulation in PEM microparticles. PEM microparticles encapsulating (a) Cy5-siRNA and (b) FITC-DNA. Shown are representative confocal images of three independent measurements. (c) FITC histogram of PEM microparticles with FITC-DNA (green) and non-fluorescent control particles (black). One representative histogram of three independent measurements is shown.

The loading efficiency of the particles was also examined through the absorbance measurements of the supernatants. A siRNA loading efficiency of ~20 % for PRM/DXS layers while a ~40 % encapsulation was observed for ARG/DXS layers for the same amount of silica PEM particles.

5.2.3 Core encapsulation in PEM microparticles

For core encapsulation, self fabricated $CaCO_3$ particles are essential as the nucleic acid needs to be encapsulated within the template core before coating of the PEM. Cy5 labeled siRNA was added during the formation of the $CaCO_3$ particles. Figure 5.6a and Figure 5.6b display the confocal micrograph and Cy5 intensity histogram of $CaCO_3$-siRNA-Cy5|PRM|DXS|PRM particles.

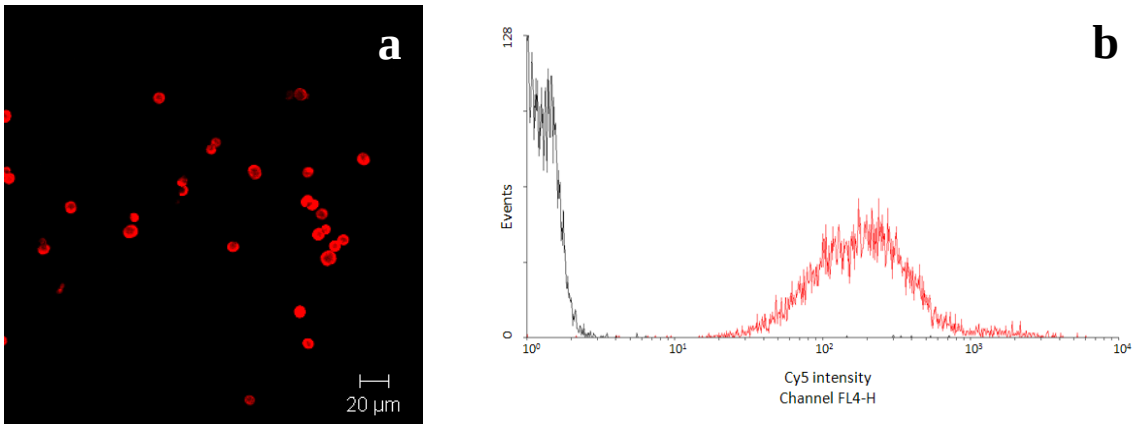

Figure 5.6 Core encapsulation in PEM microparticles. (a) Confocal micrograph of Cy5-siRNA core encapsulated PEM microparticles. (b) Cy5 intensity histograms of the Cy5-siRNA loaded particles (red) and non-fluorescent control particles (black). Shown are one representative data of three independent measurements.

From the figures, it can be observed that the core of the PEM particles were filled with fluorescent Cy5-siRNA and the increase in fluorescence intensity of the Cy5-siRNA particles (red trace) as compared to non-fluorescent control particles (black trace)

confirmed the presence of Cy5-siRNA in core encapsulated PEM microparticles. From absorbance measurements of solutions before and after fabrication of the siRNA loaded $CaCO_3$ particles, encapsulation efficiency was typically more than 50 %.

5.3 Discussion

Nucleic acids were successfully encapsulated in the layer for PEM nanoparticles, and both in the core and layer for PEM microparticles. For layer encapsulation on PEM particles, analysis of zeta potentials of nucleic acid layers proved that the negatively charged nucleic acids were successfully coated on the particles. The subsequent layering of the next positively charged layer was also unaffected, continuing the alternating zeta potential trend, and allowing further layers to be absorbed on the PEM particles.

The confocal images of PEM particles with fluorescent labeled nucleic acid confirmed the presence of nucleic acids on both types of PEM particles. PEM nanoparticles loaded with fluorescent nucleic acid appeared as fluorescent dots, while layer encapsulation on PEM microparticles displayed uniform fluorescent rings and core encapsulation in PEM microparticles exhibited filled fluorescent cores.

Together with the increase in fluorescent intensity of PEM particles loaded with fluorescent labeled siRNA, the encapsulation of nucleic acids within PEM particles is distinct. As seen from the fluorescent intensity histograms of fluorescent nucleic acid loaded PEM particles, multilayer loaded PEM nanoparticles and microparticles as well as core loaded PEM microparticles displayed higher fluorescent intensities than non-fluorescent control particles.

ARG/DXS remained the favorable choice in fabrication of PEM nanoparticles, as less aggregation of the particles was observed and higher encapsulation efficiency was attained as compared to PRM/DXS PEM nanoparticles.

Multiple layers of siRNA coating was also shown on PEM nanoparticles, with PEM nanoparticles loaded with 2 layers of siGLO exhibiting stable alternating zeta potentials. In addition, the proportional increase of fluorescent intensity with increasing number of siGLO layers further established the successive coating of multiple siRNA layers on PEM nanoparticles. This property is potentially advantageous as the siRNA dosage per unit amount of particle can be controlled.

Furthermore, the replacement of negatively charged DXS with siRNA as the alternate layer coating was explored. One advantage of this coating configuration is higher biocompatibility due to reduced externally added substance as the DXS layers are eliminated. Another benefit of replacing the DXS layers with siRNA is that it accounts for higher siRNA loading as more siRNA can be loaded per particle. However, this coating scheme would lose some manipulation factors over release control such as delayed release which could probably be accomplished by coating extra ARG/DXS polyelectrolyte layers on top of the siRNA layer(s).

More than 400 pmol siRNA could possibly be coated per layer for 0.5 mg PEM nanoparticles, as saturation is not achieved for first two siRNA layers with negligible siRNA found in the supernatant. From absorbance measurements, saturation is about 100 pmol per layer for 0.1 mg of PEM nanoparticles. However the 80 % loading observed for

the third siRNA layer was probably due to the minimal loss of particles during fabrication steps which led to extraneous siRNA in the supernatant.

Layer encapsulation of nucleic acids on PEM microparticles was achievable, which was also reported in [36] using PRM/DXS layers on silica microparticles to encapsulate plasmid. However the low loading siGLO amounts propelled experiments on core encapsulation in PEM microparticles. Layer encapsulation on ARG/DXS microparticles only slightly raised the encapsulation efficiency to 40 % from 20 % for PRM/DXS PEM microparticles. The encapsulated amounts were calculated to be insufficient for future intracellular studies. A possible method to increase the amount of nucleic acid loaded is by replacing the negatively-charged layer by nucleic acid layers as mentioned above, with the loading of multiple siGLO layers on PEM nanoparticles. Wang et al. mentioned that multiple DNA/PLL layers can be absorbed on $CaCO_3$ particles, with up to 5 bilayers [79]. This could be a future area that could be explored, layering multiple layers of siRNA/DNA with ARG layers on micro-sized particles. Although PEM microparticles offer a lower surface area to volume ratio than PEM nanoparticles, their larger cores could be functionalized for other purposes such as intracellular pH sensors [64, 65].

Core encapsulation with $CaCO_3$ particles were more promising, with encapsulation efficiency of more than 50 %. The loading amounts can probably be increased by increasing the concentration of the nucleic acids during the $CaCO_3$ fabrication step. More in depth experiments have to be carried out to encapsulate sufficient nucleic acid for the specific therapeutic purpose.

Additionally, the core loaded PEM microparticles can be exposed to dissolution conditions and from nucleic acid-filled microcapsules. These PEM microcapsules are shown and compared with PEM microparticles in the next chapter.

5.4 Conclusion

In conclusion, this chapter has summarized the successful results of loading nucleic acids on PEM particles. Layer encapsulation of nucleic acids on PEM nanoparticles was demonstrated, with ARG/DXS PEM nanoparticles as the promising choice due to less aggregation and higher encapsulation efficiency. Also, it was possible to load more than one layer of nucleic acid on these nanoparticles. The replacement of DXS layers with siRNA layers further enabled the increase of siRNA dosage per unit amount of PEM particles. The high flexibility of the LbL assembly technique could be demonstrated by PEM particle tailored to suit different dosage requirements. As for PEM microparticles, core encapsulation was more favorable than layer encapsulation as higher loading amounts were observed. This is probably because microparticles have lower surface area to volume ratio, enabling a larger amount of nucleic acid to be trapped within its core. Hence, core encapsulated nucleic acid in microparticles will be studied in the next chapters.

CHAPTER 6
Cellular processing of PEM particles

6.1 Introduction

Various cell lines were used to study the cellular processing of PEM particles, namely HEK293T, FibroGRO and HTFs. These cells were chosen for specific reasons: HEK293T cells were preferred for the investigation of plasmid delivery using PEM particles as they are easily cultured and are a highly transfected derivative of the HEK293 cell line with the insertion of the viral gene SV40.

Glaucoma is the second leading cause of blindness in the world after cataracts, according to World Health Organization (WHO) statistics gathered in 2002 [102]. It may pose a more serious public health challenge as blindness caused by glaucoma is irreversible. Increase intraocular pressure (IOP) is linked with increased occurrence of glaucoma [103]. Filtration surgery reliefs the intraocular pressures of glaucoma patients, however failure of the filtration system can be caused by deposition of scar tissue. Currently, anti-proliferative agents such as 5-fluorouracil and mitomycin C [104] are used to limit scarring. However, there is still a considerable failure rate which drives the need to find a better solution to fibrosis after glaucoma filtration surgery [105]. SPARC deficiency was demonstrated to increase chances of surgical survival after filtration surgery in SPARC-

null mice [105]. HTFs are responsible for the production of scar tissue within the eye, hence they were selected to study the delivery of siRNA by PEM particles, in the prospect for development of a sustained release carrier system for post-surgery treatments.

However, HTFs are scarce due to the limited numbers extracted from the human eye and they can only be maintained until a maximum of passage 6. Thus, a similar fibroblast model was explored and FibroGRO, a human foreskin fibroblast cell line, was chosen for the preliminary studies of siRNA delivery by LbL coated particles.

The first step in cellular processing of the PEM particles is the cellular uptake of the particles. The particles had to be attracted near the surface of the cells and then engulfed within the cell.

Encapsulation of fluorescent labeled components within the PEM particles allowed for tracking of the particles during cell interaction. First, straightforward visualization of the fluorescent PEM particles within cell was achieved using confocal microscopy, as CLSM provided a cross-section image of the cells, unlike traditional microscopes which views the whole cell volume. Particles within the cell can be easily detected at a particular z-axis while the particles attached on top of the cell will not be focused. The images from the transmission light channel allows for the visualization of the cell boundaries, while those from the fluorescent light channel enables the location of the particles. The overlay of these two channels facilitates the analysis of the fluorescent PEM particles relative to the cross sections of the cells.

Second, flow cytometry of the cells allows the study of the fluorescent intensity of each cell. If fluorescent PEM particles were attached on or within the cell, it would possess a higher fluorescent intensity than a normal untreated cell. Furthermore, trypan blue, which does not enter the membrane of live cells, was employed to quench the attached fluorescent PEM particles [82]. The comparison of the fluorescent intensities would allow the investigation of the cellular uptake of PEM particles.

After endocytosis of the particles, the particles need to escape from the endosomes before they are degraded brought upon by the fusion of enzymatic acid organelles like lysosomes. Fluorescent dyes which tag the lysosomes were utilized to visualize their location relative to the particles within the cells.

6.2 Results

6.2.1 Cellular uptake of PEM nanoparticles

For the study of cell-nanoparticle interactions, HA particles were coated with ARG|DXS|ARG|siGLO|ARG layers, resulting in fluorescent PEM particles due to the fluorescent siGLO layer. These particles were incubated with FibroGRO and HTF cells plated on 8 well chamber glass slides. After 1 day incubation, the cellular uptake of PEM nanoparticles was visualized by confocal microscopy in both transmission and fluorescent light channels.

Figure 6.1 shows the confocal micrographs of (a-c) FibroGRO and (d-f) HTF cells co-incubated with siGLO-loaded PEM nanoparticles. For both cell types, a considerable amount of dot-like fluorescence was observed on and within the cells. Furthermore, these fluorescent dots were only present in the cell cytoplasm, but not within the cell nuclei.

Additionally, ARG/DXS PEM nanoparticles encapsulating a fluorescent labeled polymer were given to HEK293T cells. Figure 6.1g displays the confocal micrograph of these HEK293T cells after 1 day incubation with CellMask Orange cell membrane stain. Likewise to FibroGRO and HTF cells, fluorescent particles were seen within HEK293T cells.

Similarly, FibroGRO plated in 6 well plates were treated with the siGLO-loaded PEM nanoparticles for 4 hours before harvesting for flow cytometry. Figure 6.2a and Figure 6.2b displays the dot plots (FSC-H vs SSC-H) of untreated FibroGRO cells and siGLO-loaded PEM particles respectively. Comparing the two dot plots, it can be seen that they were distinctively different populations. The untreated FibroGRO cells in Figure 6.2a appeared on the right portion of the dot plot, with high values for both FSC-H and SSC-H axis.

On the other hand, the siGLO-loaded PEM nanoparticles appeared on the left portion of the dot plot of Figure 6.2b, with a lower range of values for both axes as compared to the cells. Figure 6.2c displays the dot plot for FibroGRO incubated with siGLO-loaded PEM nanoparticles after 4 hours incubation. It possessed both populations similar to those showed in (a) and (b), however, the right population showed significantly higher SSC-H values than in Figure 6.2b.

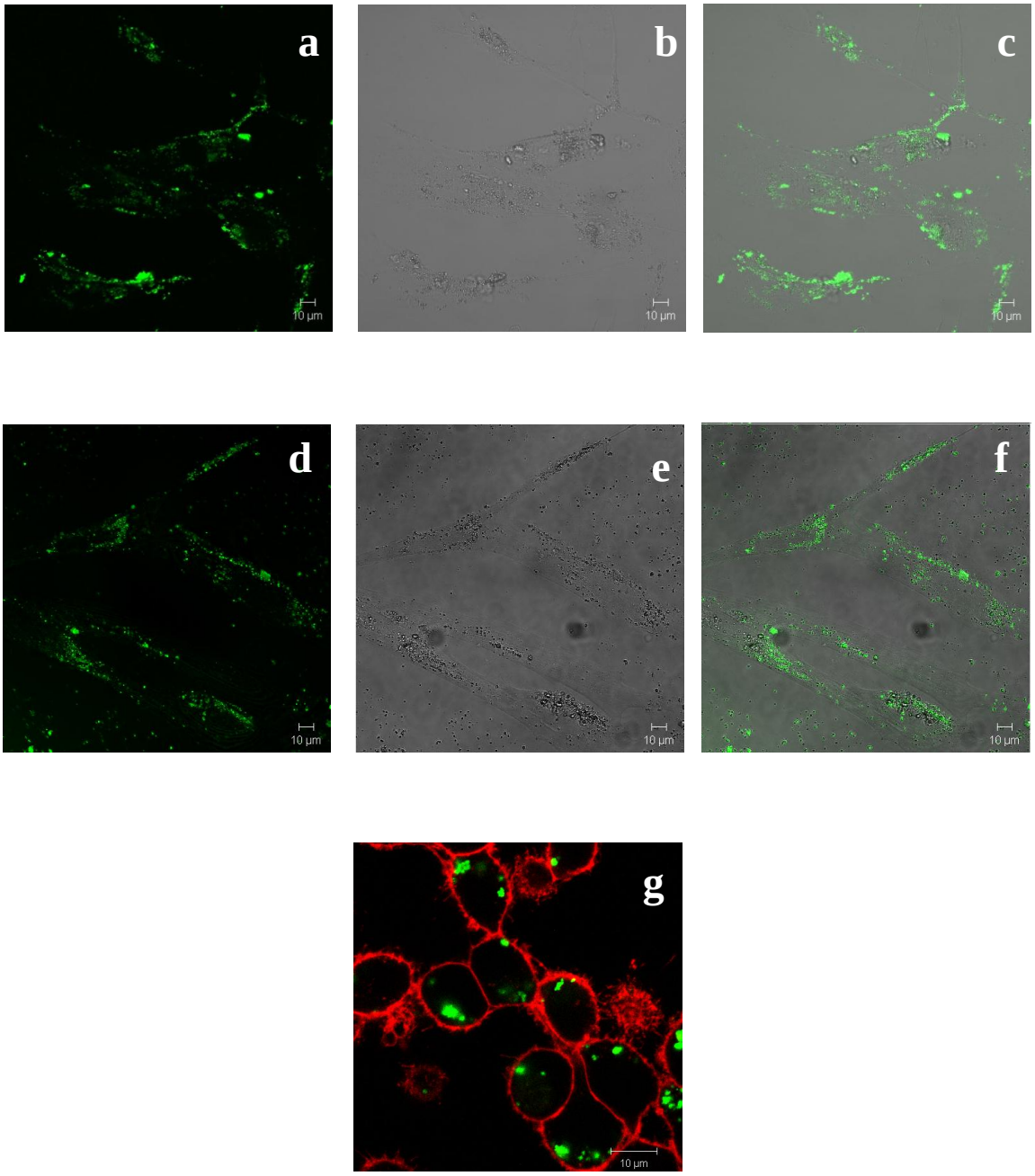

Figure 6.1 Confocal images of cellular uptake of fluorescent PEM nanoparticles. Fluorescent siGLO-loaded PEM nanoparticles within (a-c) FibroGRO and (d-f) HTF cells after 1 day co-incubation. (a,d) fluorescence channel, (b,e) transmission light channel, and (c,f) overlay of both. (g) Overlay of fluorescent PEM nanoparticles with cell membrane stained HEK293T cells. Shown are one representative data of three independent measurements.

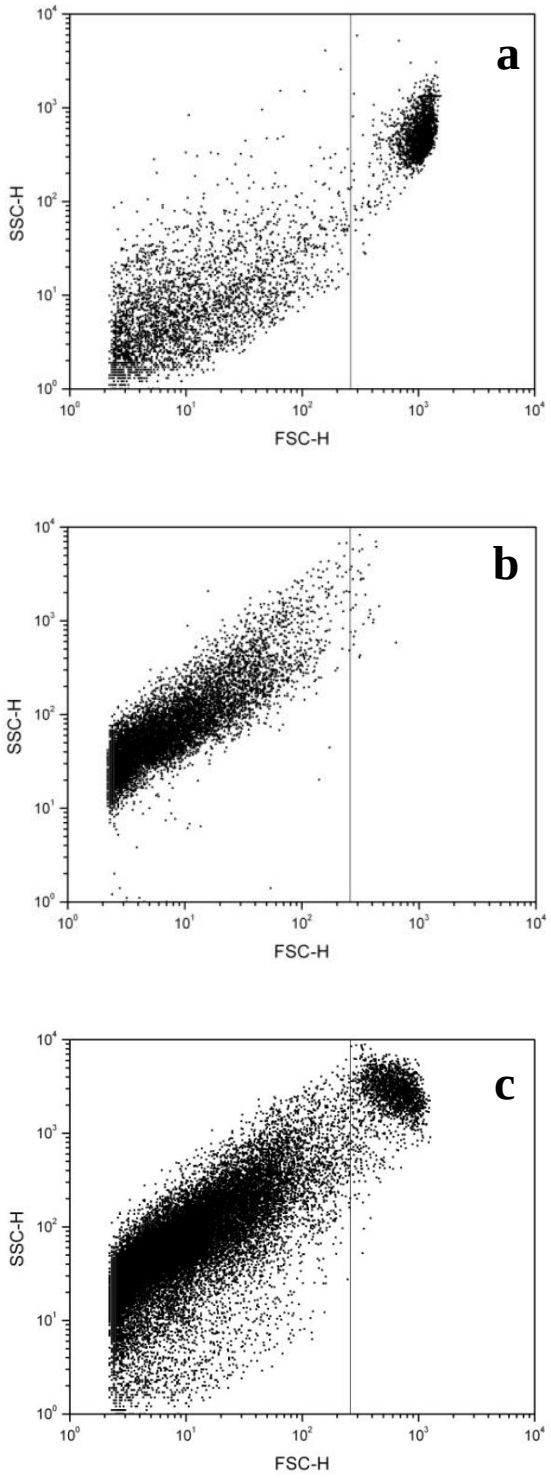

Figure 6.2 Dot plots (FSC-H vs SSC-H) of PEM nanoparticles and FibroGRO cells. (a) Untreated FibroGRO cells, (b) siGLO-loaded PEM nanoparticles, and (c) FibroGRO cell treated with siGLO loaded PEM nanoparticles after 4 hours. One representative data of three independent measurements are shown.

Figure 6.3 compares the size and FITC fluorescence intensity of untreated and siGLO-loaded PEM nanoparticle treated FibroGRO cells. The control cells clearly concentrated on the left side of the dot plot, displaying low FITC intensity as illustrated in Figure 6.3a. Conversely, FibroGRO cells treated with the fluorescent PEM nanoparticles exhibited higher FITC fluorescent intensity, as portrayed by the distinct right shift along the FITC intensity axis in Figure 6.3b. The size of the cells remained largely similar with and without PEM particle treatment.

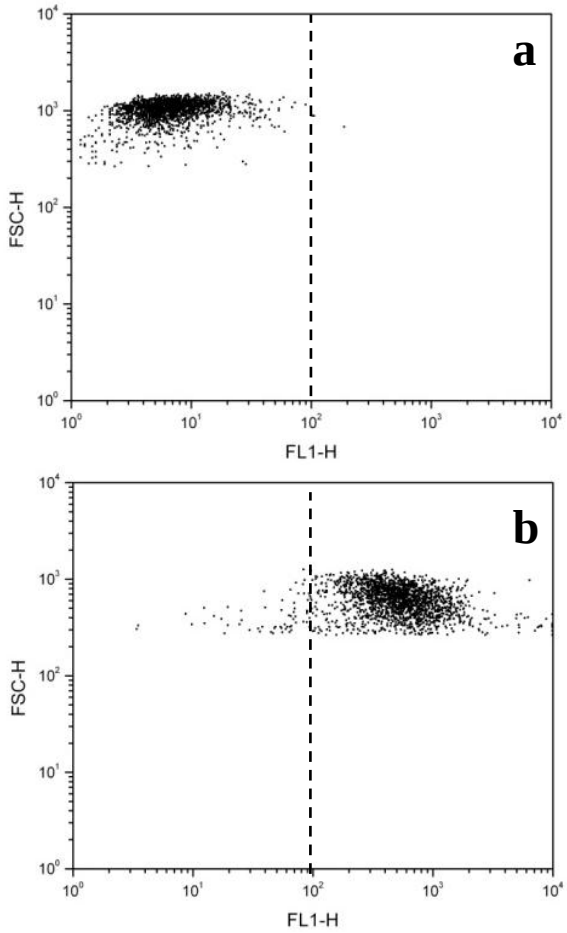

Figure 6.3 Dot plot of (FSC-H vs FL1-H) of untreated and siGLO-loaded PEM nanoparticles treated FibroGRO cells. FSC-H compares the size of the cells, while FL1-H shows the FITC intensity of the cells. Displayed are one representative data of three independent measurements.

Next, trypan blue was added to the cell-particle mixture to quench the fluorescence of the particles situated outside the cell membrane. From this, it was possible to sieve out fluorescence data from the fluorescent PEM particles attached on the membrane, and obtain data that was only from the particles within the cells. First, the quenching of the fluorescence of siGLO-loaded PEM nanoparticles was examined as illustrated in Figure 6.4a. A pronounced peak was seen in the FITC intensity histogram before quenching (black graph), but after the addition of tryphan blue, a marked reduction in fluorescence intensity was observed (grey graph).

Figure 6.4b examines the tryphan blue quenching on the particle-treated FibroGRO cells. The fluorescence intensity histogram of siGLO-loaded PEM nanoparticle FibroGRO cells (black graph) possessed noticeably greater FITC intensity as compared to the untreated control cells (grey graph), with a definite increase of the Gmean from 6 to 500. After the addition of trypan blue to the particle-treated cells, a decrease in FITC intensity was recorded (light grey graph). However, the quenched particle-treated cells still had significantly higher FITC intensity than the control cells with a Gmean of 115.

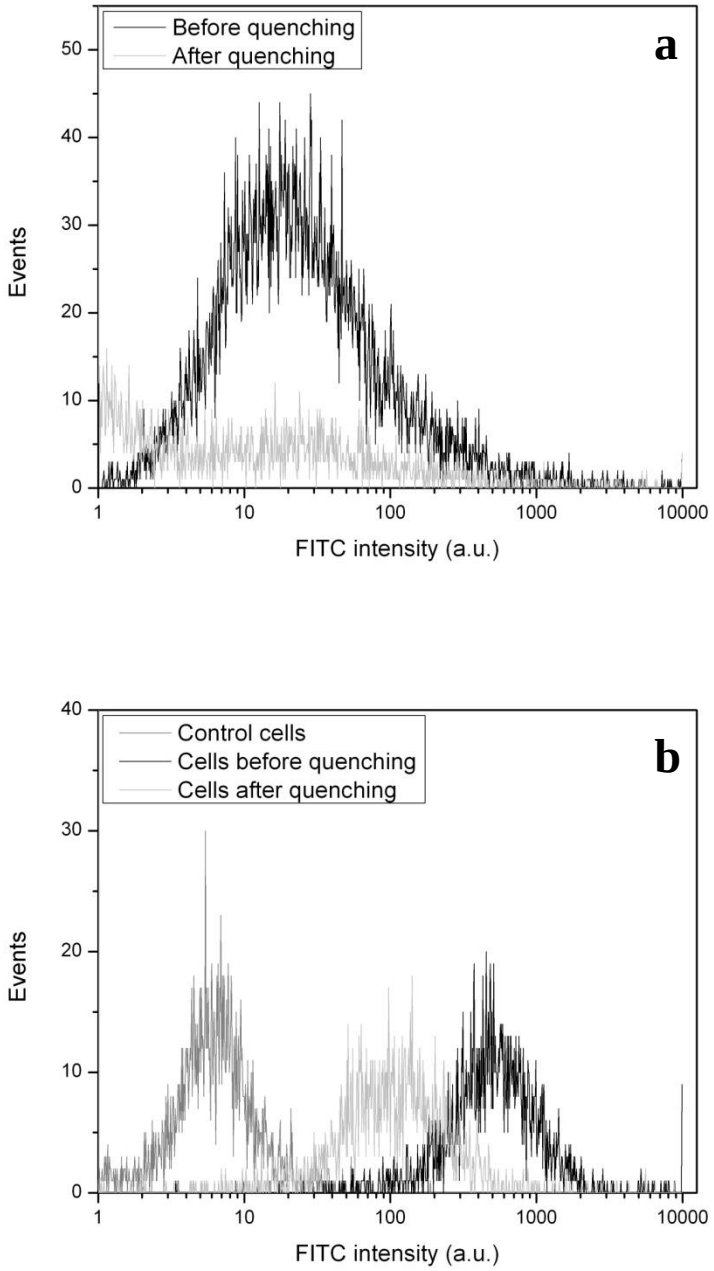

Figure 6.4 FITC intensity histograms of PEM nanoparticles and FibroGRO cells before and after trypan blue quenching. (a) siGLO-loaded PEM nanoparticles before (black graph) and after (grey graph) quenching. (b) Untreated control FibroGRO cells (grey graph) and siGLO-loaded PEM nanoparticle treated cells before (black graph) and after (light grey graph) quenching. Shown are one representative data of three independent measurements.

6.2.2 Cellular interaction of PEM nanoparticles

Cellular processing of PEM nanoparticles within FibroGRO cells was studied in further depths, through the co-staining of acidic organelles like lysosomes using the LysoTracker Red. The co-localization of the PEM nanoparticles with the LysoTracker Red would suggest that the PEM nanoparticles were within acidic environments such as endolysosomes. The cells were treated with the particles for various time points and the LysoTracker Red dye was added according to manufacturer's protocol. The cells were then imaged using confocal microscopy, and the visuals seen at 4 hour, 1 day and 3 days incubation are summarized in Figure 6.5.

As observed in column I of Figure 6.5, green fluorescent dots can already be seen within the cell membrane at 4 hours. Interestingly, many PEM nanoparticles are also attached on the cell membrane, forming a clear outline of the cell boundaries. However, no green dots were detected at the cell nuclei. Co-staining with Lysotrack Red showed that the PEM nanoparticles were mutually exclusive with the lysosomes, as there was no overlap of the red and green fluorescence (which would appear yellow in the overlap image).

After 1 day incubation (column II), the fluorescent PEM nanoparticles were mostly observed to be within the cells, with fewer particles attached on the cell membrane as compared to with 4 hours incubation (column I). Again, the red and green fluorescence was exclusive which was similarly observed for 3 days incubation. On day 3, entirely green fluorescent cells can be observed and one such cell is portrayed in column III in Figure 6.5.

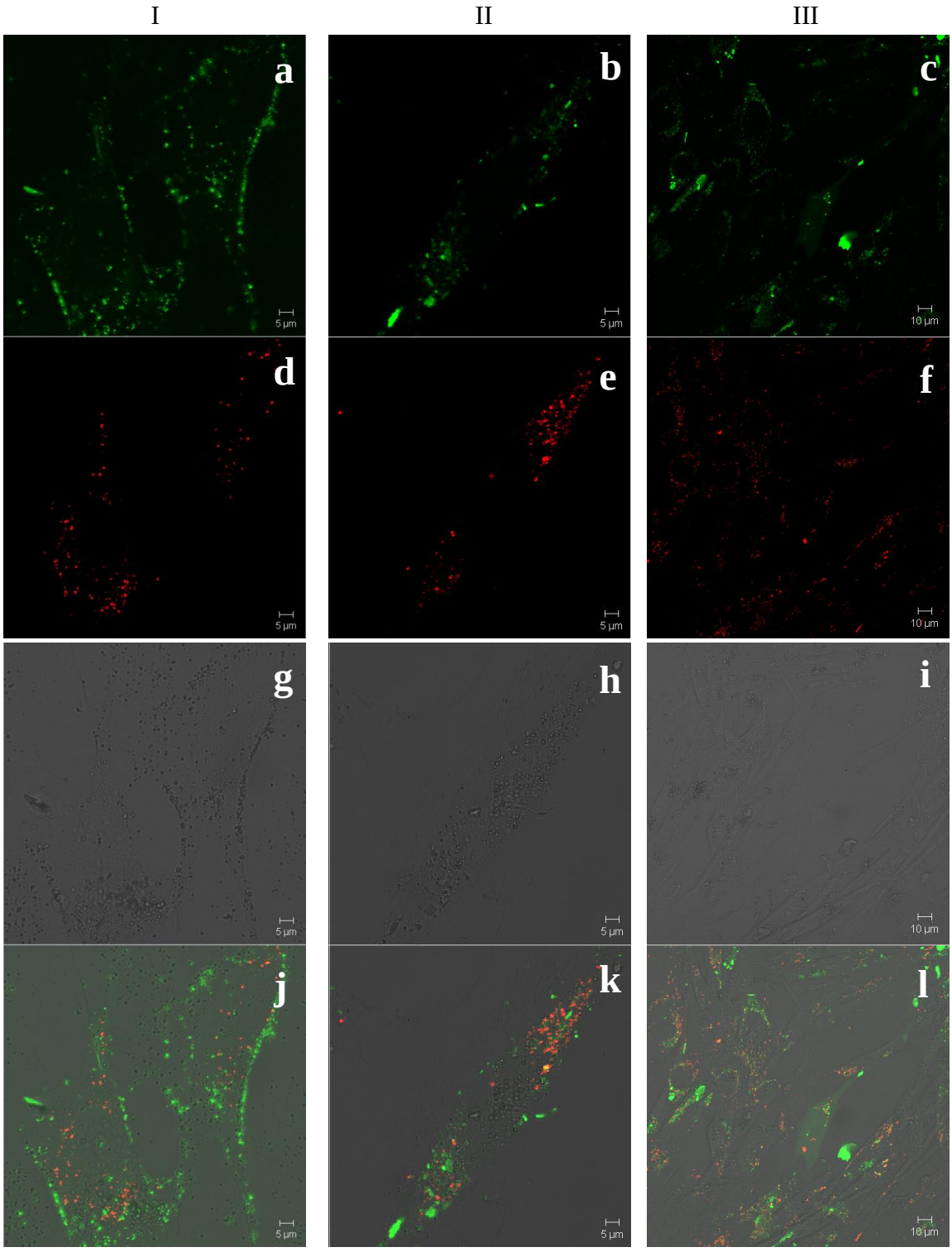

Figure 6.5 Confocal micrographs of siGLO-loaded PEM nanoparticle treated FibroGRO cells co-stained with LysoTracker Red. Column I, II, and III are 4 hours, 1 day and 3 days incubation respectively. Top to bottom: (a-c) FITC channel showing siGLO-loaded PEM nanoparticles, (d-f) RITC channel displaying LysoTracker Red stained lysosomes,

(g-i) transmission light channel, and (j-l) overlay of the 3 channels. One representative data of three independent measurements are shown.

6.2.3 Cellular uptake of PEM microparticles/capsules

The uptake of PEM microparticles/capsules were investigated with HEK293T, FibroGRO and HTF cells as shown in Figure 6.6. Due to the larger size of the PEM microparticles/capsules, they are easily identifiable from the cell structures. Dual fluorescence can be utilized, with the PEM particles possessing fluorescence, while the cell structures can be stained with fluorescent dyes of another wavelength to enable them to be differentiated easily.

FITC-PAH was encapsulated within the core of PEM microcapsules with ARG|[DXS|ARG]$_2$ layers permit the PEM microcapsules to be detected in the FITC channel in Figure 6.6a. The microcapsules were incubated with HEK293T cells for one day before staining of the cell membrane with CellMask Orange was performed. CellMask Orange allowed the visualization of the cell boundaries as portrayed in Figure 6.6b. The overlap of the confocal images in Figure 6.6c confirmed that the PEM microcapsules were found within the cells.

Staining of the HTF cell membrane with FITC-cholera toxin (FITC-CTx) was not ideal as the cell cytoplasm was also stained as seen in Figure 6.6d. Staining with CellMask Orange also posed the same problems despite reducing the concentration of the cell membrane stain. Nevertheless, PEM microparticles with PRM|DXS|PRM-RITC|DXS|PRM layers detected in the RITC channel in Figure 6.6e, were found within the HTF cells as observed from the overlap of the two channels in Figure 6.6f.

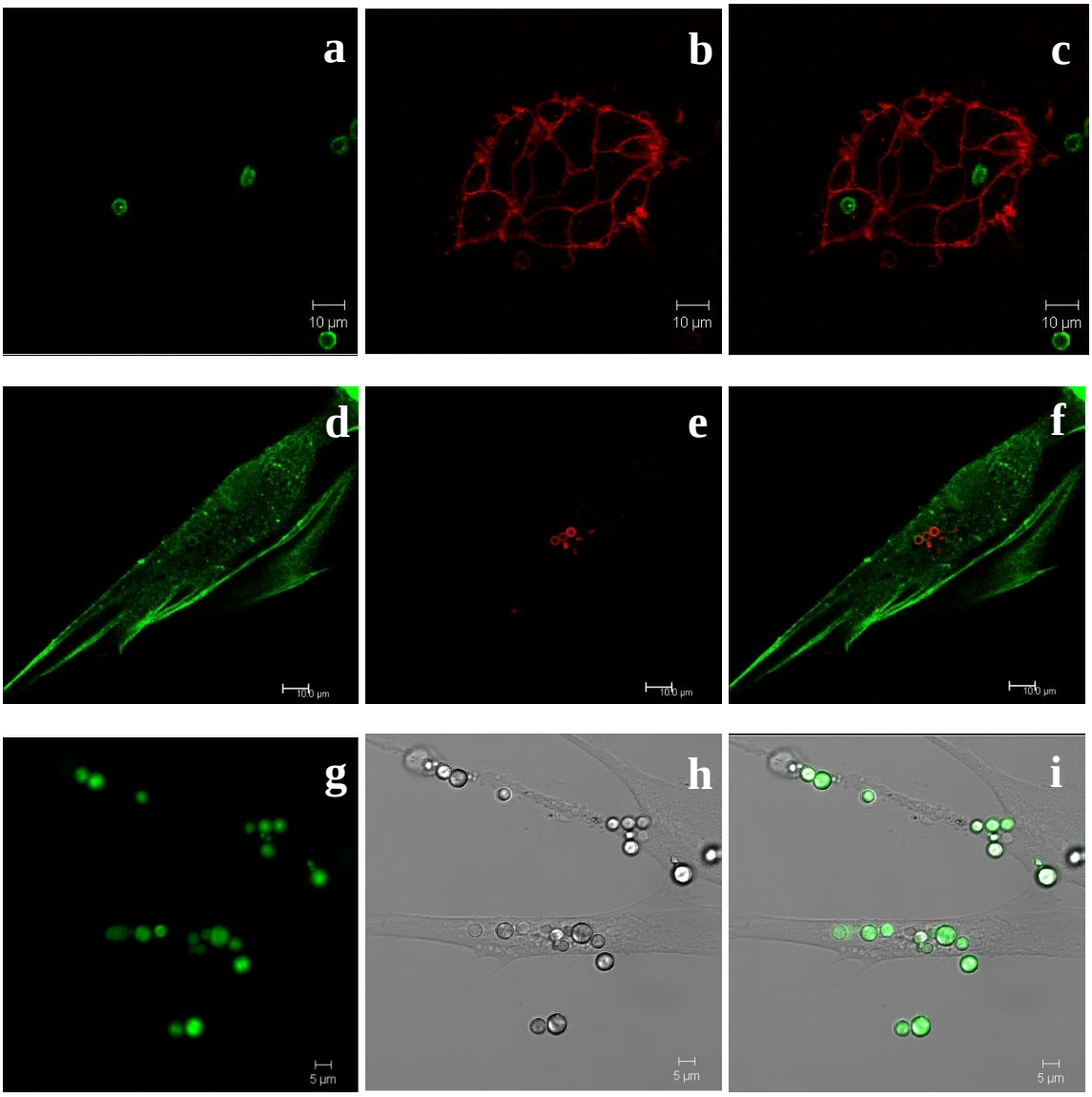

Figure 6.6 Cellular uptake of PEM microparticles/capsules. (a-c) HEK293T cells: (a) FITC channel, FITC-PAH core-encapsulated PEM microcapsules, (b) RITC channel, CellMask Orange cell membrane stain of HEK293T cells, and (c) overlay of both channels. (d-f) HTF cells: (d) FITC channel, FITC-CTx membrane stain of HTF cells, (e) RITC channel, PRM-RITC layer encapsulated PEM microparticles, and (f) overlay of both channels. (g-i) FibroGRO cells: (g) FITC channel, siGLO-loaded PEM microparticles, (h) transmission light channel, morphology of FibroGRO cells and PEM microparticles, and (i) overlay of both channels. Displayed are one representative data of three independent measurements.

Loading the core of the PEM microparticles with siGLO also produced fluorescent particles detectable in the FITC channel as seen in Figure 6.6g. Figure 6.6h shows the transmission light channel which exhibits the morphology and location of the PEM microparticles and FibroGRO cells. From the overlap image in Figure 6.6i, the PEM microparticles were also discovered to be within the FibroGRO cells.

6.3 Discussion

6.3.1 Cellular uptake of PEM nanoparticles

From the confocal micrographs in Figure 6.1, it can be observed that FibroGRO and HTF cells were able to take up a large amount of the particles, filling up the whole cytoplasm except the nuclei. This was aligned with Zhou et al. work on PEM nanoparticles made from PLGA nanoparticles and chitosan/alginate layers incubated with hepatocytes. Cellular uptake of the 400 nm particles was observed, but the confocal images showed none were observed in the nuclei [49]. The uptake of PEM nanoparticles was further demonstrated by the increase in fluorescence intensity of the cells detected using flow cytometry. First, the difference in size and complexity of particles and cells as summarized in Figure 6.2 allowed for the specific analysis of fluorescence intensities of the cells only. The population representing the cells was selected and the data from cell debris and PEM nanoparticles were gated off to obtain results that were reflective of the FibroGRO cells.

Second, although the regions reflecting the cell populations are similar in Figure 6.2a and Figure 6.2c as both possess high FSC-H values, their SSC-H axis values are slightly different. Particle-treated FibroGRO cells displayed somewhat higher SSC-H values in Figure 6.2c than untreated cells in Figure 6.2a. An increase in SSC-H values indicates an

increase in complexity of the particle-treated cells, which could probably be due to the presence of particles on and within the cells.

The increase in fluorescence intensity of the particle-treated cells is observed in Figure 6.3, while the size of the cells remained comparable to the untreated control cells. This result suggests that particle-treated cells had siGLO-loaded PEM nanoparticles either on its surface or intracellularly. Hence, quenching of the fluorescence from extracellular particles was performed to further study the cellular uptake of the PEM nanoparticles.

Trypan blue allowed for quenching of the fluorescence from the PEM nanoparticles as confirmed in Figure 6.4a. Some fluorescence from particle-treated cells was quenched as the fluorescence intensity dropped after the addition of trypan blue, implying that there are PEM nanoparticles present on the surface of the FibroGRO cells but have not entered the cell after 4 hours incubation. More importantly, the fluorescence intensity of the quenched sample still had higher fluorescence intensity than the control untreated cells as demonstrated in Figure 6.4b. As trypan blue does not enter live cells, particles within the cell membrane of live cells will be protected from quenching [82]. Hence, this meant that the presence of intracellular fluorescent PEM nanoparticles is evident.

6.3.2 Cellular interaction of PEM nanoparticles

At 4 hours incubation, PEM nanoparticles can already be observed within the FibroGRO cells. This echoes the previous flow cytometry result of observing an increase in fluorescence intensity of the cells 4 hours after particle treatment. From the different time points of 4 hours, 1 day and 3 days, the mutually exclusive fluorescence from the PEM nanoparticles and lysosomes indicate that the PEM nanoparticles are not within acidic environment, and are probably within the cell cytoplasm. This shows promising potential

of using PEM nanoparticles as a nucleic acid carrier as they are able to escape from the endosomes and have the chance to release the nucleic acid within the cytoplasm.

Although some PEM nanoparticles entered the FibroGRO cells at 4 hours, many of the particles were still situated at the cell membrane as seen in column I of Figure 6.5. At the 1 day time point, the number of particles at the cell membrane is significantly reduced, with more particles within the cell cytoplasm. Hence, 4 hours is sufficient for PEM nanoparticles to attach on the FibroGRO cell membranes and for some particles to enter the cells, but a longer amount of time is needed for the cells to take in more particles on the cell membrane.

Additionally, after 3 days the PEM nanoparticles remain within the cells and slightly green fluorescent cells can be observed like the green cell shown in column III of Figure 6.5. This proposes that the PEM nanoparticles stay within the cell and start to release the drug load, in this case siGLO, within the cell. Delivery of the nucleic acid by PEM nanoparticles will be examined more thoroughly in the next chapter.

6.3.3 Cellular uptake of PEM microparticles/capsules

Due to the LbL coating technique, the PEM particles can be fluorescently tagged in various ways and be useful in ways such as intracellular tracking of the particles. As demonstrated, encapsulation of FITC-PAH or siGLO within the core allowed for detection of the particles in the FITC channel, while coating a layer of RITC-PRM permitted the PEM microparticles/capsules to be detected in the RITC channel. The possibilities are limitless, as long as the fluorescent component is large enough to be trapped within the core and does not leak out or that the fluorescent component has to be charged to be coated as a layer within the multilayer.

The images of the fluorescent PEM microparticles/capsules were overlapped with fluorescent labeled cell membrane or transmission light pictures to analyze the location of the particles with respect to the cell boundaries. HTF cells were found to be difficult to stain ideally as not only the membrane of the cell was stained but the cytoplasm was also stained despite reducing the staining concentrations. It is understandable as the HTF cells are primary cells which may not perform as ideally as cultured cell lines. Nonetheless, for all 3 cell types, the PEM microparticles/capsules can be found inside the cells indicating the successful cellular uptake of PEM microparticles/capsules. Micron-sized PEM particles had been shown to be taken by HEK293T cells [36, 81] and another fibroblast cell line (NIH3T3) [89], but no literature has been published for the cellular uptake of PEM microparticles/capsules by HTF and FibroGRO cells.

Further experiments could be carried out to further study the processing of PEM microparticles/capsules such as the time dependent study with Lysotracker Red staining of the particle-treated cells. This would provide a basis for comparison of the processing properties of different sized PEM particles such as escape from endolysosomal compartments.

6.4 Conclusion

This chapter summarizes the results showing the cellular uptake and processing of PEM nanoparticles and microparticles/capsules. The examined cell lines readily took up both PEM nanoparticles and microparticles/capsules, as they were observed to be within the cell membrane. PEM nanoparticles could enter the cell as early as 4 hours incubation, but a significant amount of particles still remained at the cell membrane surface which signaled that longer incubations are needed to achieve maximum amount of PEM

nanoparticles within the cells. In addition, trypan blue quenching was useful in distinguishing data from PEM nanoparticles within or outside the cell membrane. Eventually, after one day incubation, a large amount of intracellular PEM nanoparticles were discovered, which were probably in the cell cytoplasm as they were not in acidic environments. Despite the larger size of PEM microparticles/capsules, their uptake by the cells was also achieved, albeit in less numbers than the nano-sized particles.

CHAPTER 7
Delivery of nucleic acids by PEM nanoparticles

7.1 Introduction

Reporter nucleic acids enabled the straightforward detection of successful nucleic acid delivery to facilitate an initial study of the ability of the carrier system. In this chapter, plasmid DNA coding for fluorescent proteins (GFP and DsRed) and siRNA transfection indicator siGLO Green were utilized. The nucleic acids were either encapsulated within the core or coated as layers on PEM particles as elaborated earlier.

siGLO-loaded PEM particles were incubated with FibroGRO and HTF cells for the study of siRNA delivery by PEM particles. siGLO Green is a commercial RNAi transfection indicator which indicates RNAi transfection success when the modified fluorescent RNA duplex accumulates within the cell nuclei. The fluorescent nuclei can be clearly visualized by confocal microscopy.

The plasmid-loaded PEM particles were given to HEK293T cells to investigate plasmid delivery by PEM particles. Fluorescent proteins will be expressed if plasmid delivery is achieved which results in fluorescent cells that can be simply detected using fluorescent and confocal microscopy.

7.2 Results

7.2.1 siGLO delivery by PEM nanoparticles

Lipofectamine 2000 was used as the positive standard transfection reagent to obtain positive controls of siGLO transfection in FibroGRO and HTF cells as shown in Figure 7.1a and Figure 7.1b respectively. Lipofectamine 2000 siGLO complex was formed with 5 µl of Lipofectamine and 200 pmol of siGLO to transfect $2x10^5$ cells. FibroGRO and HTF cells plated on 8 well chamber slides and the Lipofectamine 2000 siGLO complex was added to the cells. After 1 day incubation, analysis with confocal microscopy showed bright green fluorescent nuclei exhibited in both cell types with slightly fluorescent cytoplasm. Occasionally, a more concentrated fluorescent region can be seen within the fluorescent nuclei as seen in Figure 7.1b.

Similarly, FibroGRO and HTF cells plated on 8 well chamber slides were given siGLO-loaded PEM nanoparticles fabricated from HA nanoparticles coated with ARG|DXS|ARG|siGLO|ARG layers. The cells were examined every day using confocal microscopy. Unlike the cells treated with Lipofectamine 2000, no green nuclei were seen until after 3-4 days incubation. Figure 7.2 shows green nuclei in FibroGRO and HTF cells incubated 3-4 days with siGLO-loaded PEM nanoparticles. Like the Lipofectamine 2000 treated cells, the particle-treated cells also had slight fluorescent bodies with more strongly fluorescent cell nuclei. However, the fluorescence intensity of the cell nuclei was not as intense as those of the Lipofectamine 2000 treated cells. Additionally, many strongly fluorescent dots from the fluorescent PEM nanoparticles were still visible within the cell body. Similar concentrated fluorescent regions within the cell nuclei were also observed in the particle-treated cells.

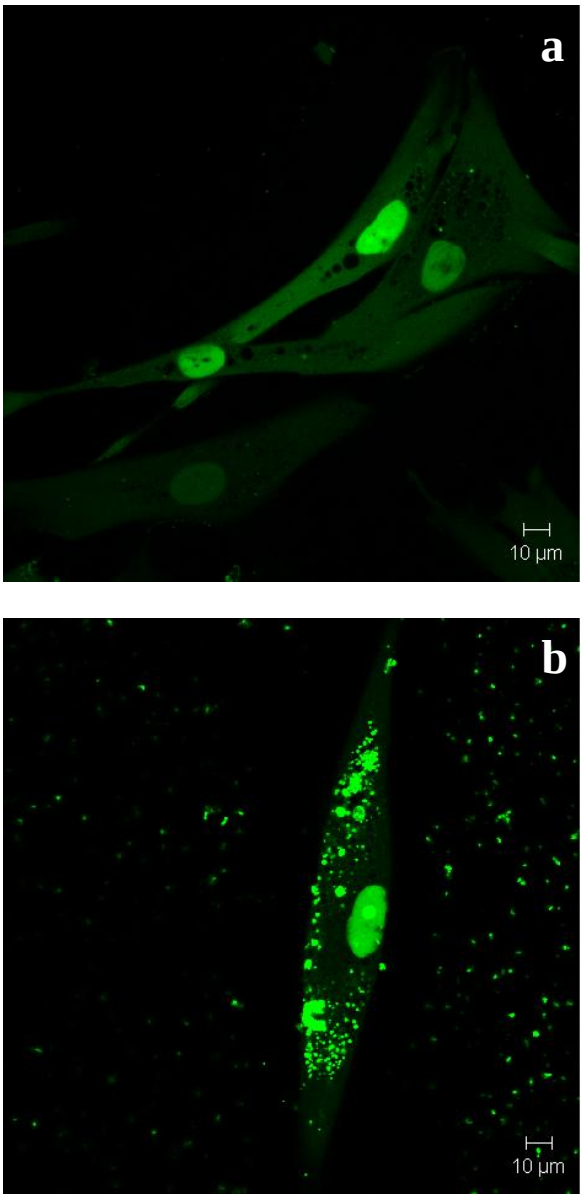

Figure 7.1 Confocal micrographs of Lipofectamine 2000 siGLO transfected cells. (a) FibroGRO cells. (b) HTF cells. Displayed are one representative data of three independent measurements.

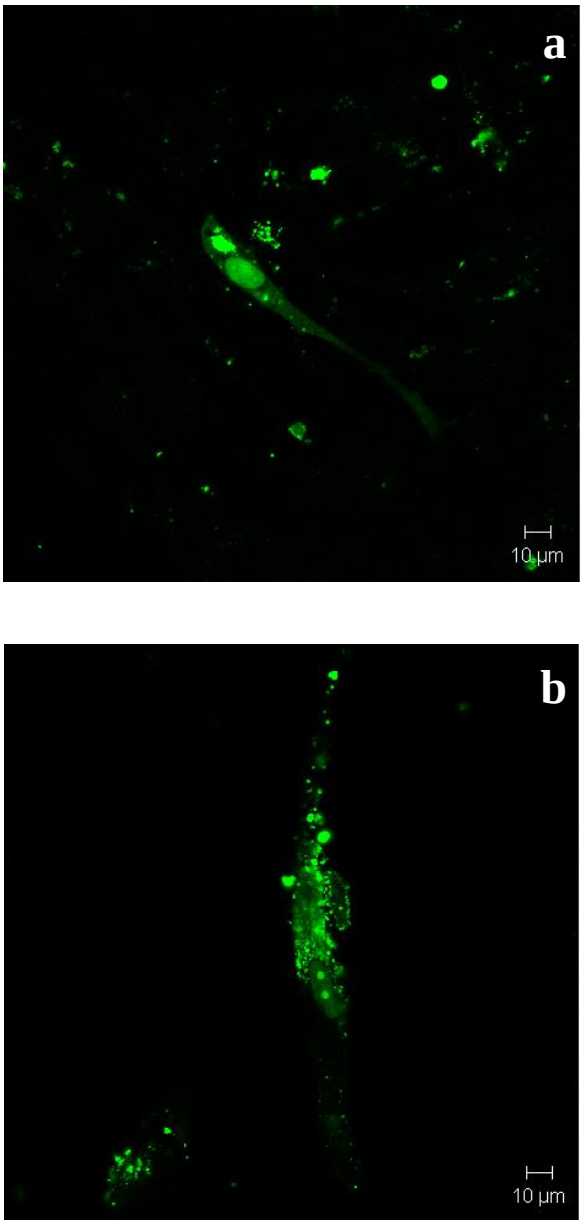

Figure 7.2 Confocal micrographs of FibroGRO and HTF cells transfected using siGLO-loaded PEM nanoparticles. (a) FibroGRO cells. (b) HTF cells. One representative data of three independent measurements are shown.

7.2.2 siGLO delivery by PEM microparticles/capsules

An amount of 200 pmol of siGLO was mixed with 50 µl of $CaCl_2$ solution before precipitation with 50 µl of Na_2CO_3 solution to form siGLO loaded $CaCO_3$ cores, which were coated with $ARG[DXS|ARG]_2$ layers. To fabricate PEM microcapsules, the PEM microparticles were subjected to EDTA. The PEM microparticles/capsules were then given to FibroGRO and HTF cells at a ratio of 1:10 to investigate their siRNA delivery capabilities. After 3 days incubation, green nuclei can be observed in FibroGRO and HTF cells treated with siGLO-loaded PEM microcapsules as shown in Figure 7.3. Similar to the above result, the cell bodies were also slightly fluorescent, with fluorescent PEM microcapsules still present within the cells. However, for cells treated with siGLO-loaded PEM microparticles, without removal of the $CaCO_3$ cores, no fluorescent cells or nuclei were observed. The PEM microparticles remained brightly fluorescent within the cells.

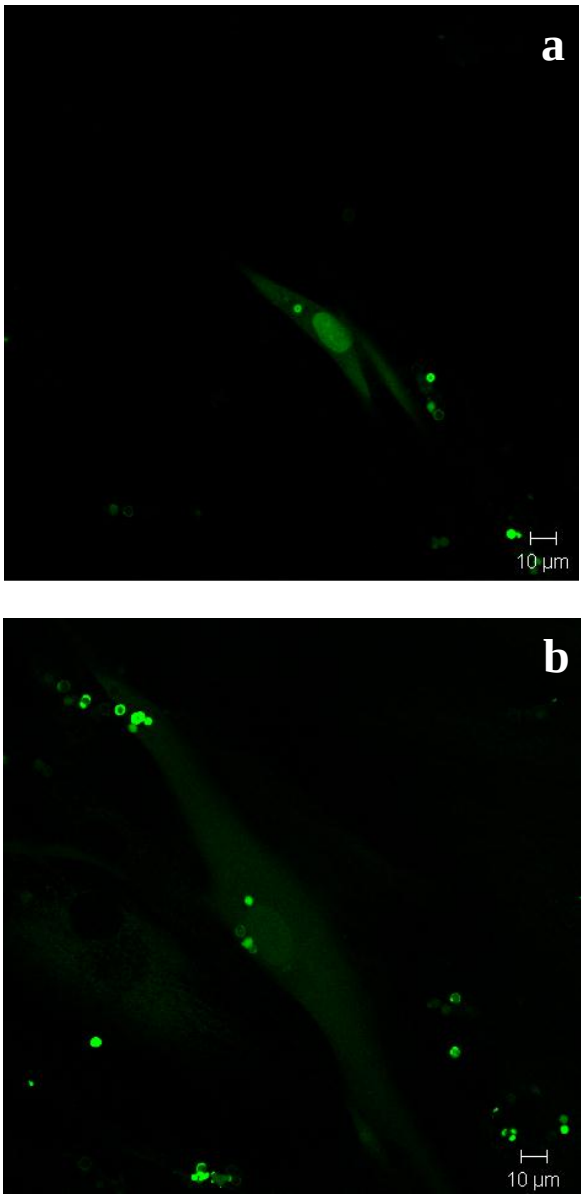

Figure 7.3 Confocal micrographs of FibroGRO and HTF cells transfected using siGLO-loaded PEM microcapsules. (a) FibroGRO cells. (b) HTF cells. One representative data of three independent measurements are displayed.

7.2.3 Plasmid delivery by PEM nanoparticles

DsRed plasmid was layer encapsulated on PEM nanoparticles in the following configuration, ARG|DXS|ARG|DNA|ARG. HEK293T cells were incubated with the plasmid loaded PEM nanoparticles for 3 days. Figure 7.4 shows the fluorescent light microscope picture of these HEK293T cells, some of the cells were observed to be expressing fluorescent DsRed proteins.

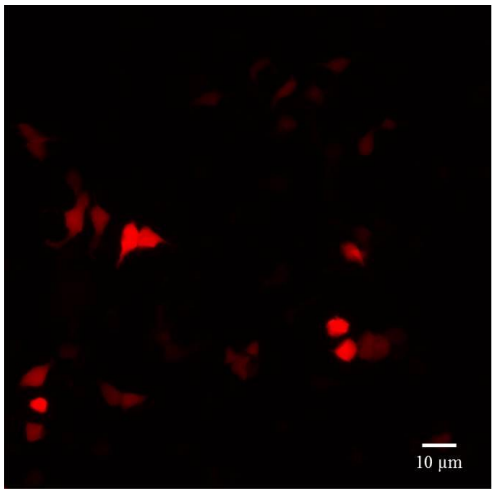

Figure 7.4 Fluorescent light microscope picture of HEK293T cells transfected by plasmid loaded PEM nanoparticles.

7.2.4 Plasmid delivery by PEM microparticles/capsules

Plasmid delivery was investigated with PEM microcapsules, where the GFP plasmid was encapsulated within the $CaCO_3$ core. Subsequent coating with $[ARG|DXS]_2$|RITC-ARG layers and core dissolution formed PEM microcapsules containing plasmid DNA within the core and with a RITC-ARG layer. Incubation of HEK293T cells with plasmid-loaded PEM microcapsules resulted in fluorescent cells, demonstrated in Figure 7.4a. The RITC-ARG layer enabled tracking of the PEM microcapsule in the RITC channel as shown in Figure 7.4b. From the overlay of the two channels in Figure 7.4c, PEM microcapsules can be observed within the fluorescent cells. Additionally, after several days within the

HEK293T cells, the PEM microcapsules appeared shrunken from the initial diameter of about 3 μm.

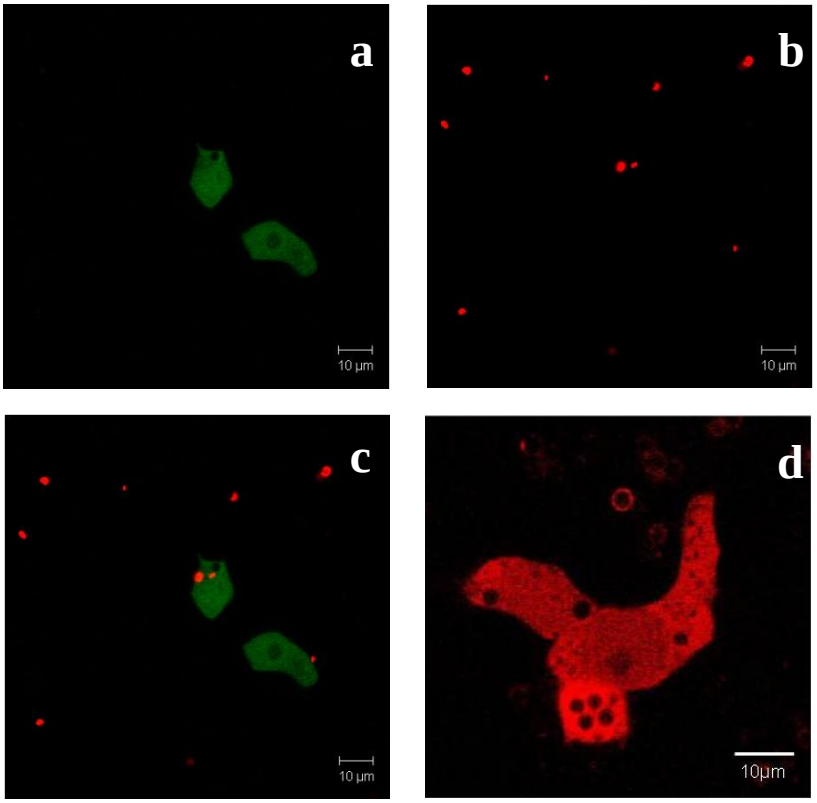

Figure 7.4 Confocal micrographs of HEK293T cells transfected using PEM microparticles/capsules. (a) FITC channel showing fluorescent HEK293T cells expressing GFP. (b) RITC channel displaying PEM microcapsules with a fluorescent layer of RITC-ARG. (c) Overlay of the two channels. (d) RITC channel showing fluorescent HEK293T cells expressing DsRed proteins with PEM microparticles possessing a fluorescent RITC-PRM layer. One representative data of three independent measurements are displayed.

DsRed plasmid was also encapsulated within the polyelectrolyte multilayer on silica particles with the following configuration: PRM|DXS|PRM-RITC|DNA|PRM. The plasmid-loaded PEM microparticles were given to HEK293T cells plated in 8 well

chambers and observed with confocal microscopy after several days. Red rings from the fluorescent PRM-RITC layer on PEM particles were detected. Fluorescent HEK293T cells such as those shown in Figure 7.4d were observed. Also, several black spheres of roughly 3 μm were seen within the fluorescent cells.

The transfection efficiency of PEM microcapsules was further studied with plasmid GFP encapsulated within the empty shell of $[ARG|DXS]_2|$ ARG layers. The microcapsules were given to HEK293T cells plated in 6 well plates and incubated for 3 days. Subsequently, the cells were detached and analyzed by flow cytometry. Figure 7.5a shows the dot plot (FSC-H vs SSC-H) of HEK293T cells, where R1 represents the cell population seen in all samples. The other events were considered as debris and gated out in subsequent analysis.

Figure 7.5b shows the FITC intensity histogram for the cell population of control untreated HEK293T cells. M1 represents 95 % of the number of events of the control cells with the lowest fluorescence intensity, and this marker was taken as non-fluorescent untreated cells. Figure 7.5c displays the result for a sample with plasmid core loaded PEM microcapsules, with marker M2 portraying the fluorescent cells. An average of about 17 % of the HEK293T cells was fluorescent after 3 days incubation with the GFP plasmid core loaded PEM microcapsules.

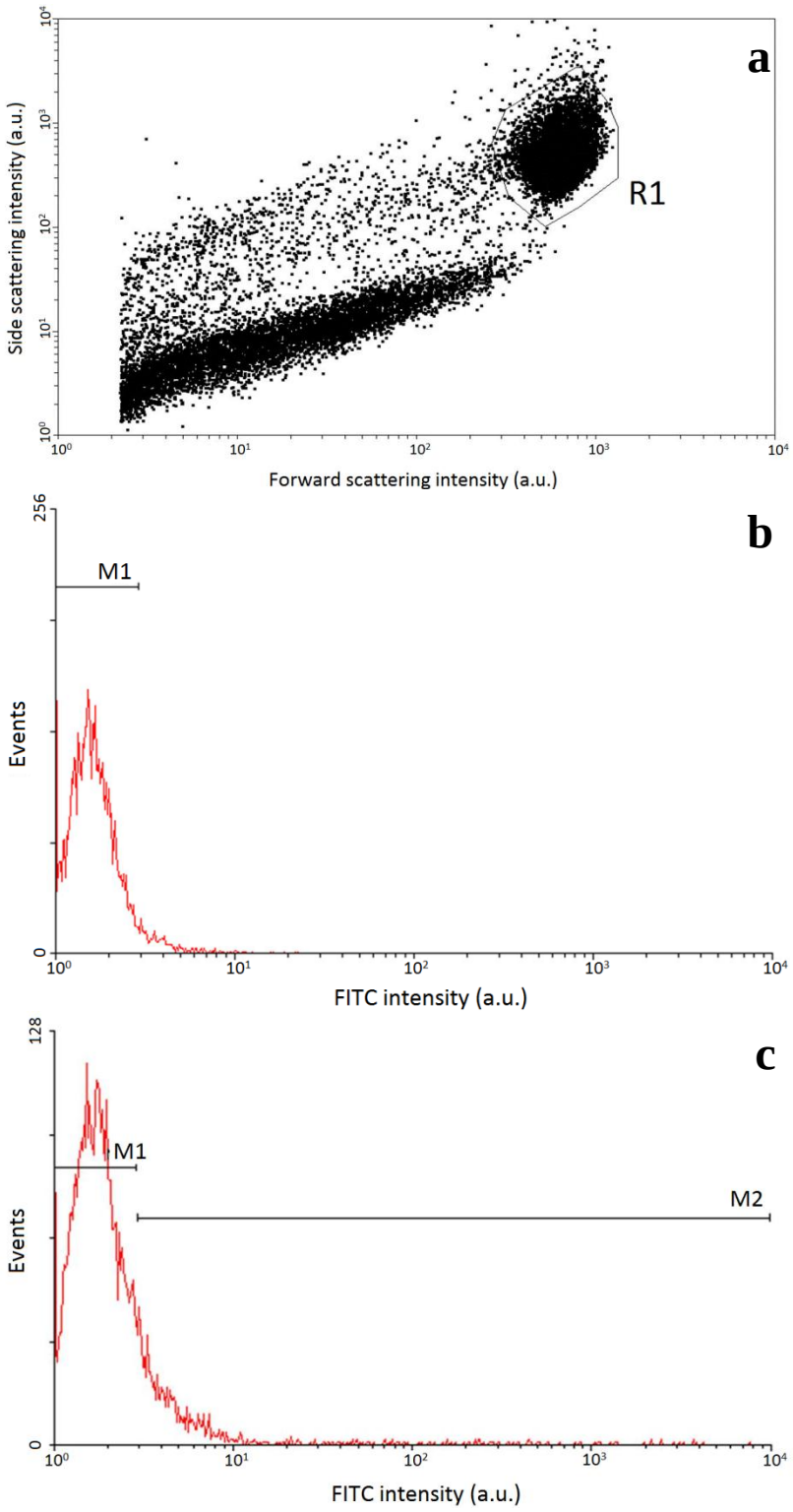

Figure 7.5 Flow cytometry of HEK293T cells transfected using plasmid core-loaded PEM microcapsules. (a) Dot plot (FSC-H vs SSC-H) of HEK293T cells. Histogram of (b) control cells and (c) capsule treated cells. M1 marks 95 % of control cells, M2 represents

fluorescent transfected cells. One representative data of three independent measurements are displayed.

7.3 Discussion

7.3.1 siGLO delivery by PEM nanoparticles

Green nuclei observed in FibroGRO and HTF cells when incubated with siGLO-loaded PEM nanoparticles indicated successful siGLO delivery via PEM nanoparticles. The polyelectrolyte layers on the PEM nanoparticles were able to degrade within the cell and release the siGLO in the intracellular spaces. The more intensely fluorescent regions within the nuclei could be the cells' nucleoli. The fluorescent nuclei only started appearing after 3-4 days incubation, unlike the Lipofectamine 2000 transfected cells which occurred after 1 day incubation. The probable reason behind the delayed transfection is degradation of the 1 layer of ARG above the siGLO layer, before the siGLO can be released from the PEM nanoparticles within the cell.

Additionally, many PEM nanoparticles still remained fluorescent and within the cells after 4 days incubation. This indicated that the siGLO layer was still present on these PEM nanoparticles. Also, the green nuclei of the particle-treated cells were not as intensely fluorescent as those treated with Lipofectamine 2000, which indicate that less siGLO was transfected. Although less siGLO is accumulated within the cell nuclei, the still siGLO-loaded PEM nanoparticles proposed the potential of being sustained release carriers. Future studies such as a prolonged investigation of the continuingly siGLO loaded PEM nanoparticles within the cells will be an interesting examination of the continued release of siRNA from PEM nanoparticles. As reported by Jacobson et al., poly-L-lactic acid and siGLO complexes can be observed in *in vivo* studies for up to 80

days [106], thus longer investigations with siGLO would be possible. Furthermore, increasing the number of layers of siGLO/siRNA as shown in Section 5.2.1 would allow the increase of the amount of siRNA loaded in each particle as more than one layer of siRNA was shown to be successfully coated. This would enable sufficient siRNA to be released to reach targeted dosage.

7.3.2 siGLO delivery by PEM microparticles/capsules

siGLO delivery was also shown to be successful by PEM microcapsules in FibroGRO and HTF cells as demonstrated in Figure 7.3. Green nuclei were observed after 3 days incubation similar to the duration of the siGLO loaded PEM nanoparticles. However, PEM microcapsules consisted of 5 polyelectrolyte layers protecting the load of siGLO in the core, whereas the PEM nanoparticles only had 1 polyelectrolyte layer on top of the siGLO layer. This suggests that the release mechanisms of PEM microcapsules and PEM nanoparticles were different, as 5 polyelectrolyte layers would require longer degradation times before the siGLO load was released. More in depth examinations of the release mechanisms within cellular spaces need to be executed to elucidate this result.

A possible rationale is the polyelectrolyte layers were weakened when exposed to dissolution conditions, resulting in faster degradation of the layers. Another possibility is the siGLO was held on more strongly by the preceding positively charged polyelectrolyte layer when coated as a layer in PEM nanoparticles, while the siGLO loaded in the hollow core of the PEM microcapsules were free to escape when pores were formed in the polyelectrolyte multilayer.

Within the cells possessing green-nuclei, fluorescent PEM microcapsules were still observed after 3 days incubation. This suggests that not all the PEM microcapsules

engulfed by the FibroGRO and HTF cells were degraded to release the siGLO load. De Geest et al. reported ARG/DXS PEM microcapsules were intracellularly degradable [92] which corresponded to the degradation of the siGLO-loaded ARG/DXS PEM microcapsules to release the encapsulated siGLO. However, the authors also mentioned after 20 hours incubation with African green monkey cells, intact ARG/DXS PEM microcapsules (8 polyelectrolyte layers) could be detected, but at 60 hours (2.5days) the microcapsules totally degraded. The comparison of these studies give an insight to cellular processing of PEM microcapsules. The degradation rate between different cell lines differs and a prolonged study is needed to elucidate the amount of time required to totally release the siGLO from PEM microcapsules in FibroGRO and HTF cells.

siGLO loaded in PEM microparticles, without core dissolution, were not yet released after 3 days incubation with no green nuclei observed and the PEM microparticles remaining brightly fluorescent. This reveals that core dissolution affected the release of siGLO in core-loaded PEM microparticles/capsules. In addition to the weakening of the polyelectrolyte layers after core dissolution, another plausible reason is that the siGLO was trapped within the $CaCO_3$ core which resulted in little or no release of siGLO from PEM microparticles. This highlights the differences in release mechanisms of PEM microparticles with and without core dissolution, which should be taken into consideration for future experiments regarding drug release from these particles.

7.3.3 Plasmid delivery by PEM nanoparticles

Incubation with PEM nanoparticles loaded with plasmid in the polyelectrolyte multilayer resulted in fluorescent cells as observed under the fluorescent light microscope. The cells expressing the fluorescent proteins coded from the plasmid signify the successful

defoliation of the polyelectrolyte layers and release of the plasmid from the PEM nanoparticles within the HEK293T cells. The successful delivery of plasmid by layer loaded PEM nanoparticles also implies that the functionality of the encapsulated plasmid was preserved during the encapsulation steps and subsequent layer adsorption.

7.3.4 Plasmid delivery by PEM microparticles/capsules

Plasmid delivery via PEM microparticles/capsules were visualized with HEK293T cells and core-loaded PEM microcapsules and layer-loaded PEM microparticles. Cells expressing the fluorescent GFP denoted the successful delivery of the GFP plasmid using PEM microcapsules and the preserved bio-functionality of the encapsulated plasmid, even when exposed to core dissolution conditions.

Similar to the siGLO core loaded PEM microcapsules, transfection was only observed after several days. In addition, after several days the PEM microcapsules were shrunken from their initial sizes of ~3 μm. This could be the collapse of the PEM microcapsules due to the instability of the degraded polyelectrolyte multilayer, thus resulting in the release of the plasmid within the hollow core. Hence, this implies that the encapsulated plasmid was released totally once the PEM microcapsule collapsed instead of a slow sustained release of the loaded plasmid. However, taken as a whole, the overall effect of a sustained release could still be achievable by PEM microcapsules. Further studies of increasing the number of polyelectrolyte layers in the multilayer to form a stronger microcapsule that is more resistant to collapsing would allow for the development of a sustained release carrier system. A mixture of these PEM microcapsules with different number of polyelectrolyte layers would result in sequential and continuous release of the drug.

DsRed plasmid coated on PEM microparticles was also successfully delivered into HEK293T cells as seen from cells expressing fluorescent DsRed proteins, which was similarly reported in [36]. However as mentioned in Section 5.2.2, the loading amounts of layer encapsulation of nucleic acids on micron sized PEM particles was relatively low. Transfection using this configuration would probably result in lower transfection efficiency. Nevertheless, it was shown that nucleic acids can be released from the polyelectrolyte multilayer. This could be coupled with core encapsulated to achieve targeted dosage of the biological drug.

An initial study of the transfection efficiency of ARG/DXS core loaded PEM microcapsules was performed by counting the number of fluorescent cells after 3 days incubation with these plasmid loaded capsules. A transfection efficiency of 17 % was observed, which reflected that not only plasmid delivery was possible by PEM microcapsules, but a certain percentage of cells can be transfected. Certainly, this drives the need to further explore PEM microcapsules as a plasmid carrier.

7.4 Conclusion

In this chapter, the potential of PEM particles in nucleic acid delivery was elucidated. Both siGLO and plasmid DNA were successfully delivered and transfected within cells using a variety of PEM particles, namely layer-loaded PEM nanoparticles and microparticles as well as core-loaded PEM microcapsules. Green nuclei, indicating RNAi transfection success, were observed in FibroGRO and HTF cells when incubated with the siGLO-loaded PEM nanoparticles and microcapsules. The still fluorescent PEM nanoparticles probe the need for prolonged study of intracellular siGLO release from

PEM nanoparticles. Incubation of HEK293T cells with plasmid loaded PEM particles and microcapsules saw cells expressing fluorescent proteins.

The successful delivery of nucleic acids by PEM particles propels further drug delivery studies of these particles including transfection efficiency, duration of nucleic acid release from the PEM particles, sufficient loading of nucleic acids to reach targeted dosage, etc. Furthermore, reporter siRNA and plasmid were used in this project, but the bio-functionality of siRNA and plasmid which specifically knockdown or express certain genes need to be examined in detail as well.

CHAPTER 8
Cytotoxicity studies of PEM particles

8.1 Introduction

An important aspect in the development of a carrier system is the study of its cytotoxic threshold levels. Besides being able to deliver the drug, the carrier itself should also have minimal undesirable effects. In this chapter, the cells were exposed to different concentrations of PEM particles and their cell proliferation profiles were determined to investigate the cytotoxic threshold amounts of PEM particles for applications in drug delivery.

A real-time cell proliferation assay, xCelligence, based on measuring the impedance of the cells was utilized [94]. Continuous information about cell growth was measured hourly for about 7 days with respect to the amount of PEM particles added. Additionally, the standard MTT cell proliferation assay was used to verify the results obtained. The MTT assay is a colorimetric assay based on MTT reduction to formazan by living cells [95, 96]. Subsequent dissolution of formazan and measurement of absorbance at 595 nm gives information of cell viability.

8.2 Results

8.2.1 Cytotoxicity studies of PEM nanoparticles

FibroGRO and HTF cells were detached and placed into special 96-well plates equipped with gold electrodes for the measurement of the cells' impedance by the xCelligence equipment. Added to 4000 cells were various amounts of PEM nanoparticles ranging from 2 μg to 20 μg, with the following layer configuration: $[ARG|DXS]_2|ARG$. Figure 8.1a and Figure 8.1b shows the cell proliferation indexes of FibroGRO and HTF cells respectively, throughout 7 days when exposed to different amounts of PEM nanoparticles.

As revealed in Figure 8.1a, a trend of increasing amount of PEM nanoparticles adversely affected cell proliferation was observed. The FibroGRO cells exposed to 2 μg, 5 μg, and 10 μg PEM nanoparticles showed similar cell index profiles which were slightly less than the untreated control FibroGRO cells. With 15 μg and 20 μg of PEM nanoparticles, the cell viability was visibly decreased, where more PEM nanoparticles caused greater cytotoxic effects.

However, Figure 8.1b demonstrates that HTF cells were less sensitive to PEM nanoparticles exposure. The HTF cells displayed largely comparable cell proliferation indexes regardless of PEM particles addition and amounts. The drop in cell viability seen in HTF cells with 5 μg of PEM nanoparticles was probably due to inaccurate readings.

The MTT assay results of FibroGRO cells with the ARG/DXS PEM nanoparticles are shown in Figure 8.2. The FibroGRO cells showed similar cell viability throughout all amounts of PEM nanoparticles. Cell viability was about 90 % as compared to control cells treated with NaCl and no particles.

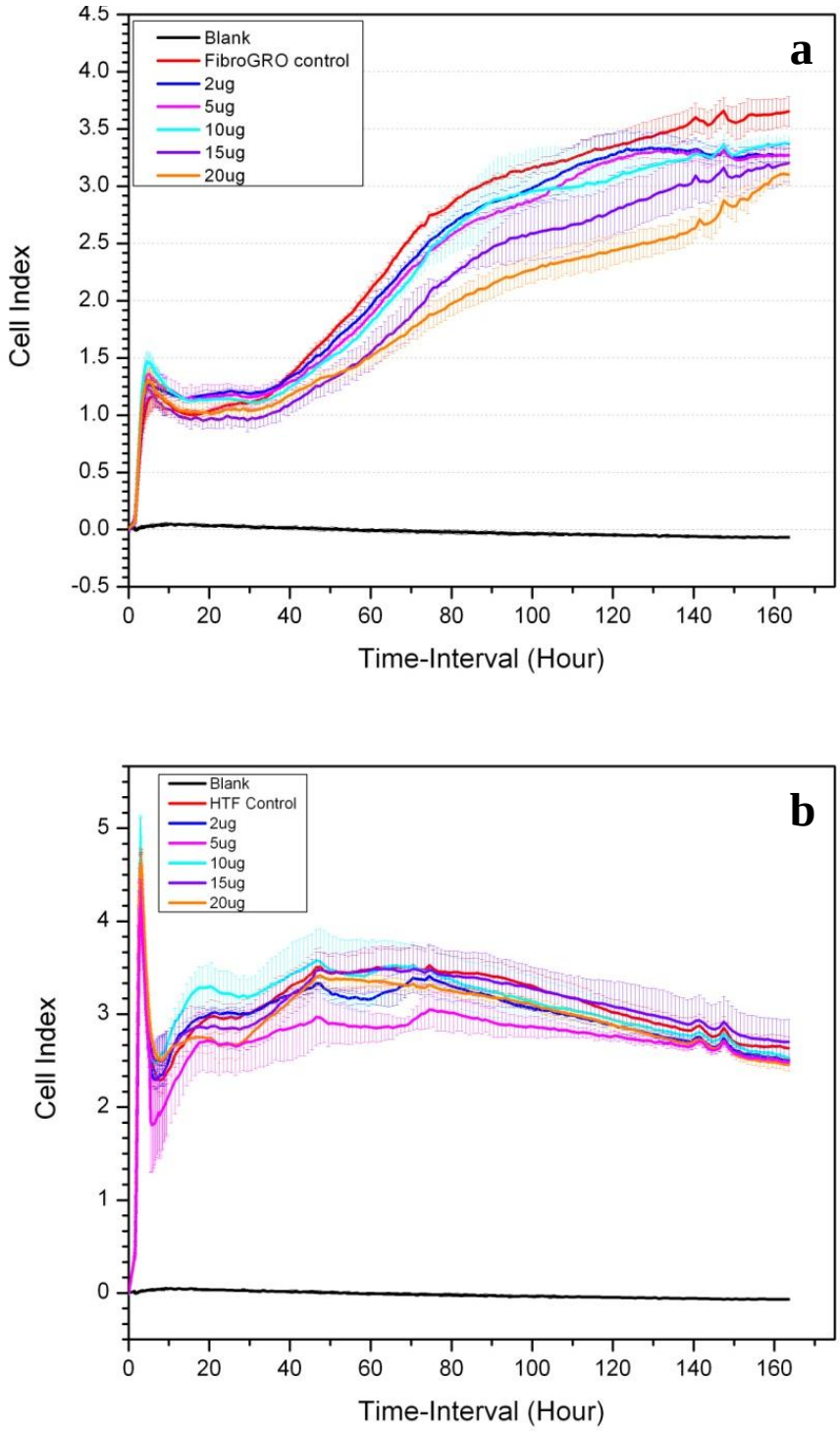

Figure 8.1 xCelligence cell proliferation indexes of FibroGRO and HTF cells exposed to PEM nanoparticles. (a) FibroGRO cells. (b) HTF cells. Blank (black line) refers to wells without cells and filled with medium only. Means and standard deviations of three measurements are shown.

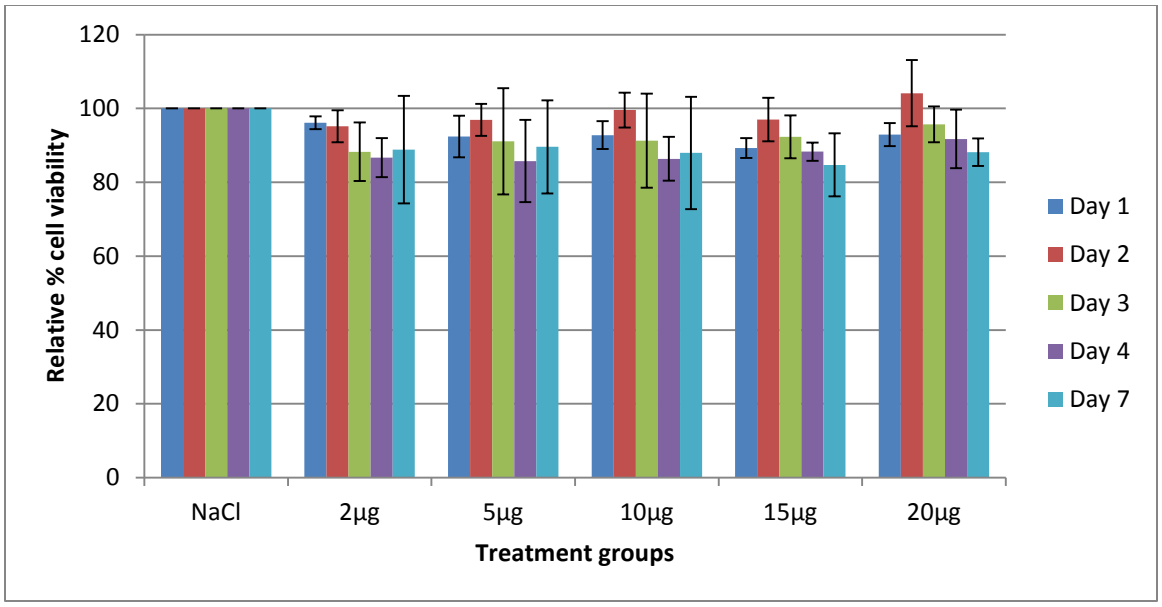

Figure 8.2 MTT assay results of FibroGRO cells with ARG/DXS PEM nanoparticles. Shown are means and standard deviations of three independent measurements.

8.2.2 Cytotoxicity studies of PEM microparticles/capsules

xCelligence cell proliferation assays were performed on FibroGRO, HTF and HEK293T cells with increasing amounts of PEM microparticles and microcapsules. $CaCO_3$ particles coated with $[ARG|DXS]_2|ARG$ formed PEM microparticles, and subsequent core dissolution resulted in ARG/DXS PEM microcapsules. They were given to the cells in the following cell-particle ratios: 1:2, 1:5, 1:10, 1:15 and 1:20.

Figure 8.3 shows the xCelligence results of FibroGRO cells with the ARG/DXS PEM microparticles and microcapsules. Increasing amounts of the PEM microparticles caused higher cytotoxic effects as depicted in Figure 8.3a. Only the cells with a cell-particle ratio of 1:2 showed similar cell growth as non particle treated control cells. Decreased cell indexes were observed with a ratio of 1:5, and cell viability was further reduced with 1:10 and 1:15 ratios.

On the other hand, PEM microcapsules with the same coating configuration except with core dissolution did not adversely affect cell growth as compared to PEM microparticles. Shown in Figure 8.3b are comparable cell index profiles detected for all cell-particle ratios, which were close to the profile of the control cells. Furthermore, cells with PEM microcapsules ratio of 1:20 showed higher cell indexes than the control cells.

Displayed in Figure 8.4a, HTF cells incubated with PEM microparticles also displayed reduced cell viability with increasing amounts of PEM microparticles. Similar to the FibroGRO cells, only the ratio of 1:2 showed similar cell growth to the control cells. The other higher ratios displayed significant reduction in cell proliferation. In Figure 8.4b, the cell index profiles of HTF cells given PEM microcapsules showed very similar growth pattern to control cells, with only a slight drop in cell proliferation initially which subsequently recovered.

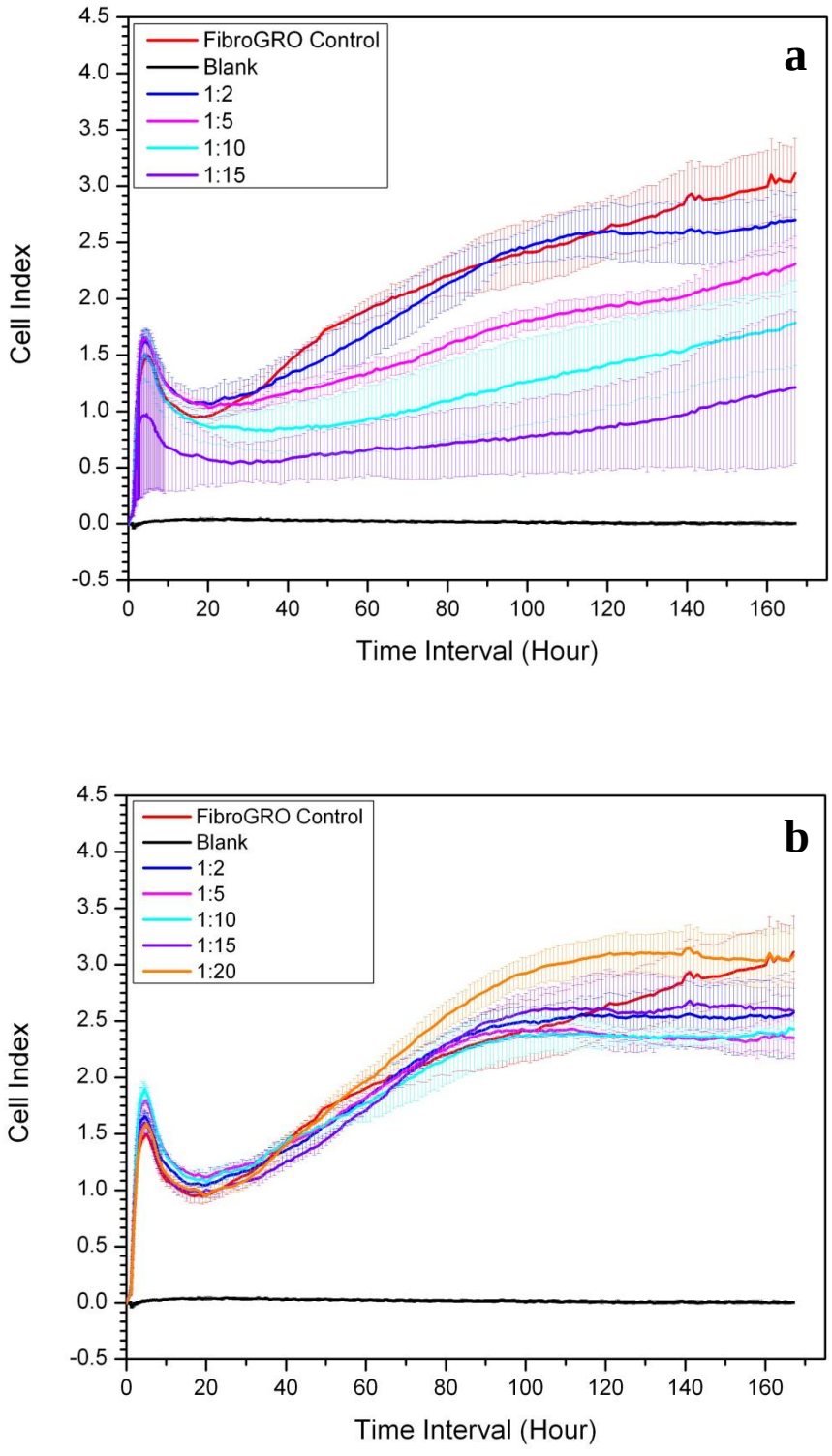

Figure 8.3 xCelligence cell proliferation indexes of FibroGRO cells exposed to PEM microparticles/capsules. (a) PEM microparticles. (b) PEM microcapsules. Blank (black line) refers to wells without cells and filled with medium only. Means and standard deviations of three measurements are shown.

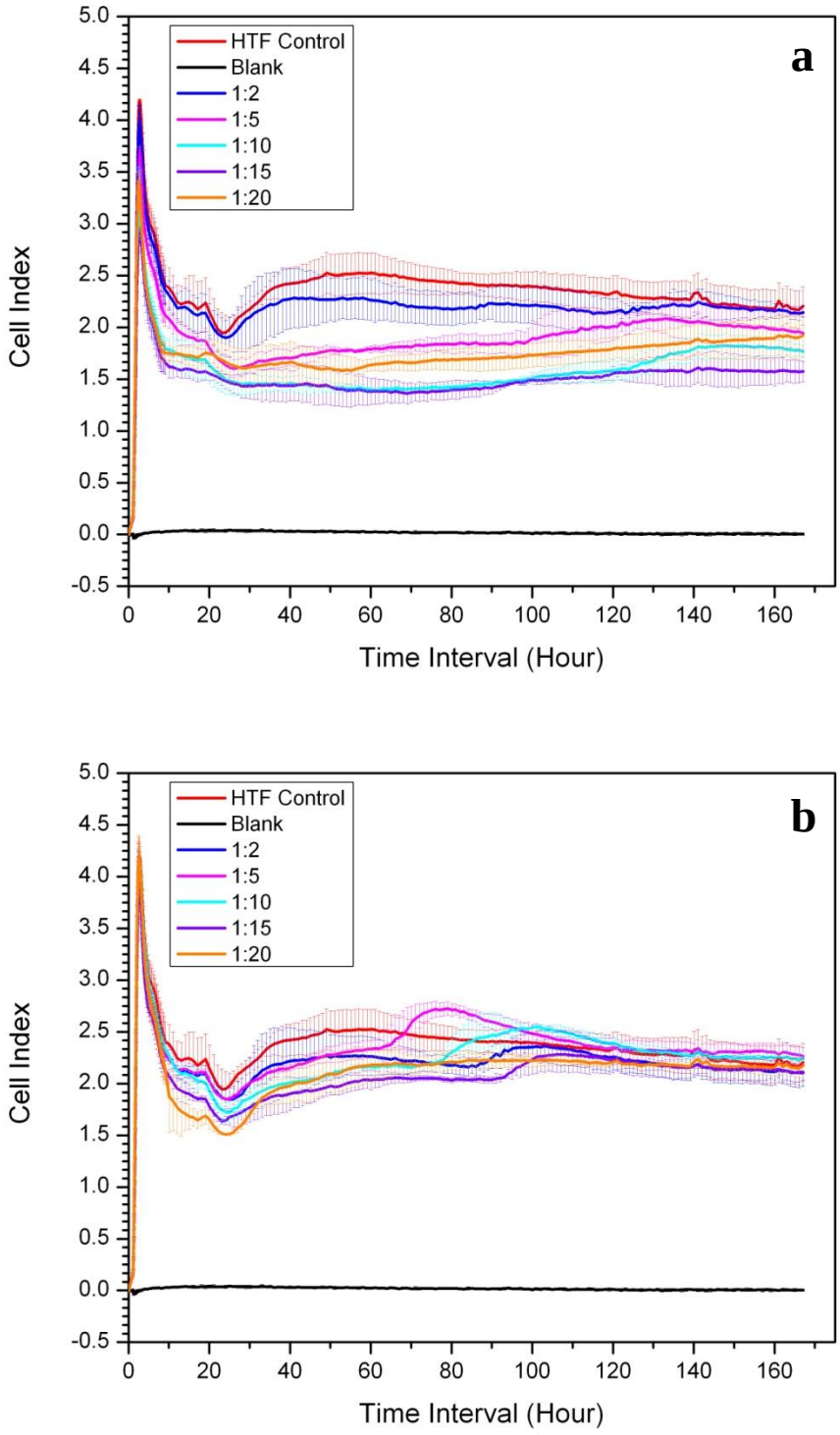

Figure 8.4 xCelligence cell proliferation indexes of HTF cells exposed to PEM microparticles/capsules. (a) PEM microparticles. (b) PEM microcapsules. Blank (black line) refers to wells without cells and filled with medium only. Means and standard deviations of three measurements are shown.

Figure 8.5 shows the xCelligence results on HEK293T cells incubated with PEM microparticles and microcapsules. As seen in Figure 8.5a, cells with PEM microparticles ratio 1:2 and 1:5 displayed comparable or better cell proliferation than the control HEK293T cells. However, a dramatic drop in cell viability was detected when the ratio was increased to 1:10. Cell proliferation was further hindered with a cell-particle ratio of 1:15.

Figure 8.5b displays the striking difference of HEK293T cell viability when incubated with PEM microcapsules as compared to PEM microparticles. All the cells throughout the different cell-particle ratios showed better cell proliferation indexes than the control cells. The cell indexes of cells with cell-particle ratio of 1:2 was slightly higher than the control cells, whereas cells with higher amounts of PEM microparticles showed similar cell proliferation profiles which were significantly higher than the control cells.

The MTT cell proliferation assay results of FibroGRO cells with PEM microcapsules are shown in Figure 8.6. The FibroGRO cell viability for cell-particle ratio 1:2 and 1:5 was almost the same as compared to control cells treated with no particles. The cells with cell-particle ratio of 1:10, 1:15 and 1:20 displayed similar cell viability as the control cells on Day 1. However, with longer incubation times of 2, 3, 4, and 7 days, cell proliferation in these cells continuously increases and were higher than the control cells. With increasing amounts of PEM microcapsules, cell proliferation increases, with FibroGRO cells exposed to 20 times the number of PEM microcapsules showing the highest cell proliferation.

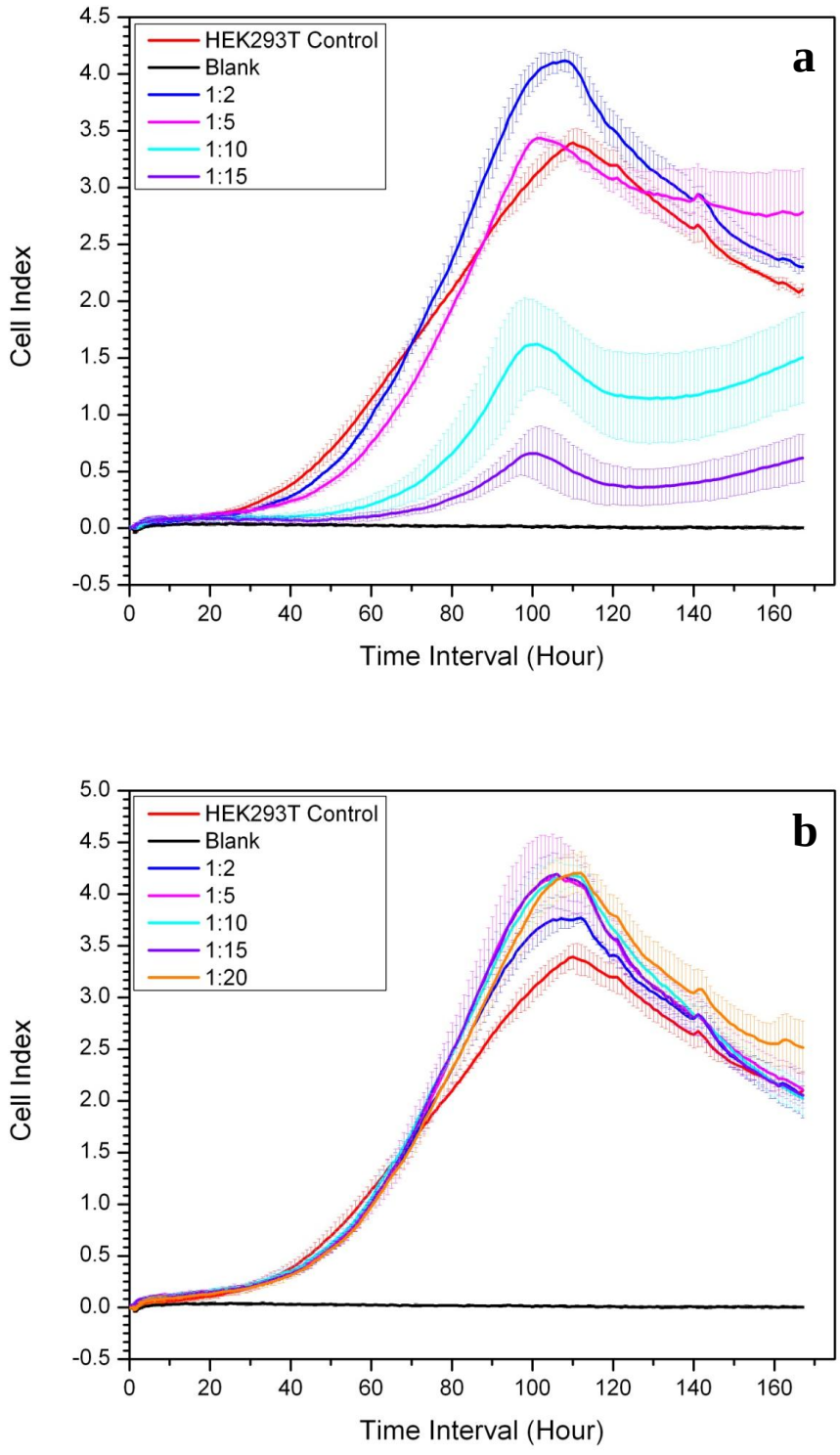

Figure 8.5 xCelligence cell proliferation indexes of HEK293T cells exposed to PEM microparticles/capsules. (a) PEM microparticles. (b) PEM microcapsules. Blank (black line) refers to wells without cells and filled with medium only. Means and standard deviations of three measurements are shown.

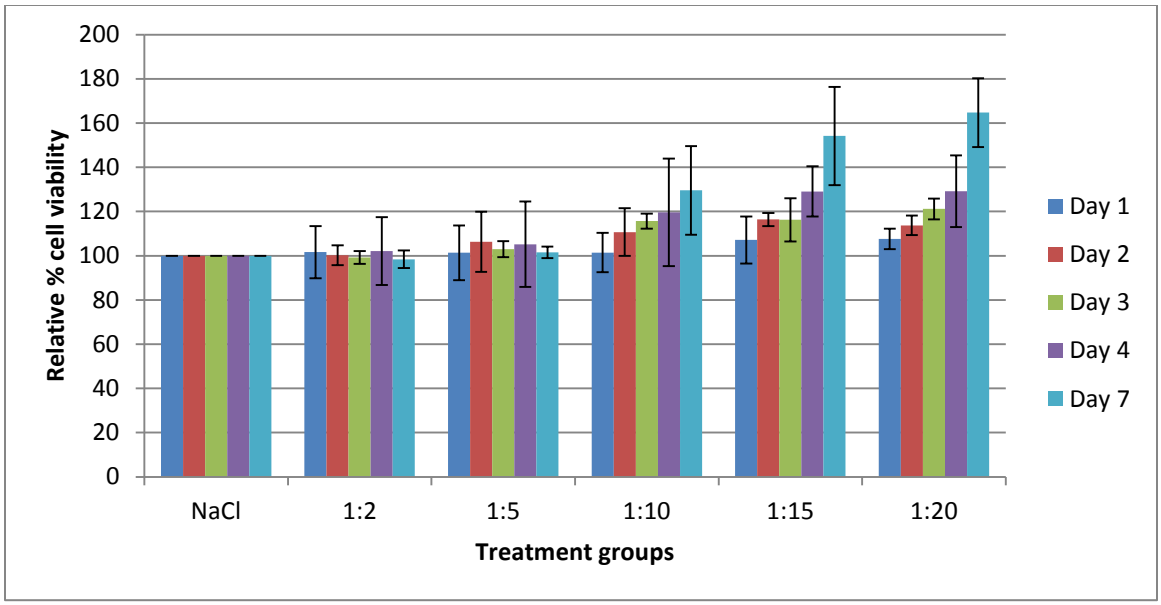

Figure 8.6 MTT assay results of FibroGRO cells with ARG/DXS microcapsules. Shown are means and standard deviations of three independent measurements.

8.3 Discussion

8.3.1 Cytotoxicity studies of PEM nanoparticles

Comparing the xCelligence data for FibroGRO and HTF cells, FibroGRO cells were more sensitive to the PEM nanoparticles than the HTF cells. Although similar cell viability was observed for all amounts of PEM nanoparticles to FibroGRO cells in the MTT assay, only lower concentrations should be used for future cellular interaction experiments for FibroGRO cells. As seen in Figure 8.1a, xCelligence assay showed 2 µg, 5 µg, 10 µg PEM nanoparticles for 4000 cells had less cytotoxic effects, while increasing to 15 µg and above greatly reduced cell viability.

On the other hand, HTF cells exposed to higher PEM nanoparticle concentrations still showed similar cell growth as those of lower particle amounts. Hence, up to 20 µg of PEM nanoparticles for 4000 cells can be explored for future studies.

xCelligence studies of HEK293T cells exposed to PEM nanoparticles as well as MTT assays of HTF and HEK293T cells can be performed to gain a more comprehensive view of PEM nanoparticle cytotoxic effects on different cell line. Additionally, besides cell viability, effects of presence of PEM nanoparticles within cells on cellular processes should also be further studied.

8.3.2 Cytotoxicity studies of PEM microparticles/capsules

The presence of the particle core versus the empty hollow capsules had significant effects on cytotoxicity throughout all 3 cell types. For FibroGRO and HTF cells, PEM microparticles did not show cytotoxic effects only at a ratio of 1:2, while higher concentrations affected the cells adversely. For HEK293T cells, a higher threshold ratio up to 1:5 was observed for PEM microparticles. Conversely, PEM microcapsules were non-cytotoxic to all 3 cell types for up to ratios of 1:20. This corresponded to work reported by De Koker et al. where 30 ARG/DXS microcapsules per cell showed low cytotoxicity at approximately 80 % viability in dendritic cells [44]. The probable explanation for this is that PEM microcapsules are more flexible and can be deformed within the cells as compared to the rigid PEM microparticles. In turn, cellular processes within the cells are less affected. Perhaps higher numbers of PEM microcapsules could be studied to discover their threshold limit in each cell type. More than 60 % cell viability was seen in dendritic cells when given much higher amounts of ARG/DXS microcapsules (125 microcapsules per cell) [44]. Additionally, PEM microcapsules will be more favorable in nucleic acid delivery applications as they are less cytotoxic when without the $CaCO_3$ core and additionally their hollow core can be utilized for loading of drugs or fluorescent materials for intracellular tracking. This finding should be taken into consideration in future studies regarding micron sized PEM particles.

Furthermore, greater cell growth was detected for PEM microcapsules for all concentrations as compared to control HEK293T cells. The higher ratios of 1:5 and above showed dramatic increase in cell proliferation. This trend of higher cell growth than control cells was also observed in xCelligence results of FibroGRO with 1:20 particles as well as MTT assay data of 1:10, 1:15 and 1:20 FibroGRO cell-particle ratios. For the MTT assays, increasing number of PEM microcapsules related to higher cell growth. The reason behind this increased cell proliferation is unclear and should be examined in further depths.

8.4 Conclusion

This chapter presented the cytotoxic studies of PEM particles to HEK293T, FibroGRO and HTF cells for both nano and micron sized. It highlights that each cell type has different threshold levels to the amounts of PEM particles it can uptake without or with minimal cytotoxic effects. For example, HTF cells can be exposed up to 20 μg of PEM nanoparticles per 4000 cells, but FibroGRO cells can only be given up to 10 μg for minimal cytotoxic effects. In addition, the presence of the $CaCO_3$ core in PEM microparticles greatly reduced cell viability in all 3 cell types. In conclusion, dissolution of the template core should be taken into consideration in future experiments and hollow PEM microcapsules will be more advantageous in future drug delivery applications of micron sized PEM particles.

CHAPTER 9
Conclusion and recommendations

In summary, PEM particles have potential as nucleic acid carriers as they were able to encapsulate nucleic acids, enter the cells, and deliver the nucleic acids (plasmid DNA and reporter siRNA) within the cells. Additionally, ARG/DXS layer pair was more favorable in the fabrication of PEM nanoparticles as well as PEM microcapsules as compared to PRM/DXS.

Nucleic acid encapsulation within PEM particles was achieved with two types of encapsulation techniques. PEM nanoparticles had a higher loading efficiency than micron-sized particles for layer encapsulation. However, PEM microparticles/capsules offer the option of core-encapsulation. Using either type of encapsulation, the results verified that nucleic acids have been successfully loaded in PEM particles. Also, more than 1 layer of siRNA was coated on PEM nanoparticles which enabled the dosage increase of each particle. Further experiments can explore the combination of both core and layer encapsulation to further increase dosage levels to reach the targeted dosage.

Cellular uptake of the PEM particles was displayed in HEK293T, FibroGRO and HTF cells as seen from confocal micrographs and flow cytometry data. Flow cytometry together with trypan blue quenching allowed the differentiation of PEM particles attached

on the cell membrane to those within the FibroGRO cells. More flow cytometry experiments with trypan blue quenching can be done in the future to further explore the uptake in HTF and HEK293T cells as well as other cell types. In addition, staining with Lysotracker Red showed PEM nanoparticles were not co-localized with lysosomes. Other stains can be utilized to discover and determine the location of the PEM nanoparticles within the cells. These experiments can also be applied to PEM microparticles/capsules, as due to their larger sizes, their location within cells might differ from the nano-sized particles.

Delivery of nucleic acids by PEM nanoparticles and microcapsules were determined straightforwardly by reporter plasmid and siRNA. The reporter properties allowed the simple study of PEM particles delivery, which could be further exploited in optimization experiments for the development of PEM particles as nucleic acid carriers. Successful delivery of nucleic acids by PEM particles paved the direction for additional studies with therapeutic plasmids and siRNA. Although these experiments would require more time including polymerase chain reaction and western blots, they would more accurately reflect the bio-functionality of the delivered nucleic acid as the increase or knockdown in expression of the genes in the RNA and protein levels will be determined.

Cytotoxicity experiments revealed that different cell types have different threshold levels to the amounts of PEM particles it can be exposed to. HTF cells can be given more PEM nanoparticles than FibroGRO cells. Hence, if future experiments call for other cell types, they should be examined individually for their cytotoxic threshold levels. Additionally, the presence of $CaCO_3$ core caused significant reduction in cell viability. The dissolution of the core to form PEM microcapsules should be taken into consideration in future

experiments with cellular interaction as they are much less cytotoxic to the cells, being non-cytotoxic for up to cell-particle ratio of 1:20. Furthermore, the increase in cell growth when the cells were given PEM microcapsules should be elucidated as it may have effects on the efficacy of the delivered nucleic acid.

In conclusion, PEM particles have shown potential to have applications in nucleic acid delivery. The results presented in this thesis propel the future studies of their true efficacy of delivering therapeutic DNA and siRNA. Due to their LbL coating technique, highly customizable and easily fabricated PEM particles can be produced for their development as multifunctional tailor-made biodegradable nucleic acid carrier systems with controlled drug release and additional functionalities.

CHAPTER 10
References

1. Decher, G., *Fuzzy nanoassemblies: Toward layered polymeric multicomposites.* Science, 1997. **277**(5330): p. 1232-1237.
2. Kotov, N.A., *Layer-by-layer self-assembly: The contribution of hydrophobic interactions.* Nanostructured Materials, 1999. **12**(5-8): p. 789-796.
3. Serizawa, T., et al., *Layer-by-Layer Assembly of Poly(vinyl alcohol) and Hydrophobic Polymers Based on Their Physical Adsorption on Surfaces.* Langmuir, 2002. **18**(22): p. 8381-8385.
4. Kozlovskaya, V., et al., *Hydrogen-Bonded Polymer Capsules Formed by Layer-by-Layer Self-Assembly.* Macromolecules, 2003. **36**(23): p. 8590-8592.
5. Liang, Z., et al., *Hydrogen-Bonding-Directed Layer-by-Layer Assembly of Conjugated Polymers.* Advanced Materials, 2004. **16**(9-10): p. 823-827.
6. Such, G.K., A.P.R. Johnston, and F. Caruso, *Engineered hydrogen-bonded polymer multilayers: from assembly to biomedical applications.* Chemical Society Reviews.
7. Johnston, A.P.R., et al., *Compositional and Structural Engineering of DNA Multilayer Films.* Langmuir, 2006. **22**(7): p. 3251-3258.
8. Sukhorukov, G.B., et al., *Stepwise polyelectrolyte assembly on particle surfaces: A novel approach to colloid design.* Polymers for Advanced Technologies, 1998. **9**(10-11): p. 759-767.
9. Schönhoff, M., *Self-assembled polyelectrolyte multilayers.* Current Opinion in Colloid & Interface Science, 2003. **8**(1): p. 86-95.
10. Joly, S., et al., *Multilayer Nanoreactors for Metallic and Semiconducting Particles.* Langmuir, 1999. **16**(3): p. 1354-1359.
11. Shi, X., M. Shen, and H. Möhwald, *Polyelectrolyte multilayer nanoreactors toward the synthesis of diverse nanostructured materials.* Progress in Polymer Science, 2004. **29**(10): p. 987-1019.
12. Trau, D. and R. Renneberg, *Encapsulation of glucose oxidase microparticles within a nanoscale layer-by-layer film: immobilization and biosensor applications.* Biosensors and Bioelectronics, 2003. **18**(12): p. 1491-1499.
13. Yang, W., et al., *Layer-by-Layer Construction of Novel Biofunctional Fluorescent Microparticles for Immunoassay Applications.* Journal of Colloid and Interface Science, 2001. **234**(2): p. 356-362.
14. Sukhorukov, G.B., et al., *pH-Controlled Macromolecule Encapsulation in and Release from Polyelectrolyte Multilayer Nanocapsules.* Macromolecular Rapid Communications, 2001. **22**(1): p. 44-46.

15. Ibarz, G., et al., *Smart Micro- and Nanocontainers for Storage, Transport, and Release.* Advanced Materials, 2001. **13**(17): p. 1324-1327.
16. Peyratout, C.S. and L. DÃ¤hne, *Tailor-made polyelectrolyte microcapsules: From multilayers to smart containers.* Angewandte Chemie - International Edition, 2004. **43**(29): p. 3762-3783.
17. Johnston, A.P.R., et al., *Layer-by-layer engineered capsules and their applications.* Current Opinion in Colloid & Interface Science, 2006. **11**(4): p. 203-209.
18. Mhashilkar, A., et al., *Gene therapy: Therapeutic approaches and implications.* Biotechnology Advances, 2001. **19**(4): p. 279-297.
19. El-Aneed, A., *Current strategies in cancer gene therapy.* European Journal of Pharmacology, 2004. **498**(1-3): p. 1-8.
20. Bessis, N. and M.-C. Boissier, *Gene therapy for patients with rheumatoid arthritis.* Joint Bone Spine, 2006. **73**(2): p. 169-176.
21. Nabel, E.G., *Gene therapy for vascular diseases.* Atherosclerosis, 1995. **118**(Supplement 1): p. S51-S56.
22. Fire, A., et al., *Potent and specific genetic interference by double-stranded RNA in Caenorhabditis elegans.* Nature, 1998. **391**(6669): p. 806-811.
23. Hannon, G.J., *RNA interference.* Nature, 2002. **418**(6894): p. 244-251.
24. Novina, C.D. and P.A. Sharp, *The RNAi revolution.* Nature, 2004. **430**(6996): p. 161-164.
25. Leung, R.K.M. and P.A. Whittaker, *RNA interference: From gene silencing to gene-specific therapeutics.* Pharmacology & Therapeutics, 2005. **107**(2): p. 222-239.
26. Aagaard, L. and J.J. Rossi, *RNAi therapeutics: Principles, prospects and challenges.* Advanced Drug Delivery Reviews, 2007. **59**(2-3): p. 75-86.
27. Verma, I.M. and N. Somia, *Gene therapy - promises, problems and prospects.* Nature, 1997. **389**(6648): p. 239-242.
28. Robbins, P.D. and S.C. Ghivizzani, *Viral Vectors for Gene Therapy.* Pharmacology & Therapeutics, 1998. **80**(1): p. 35-47.
29. Brown, M.D., A.G. Schätzlein, and I.F. Uchegbu, *Gene delivery with synthetic (non viral) carriers.* International Journal of Pharmaceutics, 2001. **229**(1-2): p. 1-21.
30. De Geest, B.G., et al., *Polyelectrolyte microcapsules for biomedical applications.* Soft Matter, 2009. **5**(2): p. 282-291.
31. Kim, B.S. and J.W. Choi, *Polyelectrolyte multilayer microcapsules: Self-assembly and toward biomedical applications.* Biotechnology and Bioprocess Engineering, 2007. **12**(4): p. 323-332.
32. Tong, W. and C. Gao, *Multilayer microcapsules with tailored structures for bio-related applications.* Journal of Materials Chemistry, 2008. **18**(32): p. 3799-3812.
33. Iost, R.M. and F.N. Crespilho, *Layer-by-layer self-assembly and electrochemistry: Applications in biosensing and bioelectronics.* Biosensors and Bioelectronics, 2011. **31**(1): p. 1-10.
34. de Villiers, M.M., et al., *Introduction to nanocoatings produced by layer-by-layer (LbL) self-assembly.* Advanced Drug Delivery Reviews, 2011. **63**(9): p. 701-715.

35. Yan, Y., et al., *Toward Therapeutic Delivery with Layer-by-Layer Engineered Particles.* ACS Nano, 2011. **5**(6): p. 4252-4257.
36. Reibetanz, U., et al., *Defoliation and Plasmid Delivery with Layer-by-Layer Coated Colloids.* Macromolecular Bioscience, 2006. **6**(2): p. 153-160.
37. Yang, X., X. Han, and Y. Zhu, *(PAH/PSS)5 microcapsules templated on silica core: Encapsulation of anticancer drug DOX and controlled release study.* Colloids and Surfaces A: Physicochemical and Engineering Aspects, 2005. **264**(1-3): p. 49-54.
38. Yu, A., I.R. Gentle, and G.Q. Lu, *Biocompatible polypeptide microcapsules via templating mesoporous silica spheres.* Journal of Colloid and Interface Science, 2009. **333**(1): p. 341-345.
39. Gao, C., et al., *The Decomposition Process of Melamine Formaldehyde Cores: The Key Step in the Fabrication of Ultrathin Polyelectrolyte Multilayer Capsules.* Macromolecular Materials and Engineering, 2001. **286**(6): p. 355-361.
40. Kato, N., et al., *Thin multilayer films of weak polyelectrolytes on colloid particles.* Macromolecules, 2002. **35**(26): p. 9780-9787.
41. Radtchenko, I.L., et al., *Assembly of Alternated Multivalent Ion/Polyelectrolyte Layers on Colloidal Particles. Stability of the Multilayers and Encapsulation of Macromolecules into Polyelectrolyte Capsules.* Journal of Colloid and Interface Science, 2000. **230**(2): p. 272-280.
42. Moya, S., et al., *Polyelectrolyte multilayer capsules templated on biological cells: Core oxidation influences layer chemistry.* Colloids and Surfaces A: Physicochemical and Engineering Aspects, 2001. **183-185**.
43. Neu, B., et al., *Biological cell as templates for hollow microcapsules.* Journal of Microencapsulation, 2001. **18**(3): p. 385-395.
44. De Koker, S., et al., *In vivo Cellular Uptake, Degradation, and Biocompatibility of Polyelectrolyte Microcapsules.* Advanced Functional Materials, 2007. **17**(18): p. 3754-3763.
45. Volodkin, D.V., N.I. Larionova, and G.B. Sukhorukov, *Protein Encapsulation via Porous CaCO3 Microparticles Templating.* Biomacromolecules, 2004. **5**(5): p. 1962-1972.
46. Antipov, A.A., et al., *Carbonate microparticles for hollow polyelectrolyte capsules fabrication.* Colloids and Surfaces A: Physicochemical and Engineering Aspects, 2003. **224**(1-3): p. 175-183.
47. Yang, Y.-W. and P.Y.-J. Hsu, *The effect of poly(d,l-lactide-co-glycolide) microparticles with polyelectrolyte self-assembled multilayer surfaces on the cross-presentation of exogenous antigens.* Biomaterials, 2008. **29**(16): p. 2516-2526.
48. Kakade, S., et al., *Transfection activity of layer-by-layer plasmid DNA/poly(ethylenimine) films deposited on PLGA microparticles.* International Journal of Pharmaceutics, 2009. **365**(1-2): p. 44-52.
49. Zhou, J., et al., *Layer by layer chitosan/alginate coatings on poly(lactide-co-glycolide) nanoparticles for antifouling protection and Folic acid binding to achieve selective cell targeting.* Journal of Colloid and Interface Science, 2010. **345**(2): p. 241-247.

50. Zhou, J., et al., *Polyelectrolyte Coated PLGA Nanoparticles: Templation and Release Behavior.* Macromolecular Bioscience, 2009. **9**(4): p. 326-335.
51. Labouta, H.I. and M. Schneider, *Tailor-made biofunctionalized nanoparticles using layer-by-layer technology.* International Journal of Pharmaceutics, 2010. **395**(1â€“2): p. 236-242.
52. Schneider, G. and G. Decher, *From functional core/shell nanoparticles prepared via layer-by-layer deposition to empty nanospheres.* Nano Letters, 2004. **4**(10): p. 1833-1839.
53. Mayya, K.S., B. Schoeler, and F. Caruso, *Preparation and organization of nanoscale polyelectrolyte-coated gold nanoparticles.* Advanced Functional Materials, 2003. **13**(3): p. 183-188.
54. Reum, N., et al., *Multilayer Coating of Gold Nanoparticles with Drug-Polymer Coadsorbates.* Langmuir, 2010. **26**(22): p. 16901-16908.
55. Poon, Z., et al., *Layer-by-Layer Nanoparticles with a pH-Sheddable Layer for in Vivo Targeting of Tumor Hypoxia.* ACS Nano, 2011. **5**(6): p. 4284-4292.
56. Hirsjärvi, S., L. Peltonen, and J. Hirvonen, *Layer-by-layer polyelectrolyte coating of low molecular weight poly(lactic acid) nanoparticles.* Colloids and Surfaces B: Biointerfaces, 2006. **49**(1): p. 93-99.
57. Hiller, S., et al., *Protamine assembled in multilayers on colloidal particles can be exchanged and released.* Biomacromolecules, 2004. **5**(4): p. 1580-1587.
58. Jin, Y., et al., *(Protamine/dextran sulfate)6 microcapules templated on biocompatible calcium carbonate microspheres.* Colloids and Surfaces A: Physicochemical and Engineering Aspects, 2009. **342**(1-3): p. 40-45.
59. Shutava, T.G., et al., *Layer-by-Layer-Coated Gelatin Nanoparticles as a Vehicle for Delivery of Natural Polyphenols.* ACS Nano, 2009. **3**(7): p. 1877-1885.
60. Yu, A., et al., *Mesoporous Silica Particles as Templates for Preparing Enzyme-Loaded Biocompatible Microcapsules.* Advanced Materials, 2005. **17**(14): p. 1737-1741.
61. Wang, Z., et al., *Construction of hollow DNA/PLL microcapsule as a dual carrier for controlled delivery of DNA and drug.* Colloids and Surfaces A: Physicochemical and Engineering Aspects, 2008. **326**(1-2): p. 29-36.
62. Zhao, Q., et al., *Hollow chitosan-alginate multilayer microcapsules as drug delivery vehicle: doxorubicin loading and in vitro and in vivo studies.* Nanomedicine: Nanotechnology, Biology, and Medicine, 2007. **3**(1): p. 63-74.
63. Heuberger, R., et al., *Biofunctional Polyelectrolyte Multilayers and Microcapsules: Control of Non-Specific and Bio-Specific Protein Adsorption.* Advanced Functional Materials, 2005. **15**(3): p. 357-366.
64. Halozan, D., et al., *Polyelectrolyte microcapsules and coated CaCO3 particles as fluorescence activated sensors in flowmetry.* Colloids and Surfaces A: Physicochemical and Engineering Aspects, 2009. **342**(1-3): p. 115-121.
65. Kreft, O., et al., *Polymer microcapsules as mobile local pH-sensors.* Journal of Materials Chemistry, 2007. **17**(42): p. 4471-4476.
66. Reibetanz, U., et al., *Flow cytometry of HEK 293T cells interacting with polyelectrolyte multilayer capsules containing fluorescein-labeled poly(acrylic acid) as a pH sensor.* Biomacromolecules, 2007. **8**(6): p. 1927-1933.

67. Liu, X., et al., *Multilayer Microcapsules as Anti-Cancer Drug Delivery Vehicle: Deposition, Sustained Release, and in vitro Bioactivity.* Macromolecular Bioscience, 2005. **5**(12): p. 1209-1219.
68. Manju, S. and K. Sreenivasan, *Hollow microcapsules built by layer by layer assembly for the encapsulation and sustained release of curcumin.* Colloids and Surfaces B: Biointerfaces, 2010. **82**(2): p. 588-593.
69. Zhu, Y. and J. Shi, *A mesoporous core-shell structure for pH-controlled storage and release of water-soluble drug.* Microporous and Mesoporous Materials, 2007. **103**(1-3): p. 243-249.
70. Qiu, X., E. Donath, and H. MÃ¶hwald, *Permeability of ibuprofen in various polyelectrolyte multilayers.* Macromolecular Materials and Engineering, 2001. **286**(10): p. 591-597.
71. Shchukina, E.M. and D.G. Shchukin, *LbL coated microcapsules for delivering lipid-based drugs.* Advanced Drug Delivery Reviews, 2011. **63**(9): p. 837-846.
72. Wang, Y. and F. Caruso, *Mesoporous silica spheres as supports for enzyme immobilization and encapsulation.* Chemistry of Materials, 2005. **17**(5): p. 953-961.
73. Garbers, E., et al., *Activity of Immobilized Trypsin in the Layer Structure of Polyelectrolyte Microcapsules (PEMC).* Macromolecular Bioscience, 2007. **7**(12): p. 1243-1249.
74. Caruso, F. and H. MÃ¶hwald, *Protein multilayer formation on colloids through a stepwise self- assembly technique.* Journal of the American Chemical Society, 1999. **121**(25): p. 6039-6046.
75. She, Z., et al., *Mechanism of Protein Release from Polyelectrolyte Multilayer Microcapsules.* Biomacromolecules. **11**(5): p. 1241-1247.
76. Petrov, A.I., D.V. Volodkin, and G.B. Sukhorukov, *Protein—Calcium Carbonate Coprecipitation: A Tool for Protein Encapsulation.* Biotechnology Progress, 2005. **21**(3): p. 918-925.
77. Hashide, R., et al., *Insulin-containing layer-by-layer films deposited on poly(lactic acid) microbeads for pH-controlled release of insulin.* Colloids and Surfaces B: Biointerfaces, 2011. **89**(0): p. 242-247.
78. Johnston, A.P.R., E.S. Read, and F. Caruso, *DNA Multilayer Films on Planar and Colloidal Supports:â€‰ Sequential Assembly of Like-Charged Polyelectrolytes.* Nano Letters, 2005. **5**(5): p. 953-956.
79. Wang, Z., et al., *Hollow DNA/PLL microcapsules with tunable degradation property as efficient dual drug delivery vehicles by Î±-chymotrypsin degradation.* Colloids and Surfaces A: Physicochemical and Engineering Aspects, 2009. **332**(2â€“3): p. 164-171.
80. Kakade, S., et al., *Transfection activity of layer-by-layer plasmid DNA/poly(ethylenimine) films deposited on PLGA microparticles.* International Journal of Pharmaceutics, 2009. **365**(1â€“2): p. 44-52.
81. Reibetanz, U., et al., *Functionalization of Calcium Carbonate Microparticles as a Combined Sensor and Transport System for Active Agents in Cells.* Journal of Biomaterials Science, Polymer Edition, 2011. **22**(14): p. 1845-1859.
82. Reibetanz, U., et al., *Colloidal DNA Carriers for Direct Localization in Cell Compartments by pH Sensoring.* Biomacromolecules, 2010. **11**(7): p. 1779-1784.

83. Ai, H., et al., *Interactions between self-assembled polyelectrolyte shells and tumor cells.* Journal of Biomedical Materials Research Part A, 2005. **73A**(3): p. 303-312.
84. Muñoz Javier, A., et al., *Combined Atomic Force Microscopy and Optical Microscopy Measurements as a Method To Investigate Particle Uptake by Cells.* Small, 2006. **2**(3): p. 394-400.
85. Cortez, C., et al., *Targeting and Uptake of Multilayered Particles to Colorectal Cancer Cells.* Advanced Materials, 2006. **18**(15): p. 1998-2003.
86. Zhou, J., et al., *Layer by layer chitosan/alginate coatings on poly(lactide-co-glycolide) nanoparticles for antifouling protection and Folic acid binding to achieve selective cell targeting.* Journal of Colloid and Interface Science. **345**(2): p. 241-247.
87. Cortez, C., et al., *Influence of Size, Surface, Cell Line, and Kinetic Properties on the Specific Binding of A33 Antigen-Targeted Multilayered Particles and Capsules to Colorectal Cancer Cells.* ACS Nano, 2007. **1**(2): p. 93-102.
88. Leßig, J., et al., *Phagocytotic Competence of Differentiated U937 Cells for Colloidal Drug Delivery Systems in Immune Cells.* Inflammation: p. 1-12.
89. Javier, A.M., et al., *Uptake of colloidal polyelectrolyte-coated particles and polyelectrolyte multilayer capsules by living cells.* Advanced Materials, 2008. **20**(22): p. 4281-4287.
90. Rathmann, S., et al., *Interaction, uptake, and processing of LbL-coated microcarriers by PMNs.* Cytometry Part A, 2011. **79A**(12): p. 979-989.
91. Han, B., et al., *Layered microcapsules for daunorubicin loading and release as well as in vitro and in vivo studies.* Polymers for Advanced Technologies, 2008. **19**(1): p. 36-46.
92. De Geest, B.G., et al., *Intracellularly degradable polyelectrolyte microcapsules.* Advanced Materials, 2006. **18**(8): p. 1005-1009.
93. Manchester, K.L., *Use of UV methods for measurement of protein and nucleic acid concentrations.* BioTechniques, 1996. **20**(6): p. 968-970.
94. Ke, N., et al., *The xCELLigence system for real-time and label-free monitoring of cell viability.* Methods in molecular biology (Clifton, N.J.), 2011. **740**: p. 33-43.
95. Denizot, F.o. and R. Lang, *Rapid colorimetric assay for cell growth and survival: Modifications to the tetrazolium dye procedure giving improved sensitivity and reliability.* Journal of Immunological Methods, 1986. **89**(2): p. 271-277.
96. Hansen, M.B., S.E. Nielsen, and K. Berg, *Re-examination and further development of a precise and rapid dye method for measuring cell growth/cell kill.* Journal of Immunological Methods, 1989. **119**(2): p. 203-210.
97. Sibilla, P., et al., *Effects of a Hydroxyapatite-based Biomaterial on Gene Expression in Osteoblast-like Cells.* Journal of Dental Research, 2006. **85**(4): p. 354-358.
98. Dasgupta, S., A. Bandyopadhyay, and S. Bose, *Reverse micelle-mediated synthesis of calcium phosphate nanocarriers for controlled release of bovine serum albumin.* Acta Biomaterialia, 2009. **5**(8): p. 3112-3121.
99. Palazzo, B., et al., *Biomimetic hydroxyapatite-drug nanocrystals as potential bone substitutes with antitumor drug delivery properties.* Advanced Functional Materials, 2007. **17**(13): p. 2180-2188.

100. Zhu, X., et al., *Characterization of nano hydroxyapatite/collagen surfaces and cellular behaviors.* Journal of Biomedical Materials Research - Part A, 2006. **79**(1): p. 114-127.
101. Cai, Y., et al., *Role of hydroxyapatite nanoparticle size in bone cell proliferation.* Journal of Materials Chemistry, 2007. **17**(36): p. 3780-3787.
102. Resnikoff, S., et al., *Global data on visual impairment in the year 2002.* Bulletin of the World Health Organization, 2004. **82**: p. 844-851.
103. *The AGIS Investigators. The advanced glaucoma intervention study (AGIS): 7. the relationship between control of intraocular pressure and visual field deterioration.* American Journal of Ophthalmology, 2000. **130**(4): p. 429-440.
104. Lama, P.J. and R.D. Fechtner, *Antifibrotics and Wound Healing in Glaucoma Surgery.* Survey of Ophthalmology, 2003. **48**(3): p. 314-346.
105. Seet, L.-F., et al., *SPARC Deficiency Results in Improved Surgical Survival in a Novel Mouse Model of Glaucoma Filtration Surgery.* PLoS ONE. **5**(2): p. e9415.
106. Jacobson, G.B., et al., *Biodegradable nanoparticles with sustained release of functional siRNA in skin.* Journal of Pharmaceutical Sciences, 2010. **99**(10): p. 4261-4266.